Simulation Modeling and Ecological Significance of Perched System Hydrology

By

RICHARD GRAY NISWONGER III
B.S. (Humboldt State University) 1997
M.Sc. (University of Nevada, Reno) 2002

DISSERTATION

Submitted in partial satisfaction of the requirements for the degree of

DOCTOR OF PHILOSOPHY

in

Hydrologic Sciences

in the

OFFICE OF GRADUATE STUDIES

of the

UNIVERSITY OF CALIFORNIA

DAVIS

Approved:

_____

_____

_____

Committee in Charge

2006

Richard Gray Niswonger
March, 2006
Hydrologic Sciences

ACKNOWLEDGEMENTS

This research was supported by California Bay-Delta Authority Ecological Restoration Program (Award # ERP-01-NO1). I would like to thank my advisor Graham Fogg for the time he gave me during our numerous meetings and for his support, scientific insight and theoretical ideas. I also extend my thanks to the other members of my committee, Jan Hopmans, for his technical help and scientific instruction, and Tim Ginn for his enthusiasm and theoretical expertise.

Numerous colleagues and friends have contributed to my work on the Cosumnes River, including Jim Constantz, Dave Prudic, Jan Fleckenstein and John Korchendorfer. These friends have accompanied me throughout my time at UC Davis and have provided valuable support and assistance in many different ways. I would also like to thank Ellen Mantalica and Diana Cummings from the UC Davis Watershed center for their help with ordering and receiving equipment during time constraints. I would like to thank Ofer Dahan of the Ben-Gurion University of the Negev, Israel, Casey Stewman, consulting biologist, Santa Cruz, CA, and Dave Prudic of the USGS, Carson City, Nevada for their help with designing field experiments and other things. I am particularly grateful for the loving support of my wife Sarah Marschall, who has helped me with her understanding and encouragement through this challenge and many others; I am also continually inspired by me daughter Emily who I am blessed to know. I would also like to thank my parents and siblings who listened and supported me throughout my life.

TABLE OF CONTENTS

LIST OF TABLES

LIST OF FIGURES

CHAPTER 1: INTRODUCTION

1.1. BACKGROUND

Groundwater levels in populated areas have been declining over the last several decades due to groundwater overdraft. For example, studies of the Central Valley aquifer (Williamson et al., 1989), synthesized data for the USA (Miller, 2000), areas in China (Kendy, 2003) and various areas of the world (Wood, 2003) have documented lowered groundwater levels of meters to tens of meters. Several studies have documented decreased flow in streams that is correlated to lowered regional groundwater levels (Fleckenstein et al., 2004; Glennon, 2002; Sophocleous, 2000; Winter et al., 1998).

Streams and their associated ecology are severely affected when groundwater levels permanently decline below the streambed elevation. Groundwater and surface water (GW/SW) interaction is important to the ecology of streams because it is responsible for the exchange of water among organisms that live within the stream (lotic), the shallow streambed sediment (benthic), the deeper streambed sediment (hyporheic), and the associated streambank and floodplain areas (riparian) (Brunke and Gonser, 1997; Tabacchi et al., 2000), (Fig. 1.1).

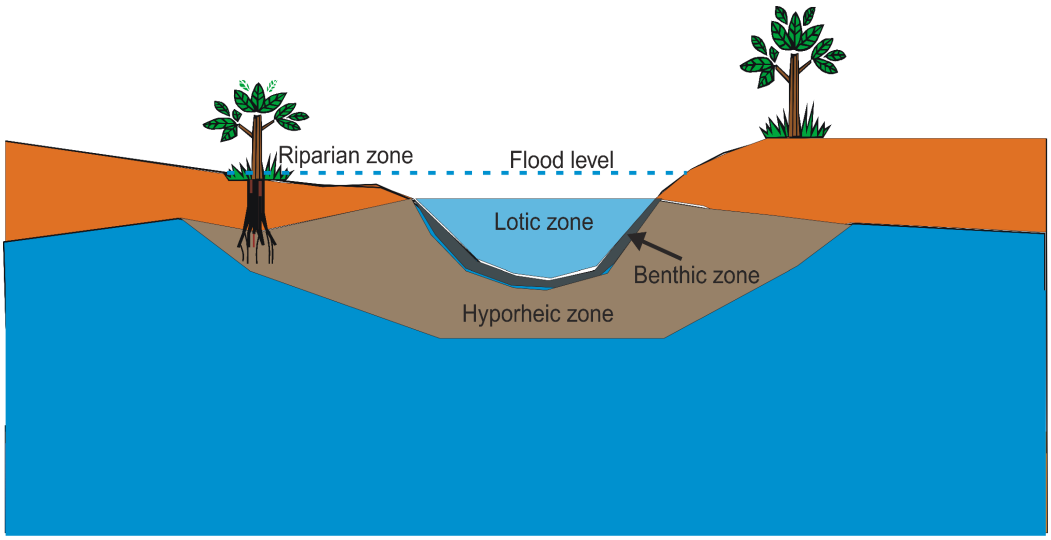

Figure 1.1: Stream zones affected by groundwater and surface-water interaction.

GW/SW interaction is important to lotic or in-stream ecosystems because groundwater keeps streams flowing (base flow) when there is no runoff to a stream. Additionally, groundwater influences the physiochemical conditions in a stream by buffering pH and temperature, cycling nutrients for biotic processing, and acting as a source or sink for organic matter (Brunke and Gonser, 1997).

Water flowing through the benthos is mainly due to hydraulic gradients created by streambed topography and stream depth, and to a lesser extent groundwater head potentials. A stream benthos is the zone adjacent to the sediment lining the channel surface that is primarily influenced by stream water conditions. However, groundwater upwelling into a stream influences the chemical and physical conditions of the water surrounding the channel bottom and is important for ecosystem functioning.

Larger scale exchanges between the stream and hyporheic corridor occur due to hydraulic gradients created by differences in stream and groundwater head potentials (Sophocleous, 2002; Brunke and Gonser, 1997). The boundary of the hyporheic corridor

is difficult to distinguish and can depend on many factors that change in space and time; however, generally it is considered to be the biologically active saturated region between a stream and phreatic groundwater. Although the benthos and hyporheic zones may overlap, the hyporheic zone is distinguished by permanent darkness, lower seepage velocities, and less mobile sediment (Brunke and Gonser, 1997).

Riparian zones near streams are often influenced by GW/SW interaction; however, the influence may be less direct further from a stream. Groundwater hydraulic heads beneath a stream often cause water seeping from the stream to flow laterally into the riparian root zone, providing water and nutrients for root uptake. Root uptake can enhance hydraulic gradients and cause water to flow toward the root zone. Streams that recharge groundwater maintain higher adjacent water table levels, which can help keep the riparian root zone saturated. Water supplied to riparian areas comes primarily from groundwater but may also be supplied by stream water during flooding or due to seepage through stream banks.

The extent that the aforementioned biological zones function in areas where groundwater does not contribute to the saturated region surrounding a stream is mostly unknown. Most streams that are exclusively effluent (stream water seeping into the subsurface) usually do not have water flowing in them continuously (intermittent or ephemeral streams). The ability of near-stream ecosystems to survive during periods of limited water availability is a key scientific question that will likely become more important as groundwater levels continue to decline near streams.

Streams in arid and semi-arid regions may be viewed as an analogue to streams in wetter regions that have declining groundwater levels. Streams traversing alluvial plains

in arid and semi-arid regions are usually separated from groundwater because regional groundwater levels, including the regional water table, become deep (Wilson and Guan, 2004). Separation from groundwater, which happens when a partially saturated zone lies between the stream and the groundwater (fully saturated) zone, results in distinct transitions of near-stream communities from lotic, hyphorheic and riparian species to drought tolerant species that do not require permanently submersed or saturated conditions. Such transitions are beginning to occur in wetter regions where groundwater levels are declining; however, the location and extent to which these transitions occur seem to depend on many geologic and geomorphic factors.

The effect of groundwater level decline on stream ecology may be dependent on the hydraulic conductivity (K) of the surrounding alluvial sediment due to the formation of perched systems beneath streams. Sediment surrounding streams may include streambed deposits that are conduits that enhance seepage, finer grained overbank deposits that inhibit flow, and consolidated alluvial deposits such as paleosols or hard pans that commonly inhibit vertical flow. Thus, where regional groundwater levels have declined, the extent to which GW/SW interaction occurs may be highly variable depending on the hydraulic properties of the heterogeneous alluvial deposits surrounding a stream and the formation of perched systems.

Studies of GW/SW interaction commonly assume that when a regional water table drops below and separates from the saturated zone associated with a streambed, the interaction between a stream and groundwater is in one direction only, where water seeps vertically from the stream toward the water table below (McDonald and Harbaugh, 1988; Winter et al., 1998). This conventional view may be sufficient in certain cases; however,

it does not consider the possibility of perched or mounded groundwater due to geologic heterogeneity that may diminish seepage losses and support gaining conditions in a stream.

There are few guidelines or general approaches for evaluating the effects of heterogeneous alluvial deposits and perched systems on exchange processes among streams and groundwater. A premise of this dissertation is that development of a basic understanding of the links between heterogeneous alluvial deposits, perched systems and water cycling near streams will greatly enhance conceptual models of SW/GW interaction.

1.2. RATIONALE AND OBJECTIVES

Historically, the study of groundwater has been motivated by the need to fulfill human consumption. Consequently, hydrogeologic research has been focused on the analysis of aquifers that could be exploited for water supply (Miller, 2000). Perched systems, which are vadose zone features, are usually considered irrelevant to groundwater supply and consequently, have been virtually ignored by the hydrogeologic community; however, perched systems may be important to streams for providing baseflow and for enhancing water availability for near-stream ecosystems.

Few studies have analyzed perched systems and these studies have been limited to either the migration of contaminants in the vadose zone (Robertson, 1977; Orr, 1999) or to lateral seepage processes beneath hillslopes (Whipkey, 1966; Betson, 1968; Hammermeister et al., 1982a,b). The shapes of steady-state perched groundwater mounds were analyzed by Khan et al., (1976) using stream functions and potential theory; however, their analysis cannot consider the geometry of a partially penetrating stream

with possible seepage faces. No research has been done to develop a basic understanding of how perched systems form beneath streams. A better understanding of perched systems beneath streams (both theoretically and applied), may lead to the possibility of managing perched systems so as to enhance baseflow and near-stream ecosystem integrity, especially in arid regions or overdrafted basins.

We hypothesize that the distribution of heterogeneous alluvial deposits may be important to streams for the following reasons: the presence of laterally extensive aquitards beneath streams may form perched systems that are surrogates for regional aquifers surrounding a stream; and the presence of smaller-scale interbedded heterogeneities that may elevate sediment saturation within the riparian-root zone. These typical features of alluvial sediment are not mutually exclusive and may occur over a spectrum of scales, such that their ability to enhance baseflow and ecosystem integrity will vary. However, because presently there is no scientific foundation that provides general understanding of the potential function of perched systems, our objective is to try and establish such an understanding with regards to stream baseflow and water availability to riparian vegetation.

1.3. DISSERTATION OUTLINE

This dissertation is generally structured according to the objectives outlined above and consists of two additional chapters. Chapter 2 addresses whether the presence of a fine-grained unit beneath a streambed could result in perched groundwater that contributes significantly to baseflow in the absence of influence from a regional aquifer in a variety of conceptual scenarios. Although the modeling analyses done in this chapter are relatively straightforward, such analyses are a first because hydrogeologists have not

considered the above-described questions regarding perched groundwater and stream/riparian-zone function.

Conceptually, the analysis in Chapter 2 is analogous to the general groundwater (fully saturated) simulations done originally by Tóth (1962, 1963), and more rigorously by Freeze and Witherspoon (1967). Their simulations have provided a widely-used foundation for understanding how groundwater behaves in typical circumstances. Due to the insights gained by these generic simulation studies, similar analysis have since been published to understand interaction among lakes and groundwater (Winter, 1976; 1978), ephemeral stream hydrology (Reid and Dreiss, 1990), and peatland hydrology (Reeves et al., 2000).

The generic simulation of stream/perched system interaction presented in Chapter 2 considers the presence of two homogeneous and deterministic geologic features, including a fine-grained-perching unit that lies beneath coarser sediment surrounding a stream. Although, in actuality these individual units are in themselves heterogeneous and thus consist of sediment of various textures, average properties are assumed to reflect their general affect on seepage processes surrounding a stream. Evapotranspiration (ET) is simulated to determine if riparian vegetation may diminish baseflow contribution by perched systems, indicating that the competition among lotic and riparian organisms may control water availability in a water-stressed environment.

Chapter 3 addresses another consequence of lowered regional groundwater levels near streams, which is the loss of riparian habitat. In this chapter, we examine whether interbedded sequences of fine- and coarse-grained sediment can store suitable amounts of water in the root zone above the regional water table to support phreatophyte vegetation.

In contrast to Chapter 2, which considered averaged properties of fine and coarse-grained units to analyze the potential of perched systems, Chapter 3 examines the heterogeneous alluvial deposits in detail by including small scale stratigraphic sequences developed using geostatistical methods.

In Chapter 3 we propose that a mechanism for enhanced water availability to riparian vegetation is the combination of coarser grained sediment deposits that are seepage pathways from the stream to the riparian root zone, and the resistance to vertical drainage by interbedded clay deposits. Unlike Chapter 2, which is hypothetical, we develop a model of stream/perched-aquifer interaction that is representative of the Cosumnes River, California to determine whether the seepage from the river can support the measured evapotranspiration (ET) demand over significant areas around the river.

In Chapter 3 we take a different approach from previous studies that have analyzed the effects of regional groundwater level decline on the growth and regeneration of phreatophyte vegetation near streams. Previous studies of phreatophyte vegetation have focused on the elevation of regional groundwater levels. These studies include the use of isotopes to determine the source of root-water uptake by phreatophyte vegetation in areas with shallow regional groundwater (Busch et al., 1992; Snyder et al., 1998), or the use of a regional groundwater level elevation criteria to determine suitable habitat for riparian vegetation (Springer et al., 1999). Because previous studies have been focused in areas with shallow regional groundwater, the possibility of phreatophyte vegetation being supported by perched groundwater has been overlooked. Thus Chapter 3 assesses the original idea that phreatophyte vegetation can grow and regenerate independently from regional groundwater elevation due to the presence of perched groundwater in the vadose

zone. Finally, Chapter 4 reviews the results of Chapters 2 and 3 and describes from an ecological perspective how perched systems may benefit streams and other surface water features. Chapter 4 also describes how perched systems might be managed to take advantage of their benefit to ecohydrology and water resources.

1.4. REFERENCES

Brunke, M. & Gonser ,T. (1997): The ecological significance of exchange processes between streams and groundwater. Freshwater Biology. 37, 1-33.

Busch, D.E., N.L. Ingraham, and S.D. Smith, (1992), Water uptake in woody riparian phreatophytes of the southwestern United States: a stable isotope study. Ecological Applications , 2, 450-459.

Fleckenstein, J.H., Anderson, Michael, Fogg, G.E., and Mount, Jeffrey (2004), Managing surface water-grondwater to restore fall flows in the Cosumnes River, American Society of Civil Engineers, Journal of Water Resources Planning and Management, vol. 130, no. 4, p. 301-310.

Freeze, R.A., P.A., Witherspoon (1967), Theoretical analysis of regional groundwater flow 2. Effect of water-table configurationand subsurface permeability variation, Water ResourcesResearch 3, 623–635.

Glennon, Robert (2002), Water follies—groundwater pumping and the fate of America's fresh water, Washington,, DC, Island Press, 313 p.

Kendy, Eloise (2003), The false promise of sustainable pumping rates, Groundwater, vol. 41, pp 1-3.

Khan, M.Y., D. Kirkham, R.L. Handy (1976), Shapes of steady state perched groundwater mounds, Water Resour. Res. Vol. 12 no. 3.

McDonald, M.G., and Harbaugh A.W. (1988), A modular three-dimensional finite-difference ground-water flow model: U.S. Geological Survey Open-File Techniques of Water-Resources Investigations, Book 6, Chapter A1, 586 pp.

Miller, J.A. (2000), Groundwater Atlas of the United States, Reston, VA, U.S. Geological Survey, 386 p.

Orr, B.R. (1999), A transient numerical simulation of perched ground-water flow at the test reactor area, Idaho National Engineering and Environmental Laboratory, Idaho, 1952-94, U.S. Geological Survey Water-Resources Investigations Report 99-4277.

Reeves, A.S., D.I. Siegel, P.H. Glaser (2000), Simulating vertical flow in large peatlands, Journal of Hydrology, vol. 227, p. 207-217.

Reid, M.E. and S.J. Dreiss (1990), Modeling the effects of unsaturated, stratified sediments on groundwater recharge from intermittent streams, Journal of Hydrology, vol. 114, p. 149-174.

Robertson, J.B. (1977), Numerical modeling of subsurface radioactive solute transport from waste-seepage ponds at the Idaho National Engineering laboratory, U.S. Geological Survey Open-File Report 76-717.

Snyder, K.A., D.G. Williams, and V.L. Gempko (1998) Water source determination for cottonwood, willow and mesquite in riparian forest stands. Pages 185-188, In Wood, E.F., A.G. Chebouni, D.C. Goodrich, D.J. Seo, and J.R. Zimmerman, technical coordinators. Proceedings from the Special Symposium on Hydrology. American Meteorological Society, Boston, Massachusetts.

Sophocleous, Marious, (2000), From safe yield to sustainable development of water resources—the Kansas experience, Journal of Hydrology, vol. 235, p.27-43.

Sophocleous, M. (2002), Interactions between groundwater and surface water: the state of the science, Hydrogeology Journal, vol. 10, 52-67.

Springer, E.S., J.M. Wright, P.B. Shafroth, J.C. Stromberg, D.T. Patten, (1999) Coupling groundwater and riparian vegetation models to assess effects of reservoir releases, Water Resour. Res. Vol. 35 no. 12.

Tabacchi, E., L. Lambs, H. Guilloy, A. Planty-Tabacchi, E. Muller, H. Decamps (2000), Impacts of riparian vegetation on hydrological processes, Hydrol. Process., 14, 2959-2976.

Tóth, J. (1962), A theory of ground-water motion in small drainage basins in central Alberta, Canada, Journal of Geophysical Research, vol. 67, no. 11, p. 4375-4387.

Tóth, J. (1963), A theoretical analysis of groundwater flow in small drainage basins, Journal of Geophysical Research, vol. 68, no. 16, p. 4795-4812.

Williamson, A.K., D.E. Prudic, and L.A. Swain (1989), Ground-water flow in the Central Valley, California, U. S. Geol. Surv. Prof. Pap., 1401-D, 127p.

Wilson, J.L., and H. Guan (2004), Mountain-block hydrology and mountain-front recharge, in Hogan, J.F., Phillips, F.M., and Scanlon, B.R., eds., Groundwater Recharge in a Desert Environment: The Southwestern United States: American Geophysical Union, Washington, D.C., Water Science and Application Series, vol. 9, p. 113-137.

Winter, T.C., 1976. Numerical simulation analysis of the interaction of lakes and ground water. Professional Paper 1001, US Geological Survey.

Winter, T.C., 1978. Numerical simulation of steady state three-dimensional groundwater flow near lakes. Water Resources Research 14, 245–254.

Winter, T.C. (1992), A physiographic and climatic framework for hydrologic studies of wetlands. In: Robarts, R.D., Bothwell, M.L. (Eds.), Aquatic ecosystems in semi-arid regions: implications for resource management, NHRI Symp. Ser. 7, pp. 127–148.

Winter, T.C., J.W. Harvey, O.L. Franke, W.M. Alley, 1998, Ground water and surface water: A single Resource, U.S. Geological Survey Circular 1139, 79 p.

CHAPTER 2: A NUMERICAL STUDY OF PERCHED SYSTEMS BENEATH STREAMS

Abstract

Analysis with a 3-D variably-saturated-groundwater-flow model provides a basic understanding of the interplay among streams and perched groundwater. Baseflow contribution from perched groundwater was evaluated with regards to varying hydrogeologic conditions, including the size and location of the perching unit and the hydraulic conductivity of the perching unit and surrounding coarser sediment. Model results indicate that perched groundwater discharge may be similar in quantity to values of regional groundwater discharge to streams, and be as high as 50 l/s (1.7 ft^3/s) averaged over a 2000 m length of channel consisting of coarse sediment. When the ratio of perching-unit K to the surrounding coarser-sediment K equaled or exceeded 2000, perched groundwater contributed baseflow for longer than 6 months; however, when the ratio was 200, perched groundwater contributed baseflow for only 11 days following the cessation of runoff. Evapotranspiration (ET) was simulated to examine the potential influence of riparian vegetation on perched groundwater discharge to a stream. Results indicate that for 100% riparian vegetation coverage with ET rates occurring at the maximum demand, perched groundwater discharge to the stream decreased by 30% when the stream was not incised; however, ET did not affect perched groundwater discharge for an incised stream.

2.1. INTRODUCTION

Restoring historic water table elevations is often impractical due to the growing consumption of water by humans. Consequently, present and future restoration of streams may benefit by taking advantage of focused areas of water availability, such as perched or mounded groundwater caused by geologic heterogeneity. Perched or mounded water tables caused by geologic heterogeneity may act as a partial surrogate for regional water tables that normally surround streams by limiting seepage loss, providing baseflow and bank storage.

Commonly, it is assumed that when a regional water table drops below and separates from the saturated zone associated with a streambed, the interaction between a stream and groundwater is in one direction only, where water seeps vertically from the stream toward the water table below (McDonald and Harbaugh, 1988; Winter et al., 1998). Furthermore, it is assumed that once this so-called "disconnection" occurs, additional declines in the water table will cause no additional increases in stream seepage losses. This conventional view may be sufficient in certain cases; however, it does not consider the possibility of perched or mounded groundwater due to geologic heterogeneity that may diminish seepage losses and support gaining conditions in a stream. Fleckenstein et al., (2005) presented model results indicating that geologic heterogeneity was responsible for localized groundwater mounding as high as the free surface of the Cosumnes River, California where regional groundwater levels away from the River were greater than 15 m below the channel.

Perched groundwater may form where focused infiltration is obstructed from flowing downward by sediment with low hydraulic conductivity (K). Because disconnected streams may be a source of high infiltration, they may create perched or mounded groundwater if they flow over stratified sediment with contrasting K. Alluvial and fluvial deposits are often interbedded with unconsolidated and partially consolidated or cemented sediment (Krumbein and Sloss, 1963; Miall, 1996), and these conditions are conducive to the formation of mounded or perched groundwater.

There have been very few studies that address the interaction between surface water and perched groundwater. Most of the work regarding perched systems has pertained to the migration of contaminants in the vadose zone (Robertson, 1977; Orr, 1999) or flow and transport in hillslopes, called subsurface storm flow, or interflow (Whipkey, 1966; Betson, 1968; Hammermeister et al.,1982a,b). However, Reid and Dreiss (1990) examined the effects of low permeable lenses on stream infiltration and tested various models for simulating this situation. Reid and Dreiss (1990) identified the formation of saturated regions above low-K lenses but their work was focused on evaluating models and not the interaction between streams and perched groundwater.

Khan et al. (1976) analyzed steady-state perched groundwater mounds to estimate the anoxic region beneath sanitary landfills. The theoretical procedure developed by Khan et al. (1976) cannot be extended to consider seepage faces or discontinuous perching units. Thus, a numerical procedure must be used to consider the effects of seepage from a free surface into a partially penetrating stream. Additionally, negative pressure gradients in the sediments surrounding the stream likely enhance perched groundwater recharge during flooding, which cannot be considered based on purely

saturated analysis. In the present study we rely on a numerical solution to Richard's equation to more realistically consider the physics of flow between perched groundwater and streams.

There have been few studies analyzing the ecological significance of perched groundwater beneath streams. Most of the ecological studies of groundwater near streams have been focused on hyporheic flow that occurs where a regional water table elevation is close to the streambed elevation (e.g. Bretschko and Klemens, 1986; Danielopol and Marmonier 1992). However, Hathaway et al. (2002) stressed the importance of lithologic characterization of the upper 15 m of an alluvial aquifer beneath a stream to account for the influence of perched groundwater on stream/groundwater exchange.

This chapter examines the interaction among perched groundwater and streams using a 3-D variably-saturated-flow model to begin to develop basic understanding of the interplay among streams and perched groundwater. A simple hydrogeologic scenario is used, consisting of a stream flowing over coarse sediment underlain by a fine-grained perching unit.

Due to the complex stratigraphic architecture of fluvial environments, there is a large amount of uncertainty regarding the effective vertical K and lateral continuity of a perching unit. Similarly, coarse-grained channel deposits are also heterogeneous and the effective K of channel deposits is highly variable. These uncertainties form the basis for simulation modeling presented herein. We use generic simulations to develop ranges in K for coarse- and fine-grained sediment that result in the formation of perched groundwater that discharges to a stream. Additionally, spatial configurations of the perching unit are varied, including the length, width and depth of the perching unit relative to the stream.

Historically, the significance of aquifers has been evaluated with regards to water resources, and it is often cast in terms of how much could be produced by wells. Similarly, an important measure of significance of a perched system would be how much can flow to an ecosystem or wetland, which is in turn also indicative of temporal persistence of the perched system. For this reason, the amount and persistence of perched groundwater discharge is compared in the simulations presented herein; the shape of the perched water tables for these simulations are included in Appendix A. Evapotranspiration (ET) is simulated to evaluate the effects of ET on perched groundwater.

2.2. CONCEPTUALIZATION OF A HYPOTHETICAL STREAM AND PERCHED SYSTEM

The general conceptual model of the hypothetical stream and perched system is based on streams that flow over alluvial deposits containing stratified sediment with contrasting K that include coarse stream deposits such as sands and gravels and fine floodplain deposits such as silts and clays. In addition to unconsolidated sediment, consolidated or partially consolidated clay layers, hardpans and paleosols that are formed by pedogenic, cementation, and fluvial processes may also be present in alluvial sediment (Maill, 1996; Weissmann and Fogg, 1999). Shallow, low-K stratigraphic units or aquitards have been documented in several studies of alluvial valleys of California as being laterally extensive and to exhibit substantial control over vertical groundwater flow (Johnson et al., 1968, Croft, 1969; Weissmann and Fogg, 1999).

In order to construct a simulation model for our analysis with the appropriate hydraulic properties and geometric configurations, it is first useful to conceptualize how a perched system might form beneath a stream. The necessary condition for groundwater to

perch is when vertical seepage from a stream is impeded by a low-K perching unit. If stream infiltration is high as compared to the underlying sediment's ability to conduct water vertically, saturated storage will accumulate around the stream. As stream infiltration saturates the sediment above a low-K perching unit, positive water pressures may form, which may cause the vertical component of the hydraulic gradient to diminish or reverse. Perched groundwater may then seep back into the stream and contribute to base flow. This conceptualization leads to the assumed simplified stratigraphic configuration shown in Figure 2, consisting of fine sediment (perching unit) positioned between coarse sediment making up the channel surface and underlying regional aquifer.

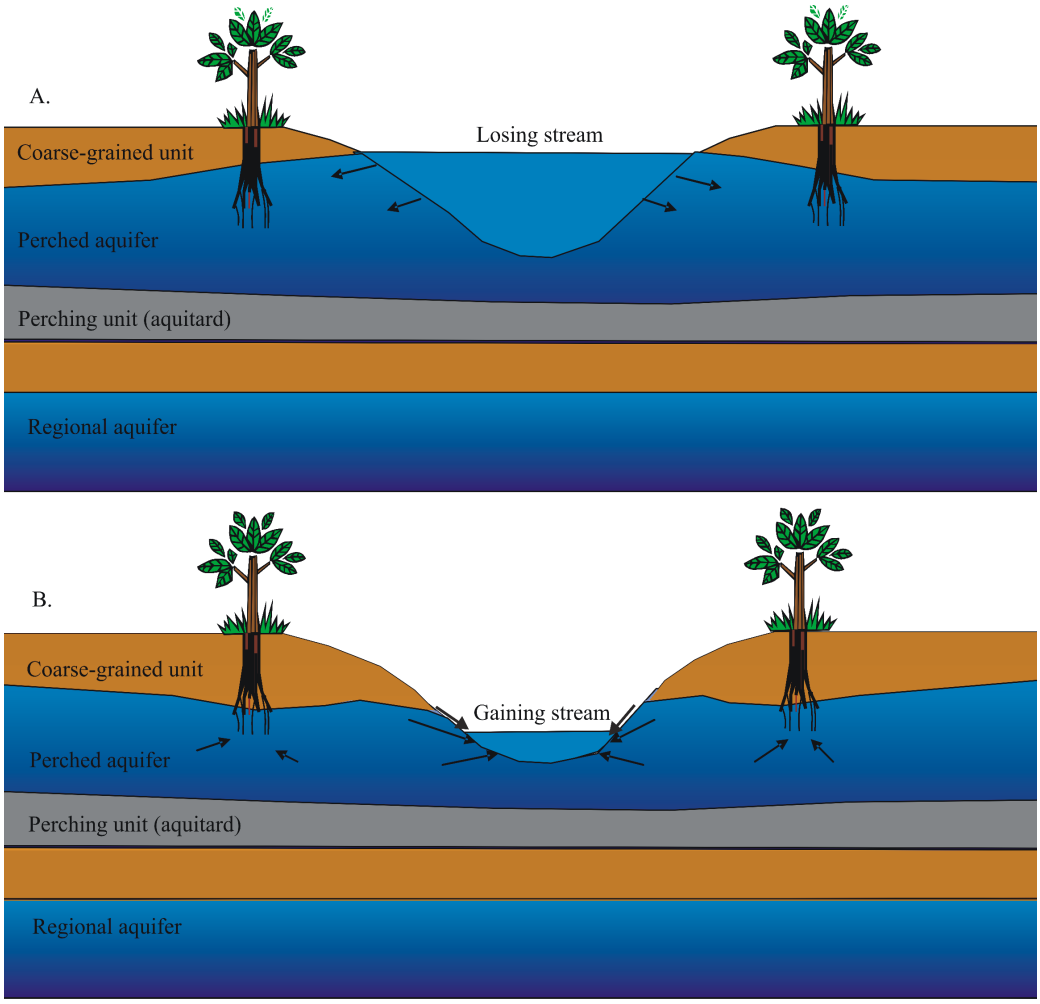

Figure 2.1: Conceptual picture of stream/perched groundwater interaction: A. during the high-flow season when the stream recharges the perched groundwater; B. during low-flow season when the perched groundwater discharges to the stream.

Constraints on the K of coarse and fine sediment may be placed based on previous studies that have measured K of sediment samples taken from streambeds and shallow alluvial depositional environments. An extensive study of alluvial sediment K of the Central Valley, California was done by Johnson et al. (1968). Johnson et al. (1968) used constant head, falling head and consolidation test results to estimate the vertical and horizontal K of 390 samples. Samples were taken from two areas, one area was located in Fresno County, which drains the western side of the Sierra Mountains, and the other area was located in Santa Clara Valley, just east of the coastal range. Despite both areas being

located in different geologic environments, both contained shallow sediment consisting of interbedded gravels, sands, silts and clays. Although the depths of individual core samples were not shown, and many samples were taken to depths greater than 50 m, Johnson et al. (1968) found vertical K for fine sediment to range between 1.0 $x10^{-5}$ and 1.0 $x10^{-6}$ md^{-1} for a majority of samples, and vertical K of coarser sediment to range between 1.0 $x10^{-2}$ and 0.4 md^{-1} for a majority of samples. Johnson et al. (1968) were not able to retrieve coarse sands and gravels so that the range in the vertical K was likely to be greater than reported. Another study by Riley (1969) took averages of K values measured using the same methods as Johnson et al. (1968) from aquitard material in alluvial sediment of California and estimated an average vertical K of 2.5 $x10^{-6}$ m/d.

These studies demonstrate the contrast in K of alluvial sediment. In addition to these works, there is also an abundance of unpublished driller's logs taken from alluvial systems that show similar variability in sediment texture. Fleckenstein et al. (2004) analyzed 350 driller's logs in order to categorize alluvial sediment surrounding the Cosumnes River, California into four different texture classes. They estimated the average thickness of these different texture classes and found them to range between 2.5-4.0 m. These data and the aforementioned published K values were used to establish ranges in the K and the perching unit thickness to simulate the interaction among a hypothetical stream and a perched groundwater.

2.3. METHODS

A numerical model was used to evaluate certain scenarios of perched groundwater near streams. Perched groundwater conditions are governed by a myriad of different combinations of system geometry, parameters and boundary conditions. It is difficult and beyond the scope of this work to define the complete solution space for such systems. Rather, the goal is to provide the first, quantitative analyses of many of the key characteristics governing perched groundwater hydrology, providing some new insights about processes as well as the foundation for future studies.

2.3.1. Model code

A three-dimensional, variably saturated groundwater flow model (TOUGH2; Pruess et al., 1990) was used to simulate stream-perched-aquifer interaction. TOUGH2 was chosen for this study because it is one of the few 3-D, variably-saturated flow codes available that has been widely used and documented. TOUGH2 has many modules that can simulate various types of problems. The module used in this study is called EOS3, which simulates non-isothermal flow of water and air through porous rock material (Pruess et al., 1990). However, isothermal conditions were assumed and the heat transport equations were not solved in these simulations. Statements of the governing equations solved by TOUGH2 are briefly described in Chapter 3 and the reader is referred to the work of Preuss et al. (1990) for a complete description.

The three dimensional flow that occurs during the interaction among streams and perched groundwater is important when considering the total inflow to a stream over a

discontinuous perching unit. It is the boundaries of the perching unit that cause the groundwater flow to deviate from being contained in a 2-D cross-sectional plane or 3-D axisymmetric domain with respect to the stream. Thus, the 3-D model will provide a better estimate of seepage from perched groundwater to a stream. Later in this chapter we compare results from 2-D and 3-D simulations of perched groundwater flow to demonstrate the difference.

2.3.2. Generalized model domain of stream/perched-groundwater system

A generalized hypothetical model was developed that consisted of a half-section of a stream profile and the surrounding sediment that includes a low-permeable perching unit beneath the stream (Fig. 2.2). Lateral extent of the perching unit is effectively 600 m perpendicular to the stream and 1000 m parallel to the stream, and the edges of the layer stop 1000 m short of the downstream model boundary and 400 m short of the distal (away from the stream) boundary. This kilometer-scale perching layer is quite common in systems containing paleosols and/or floodplain muds. The amount and longevity of perched groundwater storage will naturally depend on lateral extent of the perching layer. Some limited sensitivity to perching layer lateral extent will be examined below.

The model domain consisted of 30 cells that were 67 m long in the direction parallel to the stream, 25 cells that ranged between 5 and 50 m long in the direction perpendicular to the stream, and 20 cells that ranged between 0.5-1 m thick. The stream bank was 4 m deep, except where noted otherwise, and the active channel was 15 m wide. Symmetry was assumed along the thalweg of the stream and along one side of the perching unit perpendicular to the stream profile.

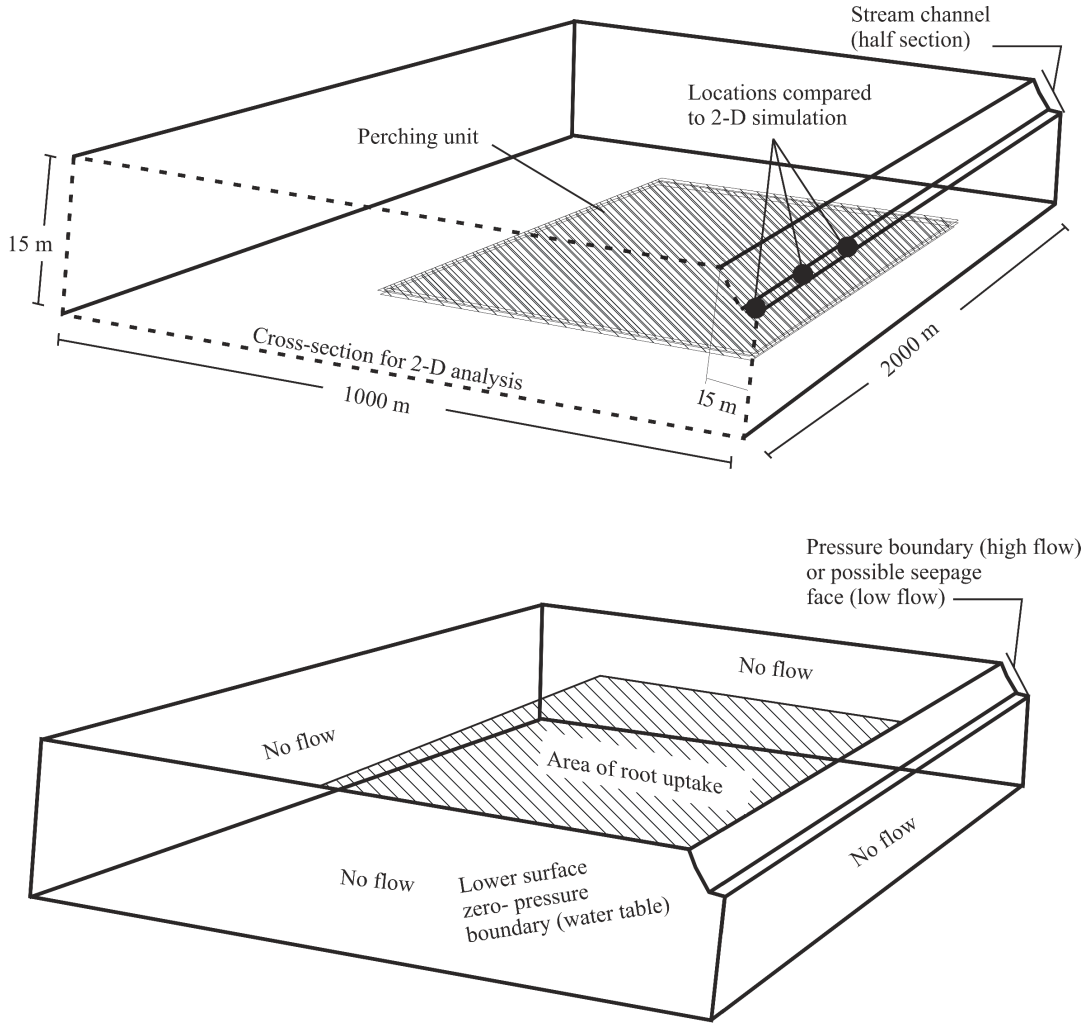

Figure 2.2: The model domain: A. model boundaries, perching unit, and location of 2-D cross-section; B. dimensions of model domain. Hatched region represents region where evapotranspiration was simulated. Root uptake extended to 4 m below top of model.

The relative permeability (relative K) and retention functions of Mualem, (1976) and Van Genuchten (1980) were used with separate sets of parameters to describe the two sediment types (coarse-grained channel deposits and fine-grained perching unit). These parameters were estimated by relating measurements of sand-silt-clay percentages, bulk density, porosity and K to relative K and retention parameters using neural networks (Minasny et al. 2004). Minasny et al. (2004) provide software that performs the neural network analysis based on a database of physical and hydraulic properties and unsaturated flow parameters calculated using the multi-step outflow method.

Unsaturated flow parameters for the two facies represented in the model were inferred based on measured sand-silt-clay percentages, bulk density, porosity and K on 9 coarse sediment and 5 fine sediment cores samples taken from the Cosumnes riverbed. Laboratory measurements were averaged within each texture group, which were used to compute the unsaturated flow parameters using neural networks (Minasny et al., 2004; Fig. 2.3).

Unsaturated flow parameters are highly variable in alluvial sediment and thus the 95% confidence intervals for the estimated function parameters result in capillary pressure curves and relative K curves that vary widely (Fig. 2.3). The 95% confidence intervals for the function parameters resulted in unrealistic curves, which is likely due to not constraining the way that the confidence intervals were calculated. For example, the capillary pressure curves predicted values of suction (negative potential) for saturation values greater than one. However, the estimated parameter values that are used in the model (solid lines in fig.2.3) resulted in curves that are realistic for the types of sediment

analyzed. The effects of varying unsaturated hydraulic properties on simulated perched groundwater were not evaluated.

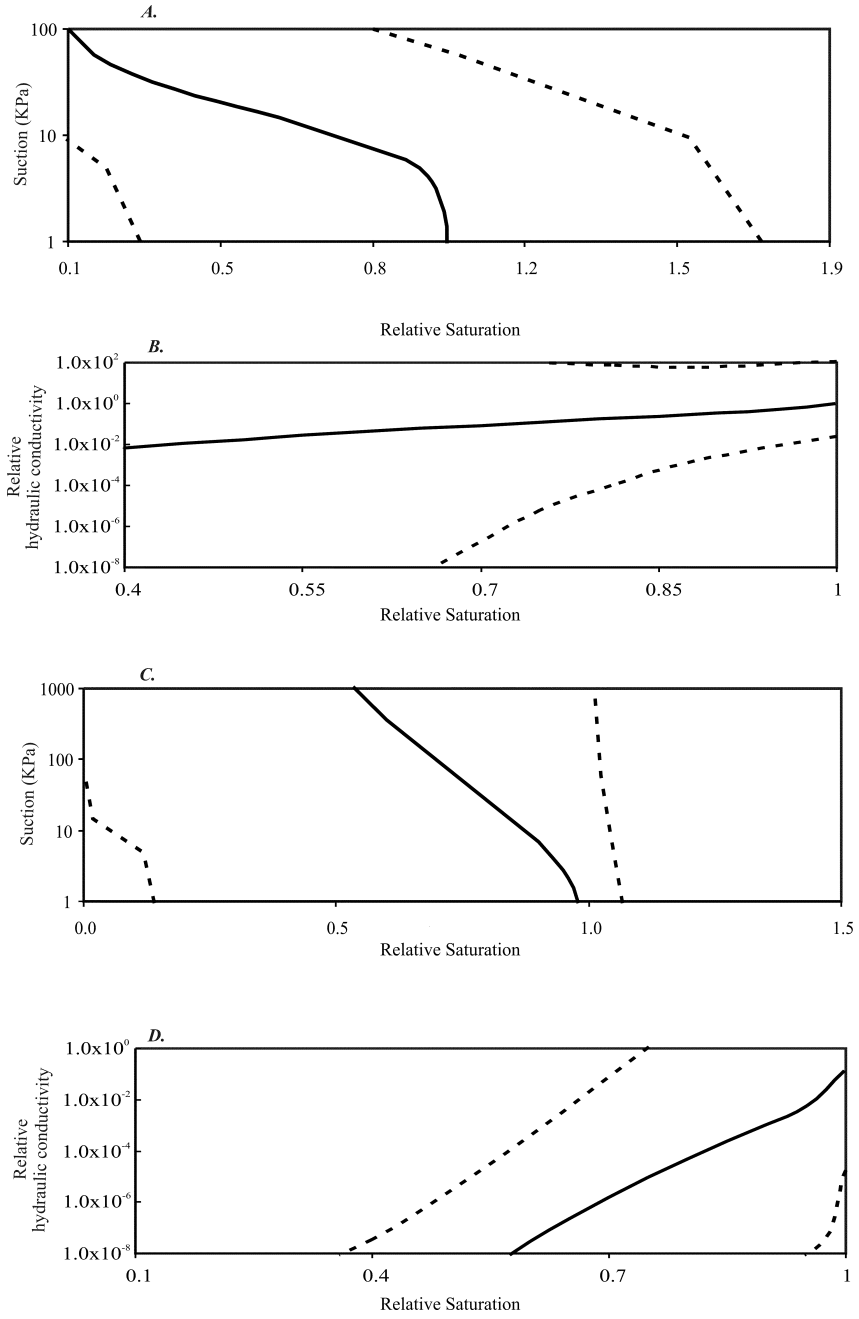

Figure 2.3: A. Capillary pressure curve for coarse sediment (called muddy sand in Chapter 3); B. relative hydraulic conductivity curve for coarse sediment; C. capillary pressure curve for fine sediment (called sandy clay in Chapter 3); and D. relative hydraulic conductivity curve for fine sediment. Dashed lines are the curves generated based on the 95% confidence intervals for the estimated function parameters. The function of van Genuchten-Mualem was used to represent the relative permeability curve (van Genuchten, 1978; Mualem, 1976) and the function of van Genuchten (1978) was used to represent the capillary pressure curve.

Each hypothetical model was run in two parts representing two periods of the annual hydrologic cycle. The first part was run with the stream at bank-full conditions represented by a constant-pressure and zero gas saturation boundary condition for three months to represent the high-flow season (January-March in Mediterranean type climates). The resulting subsurface fluid conditions at the end of the simulation were then used as initial conditions in the second simulation. The second simulation represented the low-flow season consisting of a five-month period (April-August). Consequently, the stream boundary conditions were changed such that the lower-most cells representing the stream were assigned a pressure corresponding to a stream depth of 0.25 m and boundary cells above the surface water line were assigned conditions representing the atmosphere adjacent to the stream bank.

Initial conditions for the first part of the simulation were generated by running the model until saturations were at field capacity throughout the model. Thus, there was no perched groundwater at the beginning of part one of each simulation. Although it is likely that under certain hydrogeologic conditions perched groundwater may persist for several years, the initial conditions used in this modeling neglect this condition. Assuming that the perched groundwater completely drained by the end of the previous dry season results is a conservative estimate of perched groundwater storage.

Seepage faces are simulated by TOUGH2 with the use of “atmospheric cells” that line the channel surface and floodplain above the level of the stream water surface. The atmospheric cells are made to be saturated with gas and to have an assumed mass fraction of water vapor that is representative of atmospheric conditions. A model cell can be maintained at constant gas saturation and pressure by assigning the cell a very large

volume such that flow into and out of the cell does not affect its saturation and pressure as described by Pruess et al. (1999). The volume of each cell is input as an independent value and so the volume of a cell does not have to correspond to a cell's dimensions. Each of these cells functions to connect streambed cells, located within the porous medium, with values of specified pressure representing the stream heads or specified gas saturation representing the atmosphere. Capillary pressure is turned off in the "atmospheric cells".

The modeling approach assumes that the stream depth does not change in response to seepage. This assumption is likely reasonable since the stream depth change would be relatively small given the amount of seepage that would occur over a 2000 m length of stream, even under extreme conditions. Thus, except for in very narrow streams, the dependence between changes in stream depth and seepage would be small over a 2000 m length of stream. These effects could be simulated by coupling a surface water model to TOUGH2; however, this approach is beyond the scope of the present work.

Eleven cases, herein referred to as scenarios 1-11, were simulated with varying hydrogeologic conditions. Two types of sediment were represented in the model, including the perching unit and surrounding coarser sediment. Models were constructed to evaluate the effect of: the coarse sediment and perching unit K; the horizontal extent of the perching unit; and the thickness of the coarse sediment above the perching unit. Descriptions of these hypothetical models are detailed in Table 2.1. These models were evaluated based on the amount and duration of perched groundwater discharge to the stream for a five month period.

ET losses were included to examine the influence on streamflow. Representative ET rates were determined based on ET measurements made by J. Korchendorfer and K. T. Paw U, written communication (2004) using an energy-balance method from willows trees growing along the Cosumnes River. These measurements were compared to another study by Schaeffer et al. (2000), who used sapwood flux estimates to measure transpiration from willows and cottonwoods growing along active channels in Arizona. The maximum rates measured by Schaeffer et al. (2000) of 6 mm/d compared well to the maximum rates measured by J. Korchendorfer and K. T. Paw U (2004) of 7 mm/d. These maximum rates represent an upper bound for ET rates near streams. The time variable ET demand used in hypothetical models 10 and 11 was generated as an approximation of daily ET averages from the data of Korchendorfer and Paw U (2004), (Fig. 2.4).

ET was simulated by removing water from all model cells within the assumed root zone of the riparian vegetation at a rate according to a supply-dependent root-water-uptake function. Coincident with the footprint of the perching layer, the root zone was assumed to extend 1000 m along the stream axis, 300 m laterally away from the stream, and to a depth of 4 m below the streambank, consistent with maximum root depths reported in other studies (Busch et al., 1992; Snyder et al., 1998). We used the root-water-uptake model developed by Van Genuchten and Hoffman (1984) in which the uptake is calculated in terms of sediment capillary pressure:

$$\frac{T(h)}{T_p} = \frac{1}{1 + (h / h_{0.5})^p}, \tag{1}$$

where $T(h)$ is the root uptake rate at the capillary pressure head h, T_p is the potential root uptake rate, $h_{0.5}$ is the is the value of h where the root uptake is half the potential rate, and p is an empirical parameter.

TOUGH2 (Pruess et al., 1999) in its available form does not simulate root-water uptake. The code was therefore modified to implement a root-uptake model as a function of capillary pressure (eq. 1). Excerpts of the TOUGH2 code where modifications were made are included in Appendix E. The root-uptake function was fully coupled to TOUGH2 such that the root-uptake model was implemented into the system of nonlinear equations solved by TOUGH2.

Van Genuchten and Hoffman (1984) and Van Genuchten, (1987) applied eq. 1 in a modeling study and attained good fits to data for a variety of agricultural crops with a value of p=3. Values of $h_{0.5}$ vary based on plant type and can be estimated from data provided by Feddes and Raats (2004) for many crops. Parameters used in the root-uptake function for phreatophytes were p=3 and $h_{0.5}$ = -1.0 kPa, resulting in a root-uptake curve that drops off sharply as the sediment drains below saturation, representative of phreatophyte vegetation.

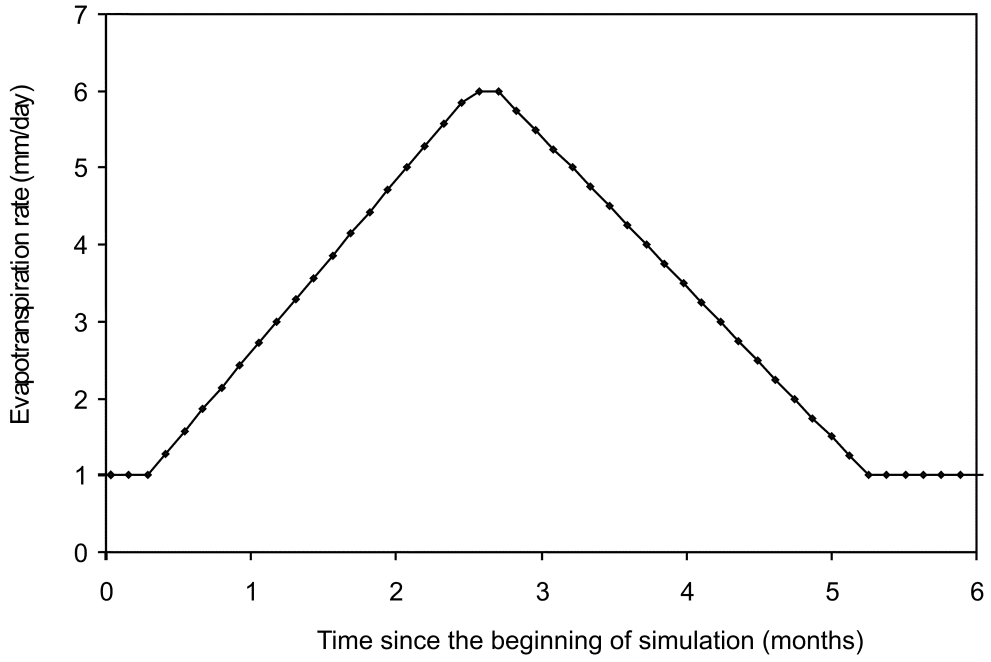

Figure 2.4: Time varying evapotranspiration rate used to simulate root-water uptake. ET rates are based on a study that used an energy-balance method above willow tree canopies along the Cosumnes River, CA (J. Korchendorfer and K. T. Paw U, written commun., 2004).

Table 2.1: Descriptions of hypothetical models used to evaluate perched groundwater conditions.

Model	Coarse sediment K (md^{-1})	Perching unit K (md^{-1})	Ratio of hydraulic conductivity (coarse sediment K divided by perching unit K)	Depth of perching unit below streambed (m)	Perching unit width (m)	Perching unit thickness (m)	Perching unit length (m)
1	0.83	$5.0x10^{-6}$	$2x10^{5}$	4.5	600	2	1000
2	5.81	$5.0x10^{-6}$	$1x10^{6}$	4.5	600	2	1000
3	0.083	$5.0x10^{-6}$	$2x10^{4}$	4.5	600	2	1000
4	0.83	$8.3x10^{-3}$	$1x10^{2}$	4.5	600	2	1000
5	0. 83	$5.0x10^{-4}$	$2x10^{3}$	4.5	600	2	1000
6	0. 83	$5.0x10^{-4}$	$2x10^{3}$	4.5	200	2	1000
7	0. 83	$5.0x10^{-4}$	$2x10^{3}$	4.5	600	2	500
8	0. 83	$5.0x10^{-4}$	$2x10^{3}$	2.5	600	2	1000
9	0. 83	$5.0x10^{-4}$	$2x10^{3}$	5.5	600	2	1000
10[1]	0. 83	$5.0x10^{-6}$	$2x10^{5}$	4.5	600	2	1000
11[1]	5.81	$5.0x10^{-6}$	$1x10^{6}$	4.5	600	2	1000

[1]Root-water uptake was included in these simulations.

2.4. RESULTS AND DISCUSSION

2.4.1. Comparison of 2-D and 3-D models

The effects of spatial dimension of the model results are analyzed by comparing the amount of groundwater flowing into the stream per unit area of streambed at three points located at different locations along the stream with respect to the edge of the perching layer (Fig. 2.5). A 2-D simulation was made that consisted of a cross-section of the 3-D model domain perpendicular to the stream axis (Fig. 2.5). The physical and hydraulic parameters used in this analysis are represented as scenario 1 (Table 2.1). Comparison among the 2-D and 3-D model results show that the 2-D model significantly over predicts the amount of baseflow contributed by perched groundwater. This result emphasizes the 3-D aspect of stream/perched system arising from the finite area of the perching unit, which causes more flow away from the stream and enhances vertical seepage around the

edges of the perching unit. The 2-D case would be suitable for perching layers that extend great distances parallel to the stream.

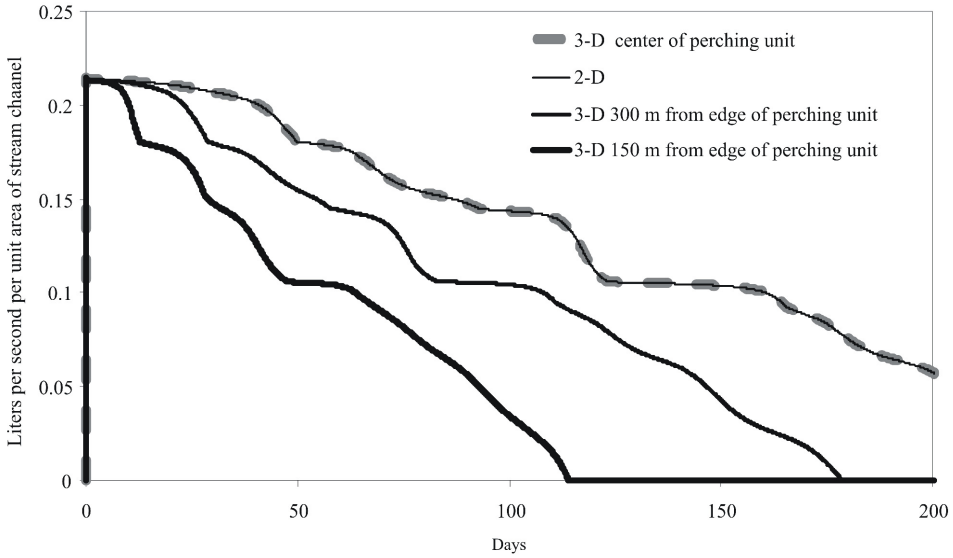

Figure 2.5: Difference between the 2-D and 3-D representation of the perched groundwater. Notice that the 2-D solution and the 3-D solution at the center of the perching unit lie on top of each other. Hydraulic properties and model dimensions are shown as scenario 1 in Table 2.1.

2.4.2. Effects of K

Four simulations were run to evaluate the influence of the coarse sediment K on perched groundwater discharge to the stream. Scenarios 1 and 2 had coarse sediment K values of 0.83 md^{-1} and 5.81 md^{-1}, respectively, and both had a perching unit 4.5 m beneath the streambed surface and with a K of $5.0x10^{-6}$ md^{-1}. A factor of 7 increase in coarse sediment K caused simulated groundwater discharge to the stream to increase by a factor of 9. The average perched groundwater discharge over the length of the stream immediately following the high-flow season was 7.6 l/s (0.27 ft^3/s) and 52 l/s (1.8 ft^3/s) for scenarios 1 and 2, respectively (Fig. 2.6).

Maximum perched groundwater discharges for scenarios 1 and 2 are consistent with measured regional groundwater discharge values reported by Conlon et al. (2003) and

Constantz et al. (2004) for two streams that are hydraulically connected to regional (non-perched) groundwater (Table 2.2). Coarse sediment K values used in scenarios 1 and 2 are also consistent with those reported in these studies. However, simulated perched groundwater discharge rates subsided to 4.9 l/s (0.17 ft^3/s) and 3.0 l/s (0.10 ft^3/s) for scenarios 1 and 2, respectively, after three months, whereas streams sustained by regional groundwater likely maintain more constant baseflow.

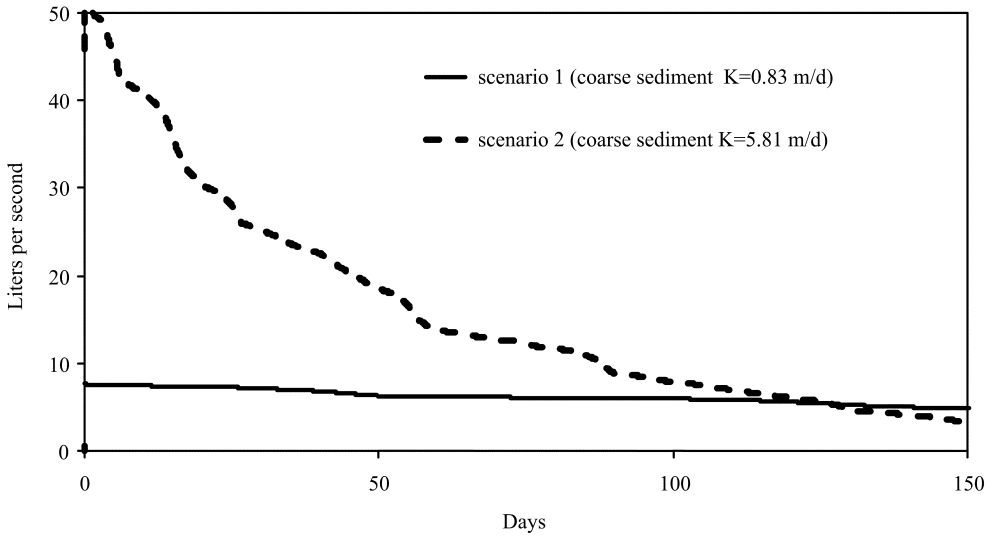

Figure 2.6: Comparison of perched groundwater discharge to stream for a medium K coarse sediment (scenario 1) and a high K coarse sediment (scenario 2).

Table 2.2: Comparisons of simulated perched groundwater discharge rates to measured discharge rates in streams sustained by regional groundwater. Groundwater discharge values were measured in all these studies by differencing streamflow at measurement points along the channels.

Location	Gain rate over 2000 m length of channel (l/s)	Sediment description	K (md^{-1}) of sediment surrounding stream	Average stream width (m)	Average flow (m^3s^{-1})
Butte Creek (Or.)[1]	5.4	Silt	0.04	~8	1.65
Cold Creek (Ca.)[2]	40	Sand	6-18	3.5	0.22
Trout Creek (Ca.)[3]	21-50	Sand	Not reported	~7.5	0.45
Upper Truckee River (Ca.)[3]	14-39	Sand	Not reported	~9	0.33
Santa Clara River (Ca.)[4,5]	33.1-52.6	Sand	36-72	~5	0.86
Scenario 1	7.5[6]	--	0.83	15	--
Scenario 2	52[6]	--	5.81	15	--

[1]Conlon et al. (2003); [2]Prudic et al. (2005); [3]Rowe and Allander (2000); [4]Constantz et al. (2004); [5]Cox et al., (2003), [6]Maximum simulated values after streamflow subsided.

Scenario 3 had the same perching unit K ($5.0x10^{-6}$ m/d) but a lower coarse sediment K than Scenario 1 by a factor of 10 (0.083 md^{-1}). Perched groundwater discharge averaged over the length of the stream was initially 3.7 l/s (0.13 ft^3/s), which is much lower than scenarios 1 and 2. However, perched groundwater discharge declined at a much slower rate for scenario 3 and is greater than scenario 2 after about 150 days (Fig. 2.7). This is an indication that the limited extent of the perching unit has less of an effect on longevity of discharge to the stream when the coarse sediment K is lower. For a fall salmon run in systems like the Cosumnes River, groundwater discharge may be most critical to systems like the Cosumnes later in the dry season (late spring and fall).

Consequently, a lower coarse sediment K may be more suitable for providing baseflow several months after runoff has ceased.

Scenario 4 is similar to scenario 1 but with a much higher perching unit K, such that the ratio of coarse sediment K to perching unit K was decreased from 20,000 to 100. Perched groundwater discharge to the stream for scenario 4 is only 2.0 l/s (0.07 ft^3/s) initially, and declines to zero after 11 days. Thus, the ratio of coarse sediment K to perching-unit K must be greater than 100 for there to be a significant contribution of perched groundwater discharge to the stream for longer than a few weeks.

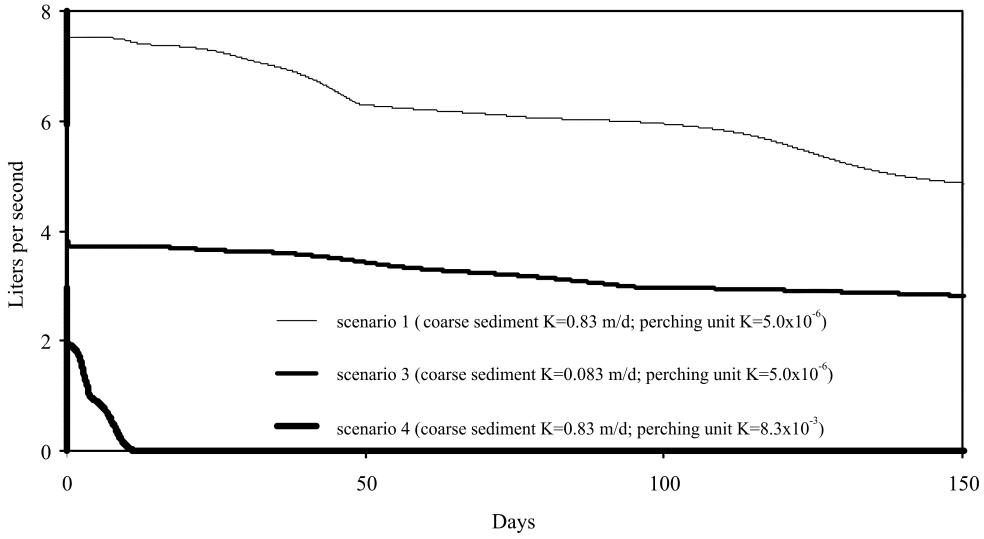

Figure 2.7: Perched groundwater discharge for coarse sediment with a low K (scenario 3), and for fine sediment with a high K (scenario 4). Scenario 1 is included for comparison.

2.4.3. Lateral extent of perching unit

Although groundwater discharge decreased at a greater rate when the perching-layer K was equal to $5x10^{-4}$ md^{-1} (scenarios 5-9) as compared to $5x10^{-6}$ md^{-1} (scenarios 1 and 2), the higher value may be more representative of the average K of a perching layer that contains some coarser sediment. Thus, simulations evaluating the lateral extent

(continuity) and thickness of the perching unit (scenarios 5-9) had a perching-layer K of $5x10^{-4}$ md^{-1}, about 1.5 orders of magnitude greater than the clay samples analyzed by Johnson et al. (1968).

Scenarios 5, 6 and 7 were used to evaluate the effect of the length and width of the perching unit beneath the stream. Scenario 5 had a perching unit length (parallel to the stream axis) of 2000 m and a width (perpendicular to the stream axis) of 1200 m. The width of the perching unit was reduced from 1200 m to 400 m in scenario 6 as compared to scenario 5. The large reduction in the perching unit width had a very small impact on groundwater discharge to the stream with a maximum difference of only 0.2 l/s (0.007 ft^3/s), (Fig. 2.8). This is because the perched system did not extend beyond 350 m away from the stream in these simulations (Appendix A). However, when the perching unit length was reduced in scenario 7 from 2000 m to 1000 m, there was a significant reduction in groundwater discharge to the stream (Fig. 2.8). These results suggest that the length of the perching unit along the stream axis is much more important than the width of the perching unit for controlling perched groundwater discharge.

The sudden changes in the discharge rates shown in Figure 2.8 is caused by the draining of cells representing the streambed and banks (seepage faces). When the total potential in a cell converts from being positive to negative due to drainage, the area contributing discharge to the stream is suddenly reduced. Thus, these changes are a model artifact caused by the spatial discretization of the streambed.

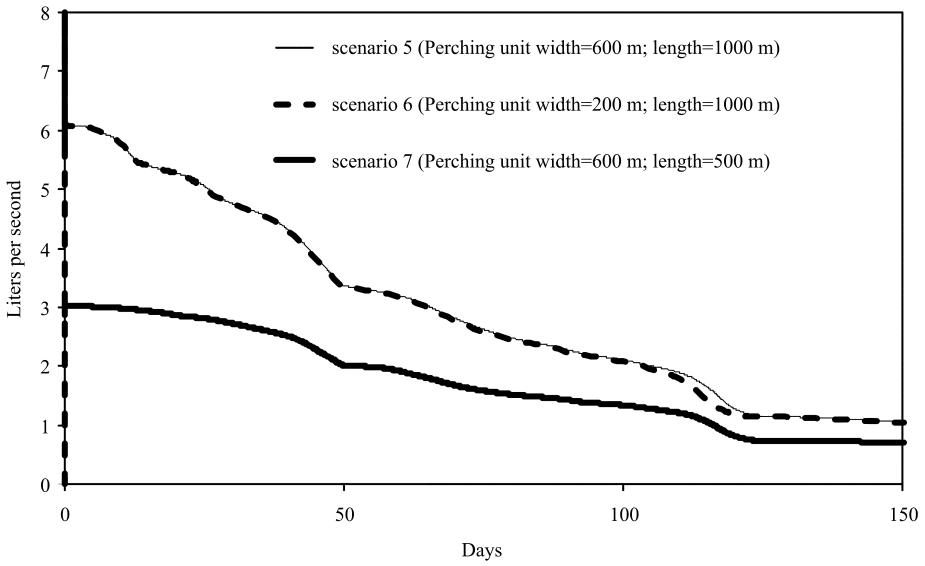

Figure 2.8: The effects of perching unit dimensions on perched groundwater discharge: the perching unit in scenario 6 extends 1/3 the distance away from the stream as compared to scenarios 5 and 7; and the perching unit in scenario 7 extends half the distance along the stream's axis as compared to scenarios 5 and 6.

2.4.4. Depth to the perching unit beneath the stream

Scenarios 8 and 9 were used to evaluate the effect of changes in the depth to the perching unit below the streambed. Increased perched groundwater storage due to a deeper perching unit, increased the maximum discharge to the stream by as much as 2 l/s (0.07 ft^3/s). However, after about 50 days, discharge to the stream was within 0.50 l/s (0.018 ft^3/s) for perching unit depths of 2.5, 4.5 and 5.5 m below the streambed (Fig. 2.9).

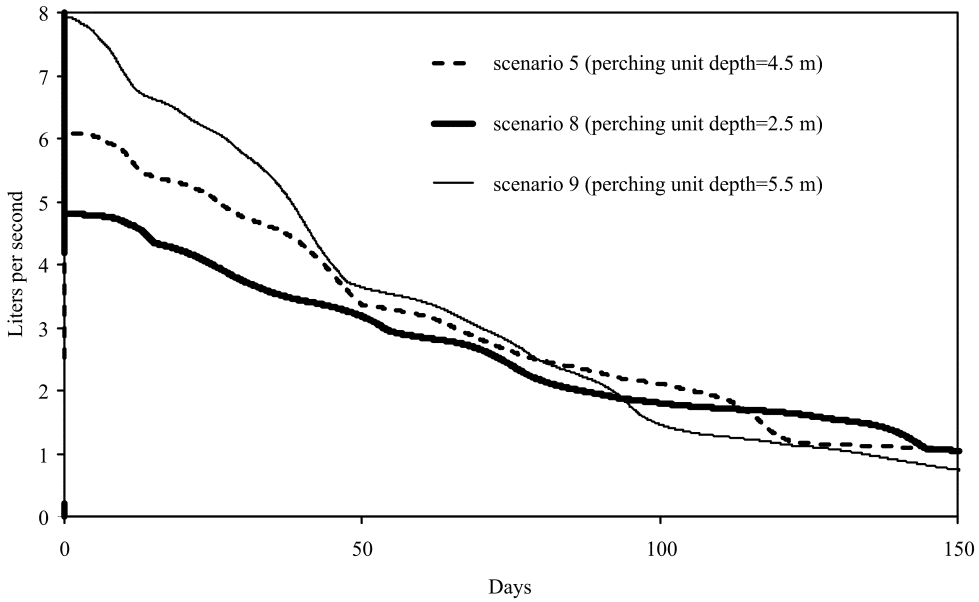

Figure 2.9: The effects of perching unit depth beneath the streambed on groundwater discharge. Perching unit depths were 4.5, 2.5, 5.5 m for scenarios 5, 8 and 9, respectively.

2.4.5. Other aspects of perched systems

This work considers the affects of perched systems on streams by examining the amount of baseflow that could be provided by perched systems. However, if a perched system does not produce appreciable baseflow to a stream, it still may benefit the stream by reducing downward seepage. In losing streams, perched systems can reduce the downward vertical hydraulic gradient, and the velocity of the stream can cause water to flow horizontally through the streambed. This phenomenon can enhance surface-water/perched-groundwater interaction (hyporheic flow), which can be extremely important for aerating fish spawning habitat and for biochemical cycling of nutrients between a stream and perched groundwater. Perched groundwater can support benthos ecosystems that would not be present beneath a stream without the influence of perched groundwater. In this case, the perched system benefits the stream indirectly by supporting benthos habitat, which directly benefits the stream.

2.4.6. Evapotranspiration

ET was simulated along the stream centered above the perching unit in order to determine if baseflow would be depleted significantly by riparian vegetation. The original models (scenarios 1-9) consisted of a stream bank that was 4 m above the stream thalweg, which represents a fairly incised stream and is typical of certain reaches of the Cosumnes River as well as other rivers in the Central Valley, California. Consequently, perched groundwater drained into the stream and the water table elevation was at or below the root zone over much of the riparian area. However, the maximum depth that tree roots can extend to find groundwater is unknown and further investigation into the maximum rooting depth for riparian plants is warranted. Young trees likely require shallow water tables and so a maximum rooting depth was limited to 4 m. For this reason, the stream-bank height above the stream thalweg in scenarios 11 and 12 were decreased to 2 m. In all other aspects besides the height of the stream bank, scenarios 11 and 12 were the same as scenario 1 and 2, respectively.

ET losses decreased perched groundwater discharge by a maximum rate of 1.4 l/s (0.05 ft^3/s) and 3.9 l/s (0.14 ft^3/s) in model scenarios 1 and 2, respectively (Fig. 2.10 and 2.11). The decrease in perched groundwater discharge for scenario 11 is equal to 12% of the total discharge over the simulation period; however, ET reduced discharge to the stream by 30% at the end of the simulation period when discharge rates were the lowest. We expected ET to reduce discharge to the stream by a larger amount for scenario 1 as compared to scenario 2 because of a lower K of the coarse sediment; however, the opposite condition occurred. This is due to the relatively large amount of water going into

perched system storage during the wet-up phase resulting because of a larger K of the coarse sediment providing more water for uptake by plants in scenario 12.

ET losses accentuated the changes in slope of the perched groundwater discharge to the stream caused by the discretization of the streambank because, unlike the previous simulations, pressure was reduced in all the seepage-face cells simultaneously due to ET (fig. 2.10).

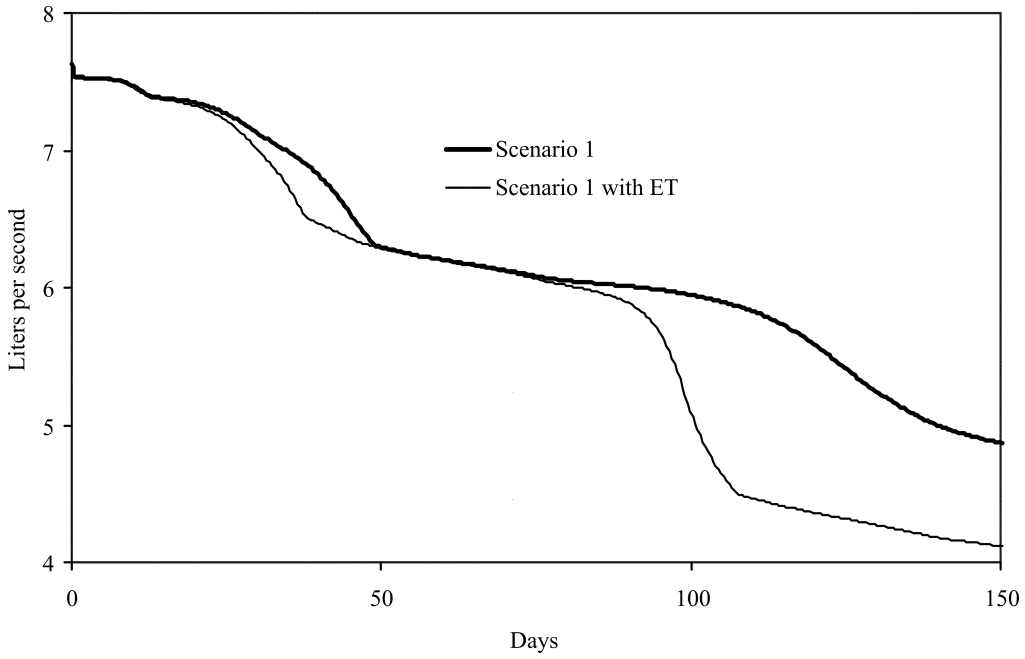

Figure 2.10: The effects of ET on perched-groundwater discharge to a stream. The coarse sediment K was 0.83 m/d and streambank was 2-m tall. The time variable ET rate was applied according to Figure 5.

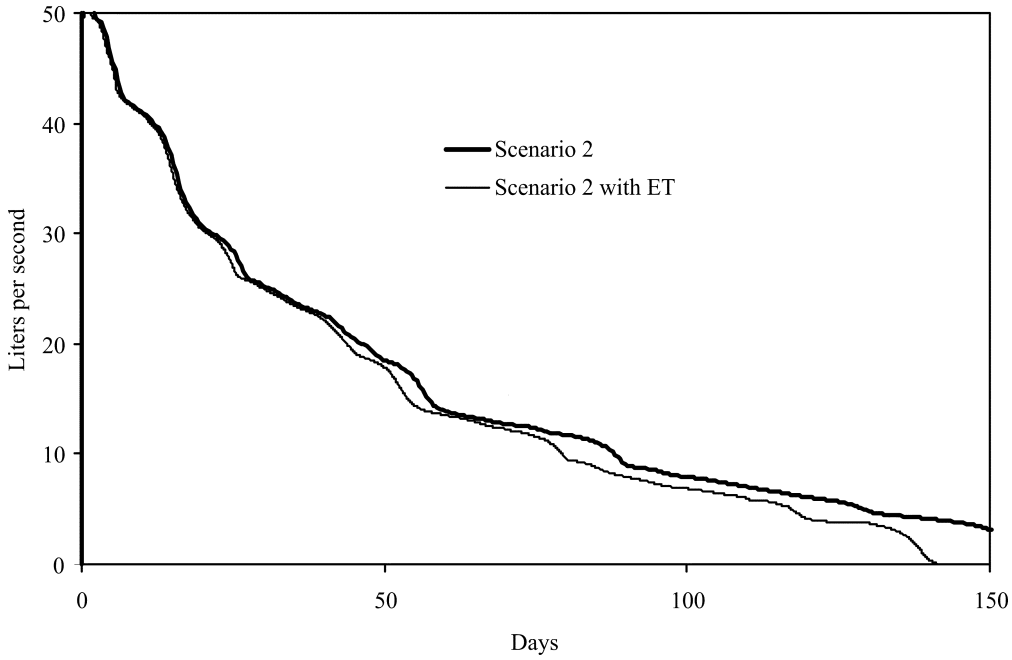

Figure 2.11: The effects of ET on perched-groundwater discharge to a stream for a high-K coarse sediment and a 2 m tall streambank. The time variable ET rate was applied according to Figure 5.

2.4.7. Model limitations and transferability

Although the present work attempts to evaluate the basic interplay among streams perched systems, we only address a few of the possible variations in stream/perched systems that may be found in nature. For example, we did not examine the effects of unsaturated flow parameters and we did not evaluate many geometric configurations of stream/perched systems such as the effects of stream-channel morphology (e.g. meandering, ripple-pool sequences) or sloped perching unit configurations.

We did not determine perched system discharge to be sensitive to the lateral extent of the perching unit perpendicular to the stream profile; however, based on the maximum lateral extent of the perched water tables (Appendix A), which was close to 350 m, perching units that are shorter than this width would likely decrease perched groundwater

discharge to a stream. Thus, more analysis is warranted with regards to small or discontinuous perching units. Another issue that was not thoroughly addressed was how climate and the resulting precipitation, recharge, and streamflow variations affect perched systems. Perched groundwater storage that persists throughout the dry season would likely increase perched groundwater storage and discharge to the stream following the wet season. We leave these analysis for future work, which may be more easily done following the development of analytical or semi-analytical solutions for stream/perched system interaction.

The model results presented herein exhibit step-like features in the simulated groundwater discharge curves. These features were caused by the spatial discretization of the cells representing the streambed and bank. The decline of the seepage-face area was approximated by the area of streambed cells that had a pressure greater than zero. Thus, when the pressure of a streambed cell decreased below zero, the area of the seepage face surrounding the stream dropped abruptly causing the seepage to the stream to drop abruptly. This artifact could be eliminated by decreasing the seepage face area contributed by a streambed cell as the pressure in the streambed cell decreases.

The analysis presented herein required 3-7 hours on a Xeon 3.2 GHz, 2.6 GB RAM computer to run each simulation because of model complexities, including 3-D geometry, both large positive and negative (capillary) pressures, and seepage faces. Despite the aforementioned limitations, this work demonstrates that perched systems can be viable contributors of baseflow to streams and that they can enhance surface-water/groundwater interaction for conditions that are somewhat typical of streams traversing alluvial depositional environments. Thus, this work provides an impetus for future theoretical

work on stream/perched systems. Another result of this work is that is shows that perched systems, which are vadose-zone features, may play a vital role in ecosystem functioning by providing saturated conditions surrounding surface-water bodies.

Competition among lotic (stream) and riparian ecosystems was addressed to a limited extent by simulating the effect maximum ET rates would have on perched-groundwater discharge to the stream. The simulations showed that perched groundwater did not support riparian vegetation beyond the immediate stream-bank area when the stream bank was as tall as the assumed maximum root depth. Thus, the roots of riparian vegetation must be able to extend below the elevation of the stream thalweg to uptake water from perched systems as simulated in this work. When the roots do extend beneath the stream thalweg, maximum ET rates by riparian vegetation diminished perched groundwater discharge to the stream by 30%.

2.4.8. Implications for vadose-zone management of stream systems

Historically, groundwater research has been focused on the analysis of aquifers that could be exploited for water supply. Perched systems are usually irrelevant to groundwater supply and consequently, have been virtually ignored by the scientific community. Thus, previous management and restoration of stream baseflow may have overemphasized regional groundwater. We begin to address this gap in groundwater research by simulating stream/perched system interaction. This work shows that streams may benefit if management and restoration efforts include the vadose zone where regional groundwater levels do not contribute to the saturated region surrounding streams. Although this work is focused on perched systems beneath streams, perched systems may also play a vital role in other ecosystems such as wetlands and floodplains.

Surface-water bodies and floodplains that are supported by perched groundwater could theoretically be managed by recognizing where conditions are suitable for perching and by maximizing recharge to perched groundwater at appropriate times. Perched systems near streams could be recharged by either diverting water from another source into the stream during the low-flow season, or by irrigating the land above the perched system. However, irrigation water could affect the water quality of perched groundwater. Another implication of this work is that the size of the stream bank can affect the amount of water available to riparian vegetation. This result has implications regarding the management and restoration of these systems since tall stream banks possibly caused by constructed levees or changes in stream discharge conditions can limit the growth of riparian vegetation and limit the competition for water among lotic and riparian ecosystems.

2.5. SUMMARY AND CONCLUSIONS

Simulations of river seepage with the presence of a low-K sediment layer resulted in a perched groundwater beneath the stream over a range in sediment K values. Perched groundwater discharged back into the stream for longer than 5 months after flow in the stream receded. Discharge rates were proportional to coarse sediment K when the ratio of coarse sediment K to perching unit K exceeded 2000. However, more work is required to further examine values of this ratio less than 2000 to refine a minimum cutoff that leads to significant perched groundwater discharge. Perched groundwater discharge rates to the hypothetical stream analyzed in this study were similar in magnitude to regional groundwater discharge rates reported for streams with similar coarse sediment K values. However, these rates receded by as much as 20% after 4 months. Nonetheless, rates of

downward seepage beneath the stream were minimized or reversed throughout the dry season, thereby allowing horizontal seepage to occur. This phenomenon can be important for supporting hyporheic and benthos habitat, aerating sediment used for fish spawning, and for biochemical cycling of nutrients.

The perched groundwater discharge rate to the stream varied by as much 60% when the depth the perching unit varied from 2.5 m to 5.5 m below the streambed surface. However, the rate became similar for all perching unit depths after 1.5 months. Discharge rates were much less sensitive to the width of the perching unit perpendicular to the stream axis as compared to the length of the perching unit parallel to the stream axis. The width of the perching unit was decreased from 1200 m to 400 m, which resulted in a negligible decrease in discharge. However, a halving of the length of the perching unit decreased the discharge rate by about 50%. A root-water-uptake function was included in the model to consider ET losses in the estimates of baseflow contribution by perched systems. ET losses reduced the perched groundwater discharge rate by as much as 30% where vegetation was dense and the roots of riparian vegetation extended below the elevation of the stream thalweg.

The present chapter analyzed perched-groundwater and surface water interaction based on hypothetical representation of systems that consisted of a coarse sediment unit and a fine-grained perching unit. These models used average hydraulic parameters to represent two facies types, whereas, in nature these units are usually not homogeneous. Despite these assumptions, Chapter 2 provided a proof of concept that a perched system can act as a surrogate for a regional aquifer by providing baseflow and enhancing groundwater and surface-water interaction.

Chapter 3 analyzes perched groundwater in a real system by taking a more detailed approach to represent sediment heterogeneity using an integrated geostatistical approach. The geostatistical approach relies on measurable data and subjective geologic information collected from the field site that describe lithologic patterns and proportions of different sediment types collected from the Cosumnes River, California. As will be described, sediment texture affects the ability for riparian vegetation to uptake water and incorporating a more detailed representation of sediment heterogeneity allows us to simulate ET more realistically. Chapter 3 addresses the question of whether perched systems can drastically affect the water budget and water cycling surrounding a river by increasing the amount of ET by riparian vegetation.

2.6. REFERENCES

Betson, R.P., Marius, J.B., and Joyce, R.T., 1968, Detection of saturated interflows in soils with piezometers, Proc. Soil. Sci Soc. Am., 32, p. 602-610.

Bretschko, G., W.E. Klemens, (1986), Quantitative methods and aspects in the study of the interstitial fauna of running water, Stygologia, 2, p. 297-316.

Brunke, M. & Gonser ,T. (1997): The ecological significance of exchange processes between streams and groundwater. Freshwater Biology. 37, 1-33

Busch, D.E., N.L. Ingraham, and S.D. Smith, (1992), Water uptake in woody riparian phreatophytes of the southwestern United States: a stable isotope study. Ecological Applications , 2, 450-459.

Constantz, Jim, Cox, H.C., Sarma, Lisa, and Mandez, Greg (2003), The Santa Clara River—the last natural river of Los Angeles, in Heat as a Tool for Studying the Movement of Ground Water Near Streams, edited by D. A. Stonestrom and J. Constantz, U.S. Geol. Surv. Circ., 1260, 81–89.

Cox, M. H., Mendez, G. O., Kratzer, C. R., and Reichard, E. G. (2003), Evaluation of Tracer Tests Completed in 1999 and 2000 on the Upper Santa Clara River, Los Angeles and Ventura Counties, California, U.S. Geological Survey Water-Resources Investigations Report 03-4277.

Croft, M.G. (1999), Subsurface geology of the late tertiary and quaternary water-bearing deposits of the southern part of the San Joaquin Valley, California, U.S. Geol. Survey Water-Supply Paper 1999-H, 29 p.

Danielopol D., P. and Marmonier, P. (1992), Aspects of research on ground water along the Rhone, Rhine and Danube, Regulated Streams, 7, 5-16.

Fleckenstein, J.H., Niswonger, R.G., and Fogg, G.E. (2005), Stream-Aquifer Interactions, Geologic Heterogeneity, and Low Flow Management, GROUNDWATER, Special issue from conference: MODFLOW and More 2003: Understanding through Modeling, Golden, CO.

Hathaway, D.L., Ha, T.S., and Hobson, A. (2002), Transient Riparian Aquifer and Stream Exchanges along the San Joaquin Stream. In Proceedings of the Ground Water/Surface Water Interactions, AWRA 2002 Summer Specialty Conference, July 1-3, 2002, Colorado, 169-174.

Johnson, A.I., Moston, R.P., and Morris, D.A. (1968), Physical and hydrologic properties of water-bearing deposits in sibsiding areas in Central California, U.S.Geol. Survey Prof. Paper 497-A, 71 p.

Khan, M.Y., D. Kirkham, R.L. Handy (1976), Shapes of steady state perched groundwater mounds, Water Resour. Res. Vol. 12 no. 3.

Krumbein, W.C. and L.L. Sloss (1963), Stratigraphy and Sedimentation, (2d ed.) San Francisco, W.H. Freeman and Company, 660 p.

McDonald, M.G., and Harbaugh A.W. (1988), A modular three-dimensional finite-difference ground-water flow model: U.S. Geological Survey Open-File Techniques of Water-Resources Investigations, Book 6, Chapter A1, 586 pp.

Miall, A. D. (1996), The geology of fluvial deposits: sedimentary facies, basin analysis, and petroleum geology, Springer Verlag, Berlin.

Minasny, B., J. W. Hopmans, T. Harter, S. O. Eching, A. Tuli, and M. A. Denton, (2004) Neural networks prediction of soil hydraulic functions for alluvial soils using multistep outflow data, Soil Sci. Soc. Am. J. 68:417–429.

Mualem, Y. (1976) A new model for predicting the hydraulic conductivity of unsaturated porous media: Water Resources Research, v. 12, p. 513-522.

Orr, B.R. (1999), A transient numerical simulation of perched ground-water flow at the test reactor area, Idaho National Engineering and Environmental Laboratory, Idaho, 1952-94, U.S. Geological Survey Water-Resources Investigations Report 99-4277.

Pruess, K., C. Oldenburg, G. Moridis (1999), TOUGH2 user's guide, version 2.0, Report No. LBNL 43134, Ernest Orlando Lawrence Berkeley National Laboratory, Ca, USA.

Reid, M.E. and Dreiss, S.J. (1990) Modeling the effects of unsaturated, stratified sediments on groundwater recharge from intermittent streams, Journal of Hydrology, vol. 114, p. 149-174.

Robertson, J.B. (1977), Numerical modeling of subsurface radioactive solute transport from waste-seepage ponds at the Idaho National Engineering laboratory, U.S. Geological Survey Open-File Report 76-717.

Rowe, T.G., K.K. Allander (2000), Surface and ground-water characteristics in the Upper Truckee Stream and Trout Creek watersheds, south Lake Tahoe, California and Nevada, July-December 1996, U.S. Geolgical Survey Water-Resources Investigations Report 00-4001, 39 p.

Snyder, K.A., D.G. Williams, and Gempko V.L. (1998), Water source determination for cottonwood, willow and mesquite in riparian forest stands. Pages 185-188, In Wood, E.F., A.G. Chebouni, D.C. Goodrich, D.J. Seo, and J.R. Zimmerman, technical coordinators. Proceedings from the Special Symposium on Hydrology. American Meteorological Society, Boston, Massachusetts.

Van Genuchten, M. Th. (1980) A closed form equation for predicting the hydraulic conductivity of unsaturated soils. Soil Sci Am J, 44, p. 892-898.

Van Genuchten, M.T. and Hoffman, G.J., 1984. Analysis of crop salt tolerance data. In: Shainberg, I. and Shalhevet, J. eds. Soil salinity under irrigation: processes and management. Springer, Berlin, 258-271. Ecological Studies no. 51.

Van Genuchten, M.T., 1987. A numerical model for water and solute movement in and below the root zone. USDA-ARS, US Salinity Laboratory, Streamside. Research Report no. 121.

Weissmann, G. S. & G. E. Fogg (1999), Multi-scale alluvial fan heterogeneity modeled with transition probability geostatistics in a sequence stratigraphic framework, Journal of Hydrology 226(1-2), p. 48-65

Whipkey, R.Z., 1966, Subsurface storm flow from forested slopes, Bull. Internat. Assoc. Sci. Hydrology, 10(2), p. 74-85.

Winter, T.C., J.W. Harvey, O.L. Franke, W.M. Alley, 1998, Ground water and surface water: A single Resource, U.S. Geological Survey Circular 1139, 79 p.

CHAPTER 3: SIGNIFICANCE OF SURFACE-WATER/PERCHED-GROUNDWATER INTERACTION AT THE COSUMNES RIVER, CALIFORNIA

Abstract

In order to examine the hydrologic significance of perched systems in situ, a simulation model was developed for a reach of the Cosumnes River, California where regional groundwater levels are greater than 15 m below the channel elevation. Sediment heterogeneity was incorporated into the model using an integrated geostatistical approach (Carle and Fogg, 1997; Carle et al., 1998). Model results corresponded well with measurements of sediment saturation at the Cosumnes, which indicated regions of perched groundwater that extend beneath the floodplain. Results were compared with a model with effective homogeneous properties. The comparison indicates that sediment heterogeneity significantly affects the water budget at the Cosumnes by increasing the occurrence of perched systems and evapotranspiration. The percentage of river seepage that was lost to ET increased from 32% to 65% when sediment heterogeneity was included in the model. The simulated recharge due to channel seepage over a 100 m reach of the Cosumnes during 2004 declined from 2,790 m^3 to 460 m^3 when sediment heterogeneity was included in the model. Floodplain inundation, which occurred 3 times during 2004, increased river seepage into the vadose zone by a factor of 6 as compared to normal flow conditions. Floodplain inundation is likely important for recharging perched systems that supports riparian vegetation growing on the floodplain. Because perched systems profoundly affect hydrologic processes at the Cosumnes, their management would likely benefit ecosystems at the Cosumnes. Management options to recharge perched systems include enhancing floodplain inundation by purposely breaching the levees along the river or by irrigating areas where perched groundwater is known to exist.

3.1. INTRODUCTION

Groundwater level decline has increased the occurrence of rivers that flow over vadose zones. Perched systems may form in the vadose zone when seepage is obstructed from flowing to regional groundwater by low-permeable deposits underlying permeable riverbed deposits. Because alluvial sediment is often heterogeneous, perched systems may be a common occurrence where regional groundwater does not contribute to the saturated region beneath a river. Although perched systems may be important to ecological functioning, water cycling, and the water budget near rivers, their significance has been mostly overlooked by the hydrogeologic community.

Conventional approaches for simulating groundwater/surface-water interaction calculate seepage based on linear functions of the riverbed conductance, surface-water elevation, and the groundwater level elevation (Dunlap et al., 1984; Vionnet and Maddock, 1992; Prudic and Herman, 1996). This calculation is modified slightly when the regional groundwater elevation is below the riverbed elevation by assuming a unit gradient beneath the riverbed (Prudic, 1989). This modeling approach has proven effective for many problems; however, it is not suitable to for simulating interaction between rivers and heterogeneous vadose zones. Another limitation of this approach is that the entire riverbed and adjacent floodplain must be contained within a single groundwater flow cell and there is no way for including heterogeneity within the riverbed and floodplain cross section.

Numerical models that can simulate variably-saturated flow through heterogeneous vadose zones may be useful for assessing the hydrologic significance of perched systems

and their effects on the water budget near rivers. However, it is often impractical to collect enough data to perfectly characterize the distribution of heterogeneous sediment within a particular area. Carle and Fogg (1997) suggest using an integrated geostatistical approach that relies on measurable data and subjective geologic information to create models of sediment heterogeneity that include important lithologic patterns and proportions of different sediment types. Several studies have demonstrated the use of conditional indicator simulation for creating realistic images of alluvial sediment heterogeneity as distributions of discrete hydrofacies (e.g. channel or flood plain hydrofacies; Deutsh, 2002; Carle et al. 1998; Weissmann and Fogg 1999; Ritzi et al. 1995). Although hydraulic properties of sediment can be difficult to define based on texture alone, the variability within a particular texture class or hydrofacies category tends to be much less than among different texture groups. Thus, defining heterogeneity according to distinctly different texture groups provides a means of simulating the important effects of heterogeneity on perched-groundwater/surface-water interaction. Although these geostatistical methods have been applied in several hydrogeologic studies, they have not been applied to simulate 3-D variably-saturated flow and groundwater/surface-water interaction.

Riparian vegetation may persist in areas where regional groundwater levels decline below the riparian root zone if water is provided by perched groundwater. A possibly important hydrologic significance of perched systems is that they may alleviate water stress to riparian vegetation when regional groundwater levels decline. Riparian vegetation is considered beneficial to river ecosystems because it provides habitat for river fauna, enhance nutrient cycling, reduce sediment load, and regulate stream

temperatures by providing shade (Brunke and Gonser, 1997). However, riparian vegetation may lower the water table adjacent to rivers and decrease groundwater/surface-water interaction, which would negatively impact fish and other river ecosystems (Tabacchi et al., 2000). Because riparian vegetation may affect perched groundwater storage, the feedback between water availability to riparian vegetation and perched groundwater storage must be included in models of perched-groundwater/surface water interaction.

Several studies indicate that the arrangement of alluvial deposits affects water availability to riparian plants, such as sand deposits overlaying clay beds that allow water to seep laterally from a river into the root zone (Schnabel et al., 1994; Correll et al., 1997; Cooper et al., 1999). Sediment texture may also affect the growth of riparian plants due to capillary pressure. Obligate or facultative phreatophytes may be especially sensitive to capillary pressure when they are not directly tapped into groundwater. Schaff et al. (2003) evaluated post-riparian rehabilitation projects and found that willows cuttings grew 10-15 times better in sandy sediment as compared to silt and clay soils with similar slopes and saturations. Several researchers have reported signs of water stress in willows, such as increases in osmotic pressures within a plant cortex, decreases in leaf water contents, and defoliation during moderately low sediment capillarity (Tabacchi et al., 2000; Snyder et al., 1998).

In this chapter, we simulate groundwater/surface-water interaction at the Cosumnes River, California to investigate whether perched systems may affect components of the water budget surrounding rivers. Components of the water budget that are considered in this chapter include seepage to and from the river, ET, changes in vadose zone storage,

and regional-groundwater recharge. The Cosumnes provides a useful test case for this study because regional groundwater levels are greater than 15 m below the elevation of the riverbed and field studies indicate the presence of perched groundwater near land surface that is attributed to heterogeneous alluvial deposits. This chapter examines whether typical heterogeneous alluvial deposits, such as those found at the Cosumnes and many other rivers, cause groundwater to perch in the vadose zone and significantly affect groundwater/surface-water interaction.

We present an approach for simulating perched groundwater/surface-water interaction using a 3-D variably-saturated flow model that combines automated parameter estimation with geostatistical modeling of sediment heterogeneity. The basic scientific question addressed in this chapter is whether the consideration of perched systems is important when assessing the effects of lowered groundwater levels beneath rivers, and whether perched systems may alter the water budget near rivers and enhance ET by riparian vegetation. There are two aspects of perched system hydrology that are considered: the hydrologic benefit of perched systems, which is to potentially increase the amount of baseflow to a river and enhance the growth of riparian vegetation, and the possible negative impacts caused by enhanced ET that may decrease baseflow and regional groundwater recharge. These aspects are addressed in the context of an actual river-aquifer system, the Cosumnes River, using vadose and saturated zone monitoring data that help calibrate and test the conceptual-numerical model.

3.2. FIELD-SITE DESCRIPTION

3.2.1. Geology and climate

The Cosumnes River drains the western slope of the Sierra Nevada, California and is characterized by an upstream section traversing Mesozoic bedrock and a downstream section traversing alluvial fan sediments located on the eastern side of the Central Valley. The Cosumnes watershed area is approximately 1900-km^2 with an elevation of 2,400 m above mean sea level (amsl) at its headwaters, and an elevation of less than 10 m amsl at its confluence with the Mokelumne River in the Central Valley. The Cosumnes River has no major dams along its entire course.

The study area is located in the lower section of the river where it flows beneath State Highway 99 in Sacramento County just above the McConnell stream gage (Fig. 3.1). In this area, the river is surrounded by flat and partly dissected alluvial plains in the east and alluvial plains in the west (Piper, 1939; Shlemon, 1998). The study area consists of a 125 m section of the stream and extends 165 m southwest of the stream to include an adjacent riparian forest (Fig. 3.1). The stream is somewhat incised over part of the study area, such that the streambanks are 0.5-2 m tall; however a constructed levee on the south side of the stream was breached, apparently during flooding. Beyond the breached levee, there is an extensive floodplain that is typically inundated a few times a year.

A Mediterranean-type climate exists within the Cosumnes basin with strong seasonality in rainfall. Discharge in the Cosumnes comes from snowmelt and rainfall, and about 75% of the annual precipitation occurs between November and March. During the period of July–September at this site the river is usually dry downstream of the Michigan

Bar gauging station (Fig. 3.1). During this time evapotranspiration is the highest and groundwater levels are the lowest. Groundwater levels beneath the river at the site fluctuate ~ 2 meters seasonally at a depth of about 15 meters below the elevation of the channel thalweg.

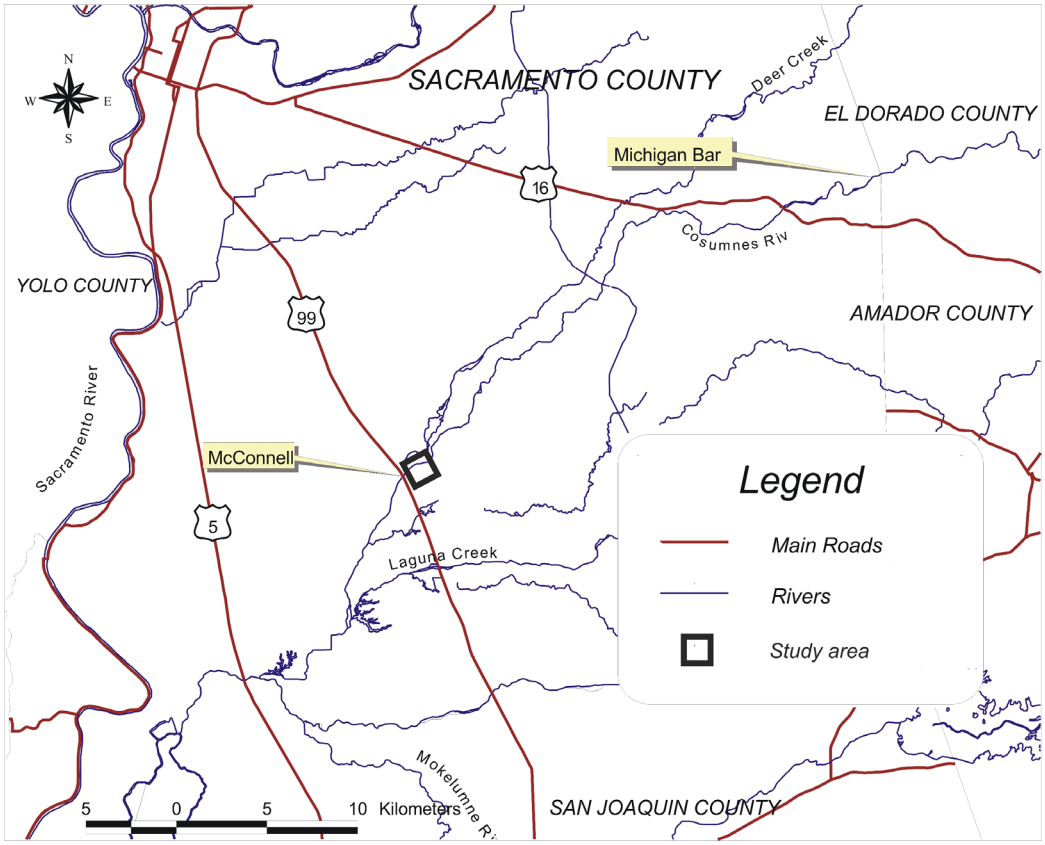

Figure 3.1: Map of the Cosumnes River, gauging stations and study area.

3.2.2. Vegetation

Stands of native riparian vegetation along the stream include mixed willow series, composed of a mixture of narrowleaf and arroyo willow, valley oak series and Fremont cottonwood series (Sawyer and Keeler-Wolf, 1995), (Fig. 3.2). While old growth stands of valley oak occur along the banks of the Cosumnes River above the junction with Deer Creek, large stands of Fremont cottonwood extend up Deer Creek and downstream of the junction with the River. The largest willow stand in the project area occurs on the

southern bank of the River directly across from the junction with Deer Creek. This stand extends into a sand splay feature and is surrounded by patches of creeping ryegrass (Leymus triticoides) grassland with oak and cottonwood regeneration (i.e. saplings) extending further out into the floodplain away from the channel. There are patches of willow and cottonwood trees in some areas between 2 and 5 m tall, indicating that these trees are actively persisting under present-day hydrologic conditions. Large stands of old growth valley oak also grow further south of the stream where agricultural activities have not cleared vegetation. In general, riparian forests grow within 50 m of the stream channel, with the exception of areas near the confluence with Deer Creek, and extended floodplain areas. All other upper historic floodplains within the project area are dominated by non-native annual grasslands or agricultural lands. Groundwater level declines have likely contributed to a reduction in the successful establishment of young riparian trees in areas where perched water tables do not occur.

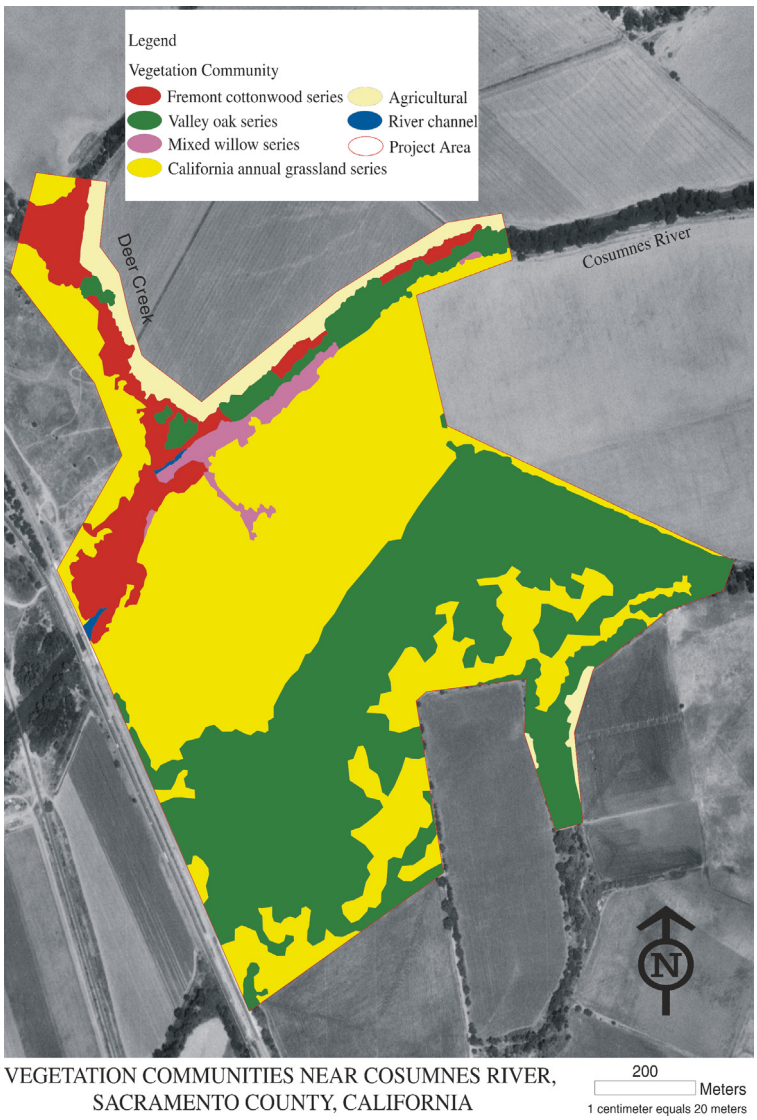

Figure 3.2: Map of vegetation at the Cosumnes within the vicinity of the study area.

3.3. METHODS

3.3.1. Data collection

Table 1 lists the types of data that was collected at the field site. These data were used to characterize the heterogeneous alluvial deposits for geostatistical modeling, to define model boundaries and to estimate the various thermal and hydraulic properties that are needed for simulating non-isothermal, variably-saturated flow.

Eighteen boreholes were auguered within the vicinity of the study area using a 3-inch diameter hand auguer to depths ranging from 6 to 11 m below the riverbed. Recovery was nearly 100% except when we intercepted coarse sand and gravel lenses and dense clay. Sediment removed from the auguer bucket was described based on texture and color and were categorized into three texture groups. Twenty-six 2.5-inch diameter 3-inch long cores were taken to represent the variability in sediment texture encountered during the auguering. These cores were sealed and brought to the laboratory for further analysis.

Sediment temperature was measured continuously in situ from December 2002 to January 2005, and sediment water content was measured continuously from January 2002 to August 2004 to aid in model calibration. Fifteen of the boreholes completed within the main channel were instrumented with thermocouple (TC) probes for measuring temperature on an hourly basis (Figure 3.3). Each TC nest consists of six TCs located at incremental depths to about 7 m below the riverbed. TCs were wired to data-loggers mounted on poles above the riverbanks.

Two boreholes were drilled, one in the riverbank and another on the floodplain, and were instrumented with eight borehole Time Domain Reflectometry probes (bTDR; Dahan et al., 2002) and eight TC probes (Figure 3.3). The bTDR and TC probes were installed at incremental depths with equal spacing to 11 m below the top of the riverbank in order to measure soil moisture and temperature on an hourly basis.

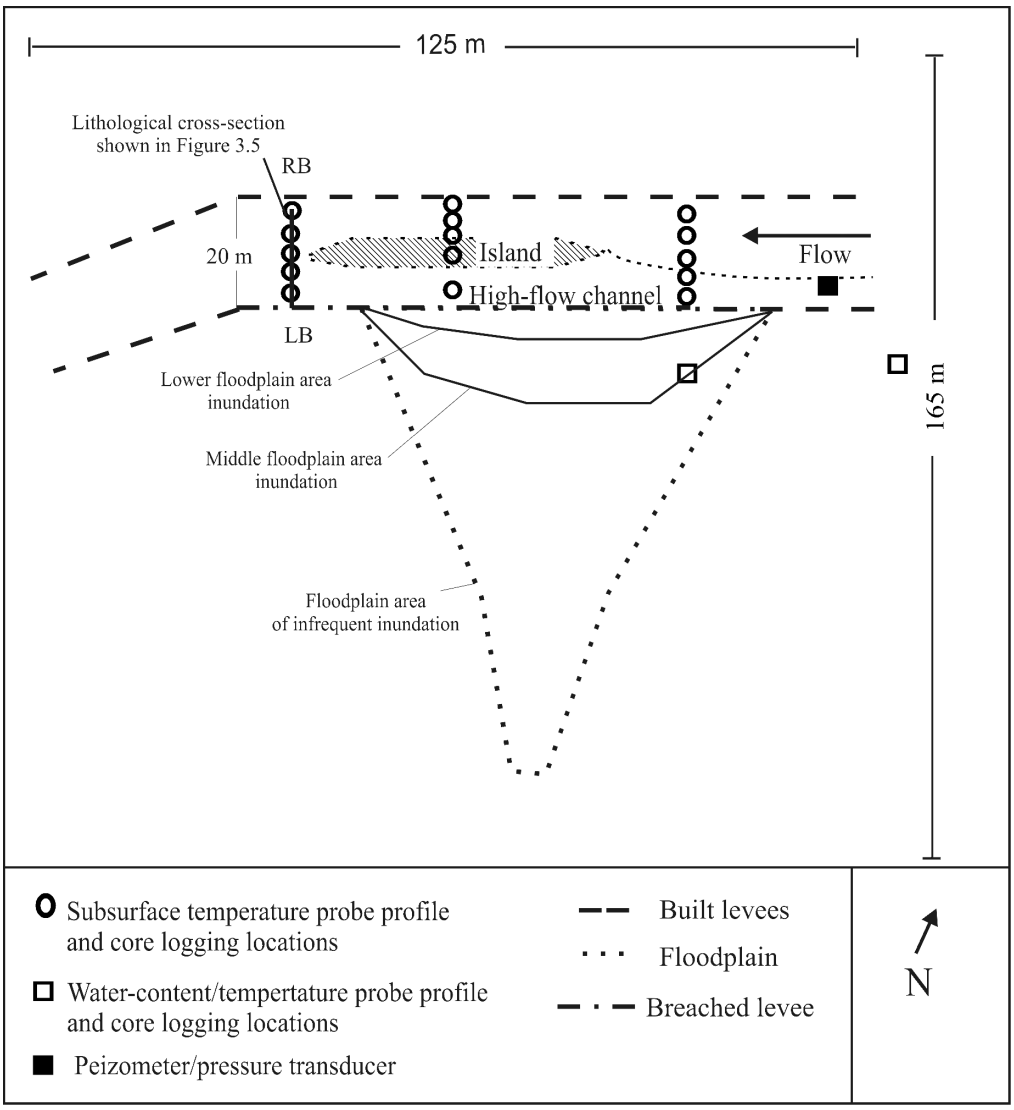

Figure 3.3: Diagram of study area showing monitoring locations, levees and floodplain area. LB and RB designate left bank and right bank, respectively, looking down channel.

Table 3.1: Hydrologic and geologic field activities at the Cosumnes River, 38° 21' 90" N, 121° 20' 28" W.

Data collection/activity	Location	Distribution	Measuring frequency
Sediment temperature	Channel and banks	17 boreholes, 7-11m depth, 5-6 probes per borehole	Hourly
Sediment water content	Banks	2 boreholes, 11m depth, 8 probes per borehole	Hourly
Regional groundwater levels	Channel	1 borehole	Hourly
Core sampling	Channel and banks	1-3 samples per borehole	26 samples
Visual texture analysis of borehole cuttings.	Channel and banks	17 boreholes, 7-11m depth	Continuous in all boreholes
Survey channel and flood plain surface elevations	Channel, banks and floodplain	15 transects	--
Survey hydrofacies outcrops	Channel and banks	Vicinity of study area	--

Physical and hydraulic properties of core samples were measured in the laboratory to characterize and help parameterize each hydrofacies for the flow modeling (Table 2). Laboratory measurements of core samples included sediment water content, bulk density, saturated hydraulic conductivity and porosity. Water content, bulk density, and porosity were measured for 12 of the 26 core-samples, 4 from each texture class, using sediment sample mass before and after oven drying and an assumed grain density of 2.65 g/cm^3 (Mason and Berry, 1968). Fractions of sand, slit and clay particles were measured for these 12 samples using a Coulter laser particle-size analyzer. Saturated hydraulic conductivity was measured on each of the 26 core samples using the falling-head method. Plots showing the falling head measurements are included in Appendix B.

Averages of the physical and hydraulic properties within each texture group were used as input data into the software NeuroMultistep for the estimation of unsaturated hydraulic conductivity and retention parameters for each hydrofacies (Minasny et al.,

2004). NeuroMultistep uses neural networks to relate physical and hydraulic properties to unsaturated flow parameters estimated based on the multi-step outflow method. Unsaturated hydraulic conductivity and retention characteristics were represented by the functions developed by Mualem (1976) and Van Genuchten (1980; Fig. 3.5).

Thermal conductivity was measured on 12 samples near saturation and near residual water content to estimate average thermal properties of each facies for input into the non-isothermal flow model (TOUGH2) (Pruess et al., 1999). Thermal properties were measured by submersing sealed sediment samples into a hot-water bath with a thermocouple imbedded into the center of the sample and measuring changes in temperature with time. The resulting temperature time series for each sample were modeled using TOUGH2, and the thermal conductivity was adjusted until the simulated and observed temperatures corresponded (Appendix C). This approach was used by Hopmans and Dane (1986) to estimate thermal conductivity of sediment with analytical equations for heat conduction through variably saturated sediment. TOUGH2 was used in the present work to avoid restrictions on sample size that are required by the analytical equation used by Hopmans and Dane (1986). The heat capacity of dry sediment was inferred based on the sample bulk density using data published by Lapham (1989) and heat capacity of saturated sediments was calculated as the volume average of the heat capacity of water and dry sediment. Linear relations were assumed for thermal conductivity and as a function of sediment saturation.

Table 3.2: Laboratory analysis on core samples taken from the Cosumnes River.

Laboratory analysis	Number of samples	Method
Bulk density	12	Sample volume divided by dry mass
Porosity	12	Based on bulk density and assumed grain density of 2.65 g/cm^3
Particle size fractions	12	Coulter brand laser particle size analyzer
Saturated hydraulic conductivity (K)	26	Falling head method
Thermal conductivity	12	Submerse sealed sample in hot-water bath, inverse solution using TOUGH2
Heat capacity	12	Inferred based on bulk density from data of Lapham (1989)

3.3.2. Measurement of Canopy transpiration

Due to inadequate fetch in the prevailing wind directions and due to heterogeneous vegetation, conventional micrometeorological techniques were not adequate for measuring transpiration from the riparian corridor surrounding the Cosumnes (J. Korchendorfer and K. T. Paw U, written communication, 2004). Consequently, a method was developed by Korchendorfer and K. T. Paw U (2004) to measure transpiration specifically for these conditions. The amount of evapotranspiration was estimated by measuring the surface temperature, net radiation, air temperature, relative humidity and ground heat flux. The energy budget of the control volume surrounding the trees was expressed as follows (Monteith, 1965):

$$R_n - G = H + LE \ , \tag{1}$$

$$H = \frac{\rho \cdot C_p}{r_h}(T_s - T_a) \ , \tag{2}$$

$$LE = \frac{\rho \cdot C_p [e_s(T_s) - e_a]}{\gamma (r_h + r_c)} \ , \tag{3}$$

where r_n is the net radiation that is positive for incoming energy (W/m^2). G is the ground heat flux that is positive into the ground (W/m^2), H is heat flux that is positive into the atmosphere (W/m^2), LE is the latent energy flux that is positive into the atmosphere (W/m^2), r_h is the aerodynamic resistance to heat transfer, assumed equal to the aerodynamic resistance to water vapor transfer and r_c is the net stomatal resistance of the canopy (s/m), T_s is an integration of leaf, trunk, and understory temperature measured with an infrared thermometer, and T_a is the air temperature, (°C), ρ is the air density (kg/m3), γ is the psychrometric constant, C_p is the specific heat of air at a constant pressure (W/kg°C), e_s and e_a are the saturation vapor pressure at the surface and the vapor pressure above the canopy, respectively (Pa).

When solving for LE as a residual in the energy budget, r_h is unknown and cannot be estimated or measured during typical daytime conditions. Consequently, Korchendorfer and K. T. Paw U (2004) solved for r_h when the atmosphere was artificially saturated with vapor using sprinklers and described r_h as a function of wind velocity and stability parameters. The estimated r_h values were used to calculate LE at ½ hour intervals during normal atmospheric conditions. This was carried out by first solving for r_h during saturated vapor conditions when stomatal resistance is assumed negligible:

$$r_h = \frac{\rho \cdot C_p}{(R_n - G)} \left\{ (T_s - T_a) + \frac{[e_s(T_s) - e_a]}{\gamma} \right\}. \quad (4)$$

A 500 gallon tank of water and a pump were placed near the tower base and a sprinkler head was installed at the top of the tower that sprays water in a 20 m radius. The instruments on the tower were covered to protect them from water while sprinkling and then uncovered immediately following spraying.

Aerodynamic resistance was estimated using nighttime data, and eliminated the possibility of condensation by using data on nights with low humidity. The stomata were assumed closed and that *LE* was assumed negligible during the night. r_h was then calculated as the only remaining unknown in the energy budget:

$$r_h = \frac{\rho \cdot C_p}{(R_n - G)}(T_s - T_a) \quad . \tag{5}$$

After estimating r_h as a function of the measured micrometeorological variables, *LE* was estimated based on equations (1-3). The measured ET based on this approach incorporated transpiration from willow tree canopies, under-story grasses and evaporation directly from land surface. We assumed the measured seasonal variation in ET was the same as the maximum ET rate for a riparian tree and under-story vegetation with no limit on supply. This is likely a good assumption because ET was measured above willow tree canopies within 15 m of main channel and because the values were greater than pan evaporation. The measured ET rates per unit canopy area were used as the ET demand in the model.

3.3.3. Supply-dependent root-uptake model

Several models of supply-dependent root uptake have been presented in the literature, and an extensive review of early works on the subject is presented by Molz (1981) and more recently by Hopmans and Bristow (2002). Most models of water uptake by roots at the macroscale are based on the incorporation of a head-dependent sink term into the governing equation for variably-saturated flow (Whisler et al., 1968; Molz and Remson, 1970). The sink term is represented by a function of root and sediment hydraulic conditions and is derived based on a description of flow over the sediment- root interface.

Macroscale models of supply-dependent root-uptake are derived by upscaling flow from a single root to a bulk mass of roots. Several studies have used these models to simulate supply-dependent root uptake with Richards' equation by adjusting empirical parameters to fit measured data such as sediment water content or capillary pressure (Feddes et al., 1974, Vrugt, et al., 2001; Zuo and Zhang, 2002; Van Genuchten and Hoffman, 1984; Van Genuchten, 1987).

Most root-water uptake models are linear functions of the hydraulic gradient among the plant and the sediment surrounding the root system (Molz, 1981). Exceptions include, the functions presented by Gardner (1991) that considers a moving uptake region that corresponds to the region of greatest sediment-water storage, and the function developed by Van Genuchten and Hoffman (1984) that assumes an s-shape response in root uptake as a function of capillary pressure. We adopted the root-uptake model developed by Van Genuchten and Hoffman (1984) in which the uptake is calculated in terms of sediment capillary pressure:

$$\frac{T(h)}{T_p} = \frac{1}{1 + (h / h_{0.5})^p}, \tag{6}$$

where $T(h)$ is the root uptake at the capillary pressure head h, T_p is the potential root uptake, $h_{0.5}$ is the is the value of h where the root uptake is half the potential rate, and p is an empirical parameter. We chose equation 6 because it provides flexibility to consider abrupt declines in root-uptake as a function of capillary pressure that is representative of phreatophyte vegetation.

Van Genuchten and Hoffman (1984) and Van Genuchten, (1987) applied equation 6 in a modeling study and attained good fits to data for a variety of agricultural plant types with a value of p=3. Values of $h_{0.5}$ vary based on plant type and can be estimated from

data provided by Feddes and Raats (2004). However, there are no such data available in the literature for estimating root uptake parameters for riparian vegetation.

There is conflicting evidence regarding whether willow and cottonwood trees can tolerate capillary suction. Busch et al. (1992) used stable isotope data to show that willows derive their water only from groundwater and not from the overlying vadose zone. However, in the study by Busch et al. (1992) groundwater was less than 4 m below land surface and there was no way of differentiating among groundwater and capillary water below 1 m. In contrast to the results of Busch et al. (1992), Snyder et al. (1998) presented evidence based on stable isotope data that cottonwood trees get water from the vadose zone after monsoon rainfall.

In general, studies of cottonwood and willow trees have shown that phreatophytes grow in nearly saturated conditions and exhibit signs of water stress during moderate droughts. This evidence suggests that phreatophytes such as willow and cottonwood trees have very little tolerance to capillary pressure and thus very low values of $h_{0.5}$ are likely representative for riparian vegetation. Requiring zero capillarity for phreatophyte uptake is likely too stringent and causes convergence problems in TOUGH2 due to a step-like sink term. Parameters used in the root-uptake function for phreatophytes were p=3 and $h_{0.5}$=-1.0 kPa, resulting in a root-uptake curve that drops off sharply as the sediment drains below saturation (Figure 3.4).

The rooting depth was set equal to 4 m for phreatophytes and equal to 0.40 m for understory vegetation. Rooting depth varies greatly depending in vegetation type and location. Busch et al. (1992) and Snyder et al. (1998) reported uptake by phreatophytes to

depths of at least 4 m. Roots that extend deeper than 4 m would indicate that the modeling presented herein is conservative.

The root-water uptake function representing pasture vegetation was applied to the top model layer only; whereas the function representing phreatophyte vegetation was applied from the second layer down to the tenth layer, which is located 4 m below land surface. Root uptake was calculated beginning with the uppermost layer, and if the demand was not satisfied, uptake was calculated for lower layers until the demand was satisfied or else the bottom of the root zone was reached. Homogeneous root distributions were assumed, which is a common assumption since root distributions vary greatly and are difficult to measure (Molz, 1981).

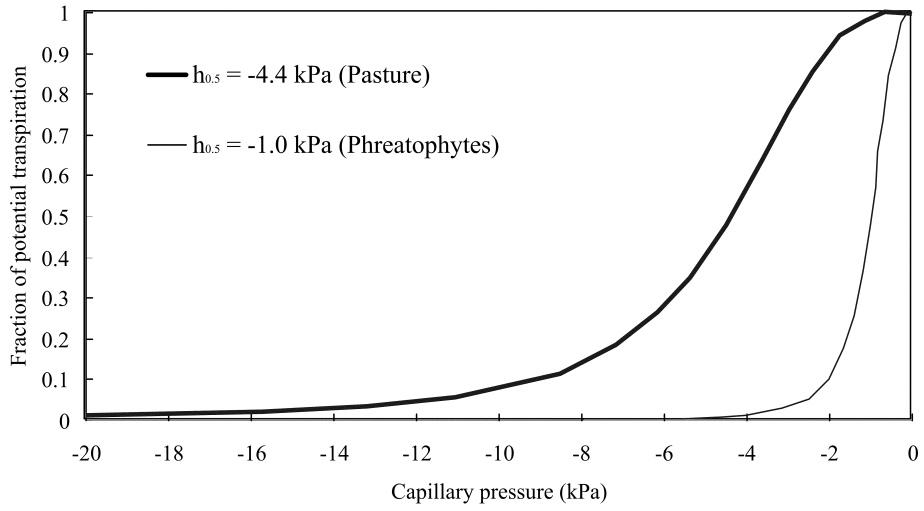

Figure 3.4: Root uptake curves used in this study as a function of capillary pressure. Curves were developed based on the function developed by Van Genuchten and Hoffman (1984) and parameter values for pasture were based on data provided by Wesseling (1991). Parameter values for phreatophytes were assumed.

3.3.4. Development of hydrofacies model

Previous studies have applied the transition probability-based geostatistical approach using TPROGS (Carle, 1999) to develop geologic models of the alluvial sediments in the central valley of California. Weissmann and Fogg (1999) studied the King's River alluvial fan and categorized hydrofacies according to 1) mud which typically represent floodplain deposits, composed predominately of silts and clays; 2) muddy sands comprised of silty and clayey sands and sandy silts and clays that characterize the transitional zone between channel and floodplain deposits; and 3) channel deposits made up of gravel and relatively clean sand. Another study by Fleckenstein et al. (2005) analyzed 230 driller's logs from the Cosumnes River basin to apply TPROGS (Carle, 1999) and categorized hydrofacies of the Pleistocene Riverbank Formation into gravel and coarse sand, sand, muddy sand and mud (silt and/or clay undifferentiated).

Core and drill cuttings collected from the our study area and descriptions by DWR (1974) show shallow sediments within our study area consist of a brown to tan assemblage of granitic sand, silt and clay and a small amount of discontinuous gravel bodies comprised of metamorphic rock fragments. The apparent lack of gravel is likely because there is not much gravel in the relatively small study area, and because gravel deposits lie at the bottom of channel deposits, too deep to be reached by our shallow drilling. Another possibility is that the position of the study area is lower on the fan such that channel deposits are mainly fine sands. Due to uncertainty in defining facies based on depositional origin as in Weissmann and Fogg (1999), we followed the approach of Fleckenstein et al. (2005) and relied on textural facies to categorize the alluvial geology for the application of TPROGS.

We observed vertical changes in the lithology on a 50 cm scale (Figure 3.5), and there were perched saturated regions in the vadose zone that were decimeter-scale in thickness and supported by thin layers of clay. Descriptions of lithology for other boreholes drilled in the study are shown in Appendix D. In order to incorporate these small-scale variations in sediment into the geostatistical model, we included much more detail in lithology as compared to Fleckenstein et al. (2005), who relied on drillers' logs.

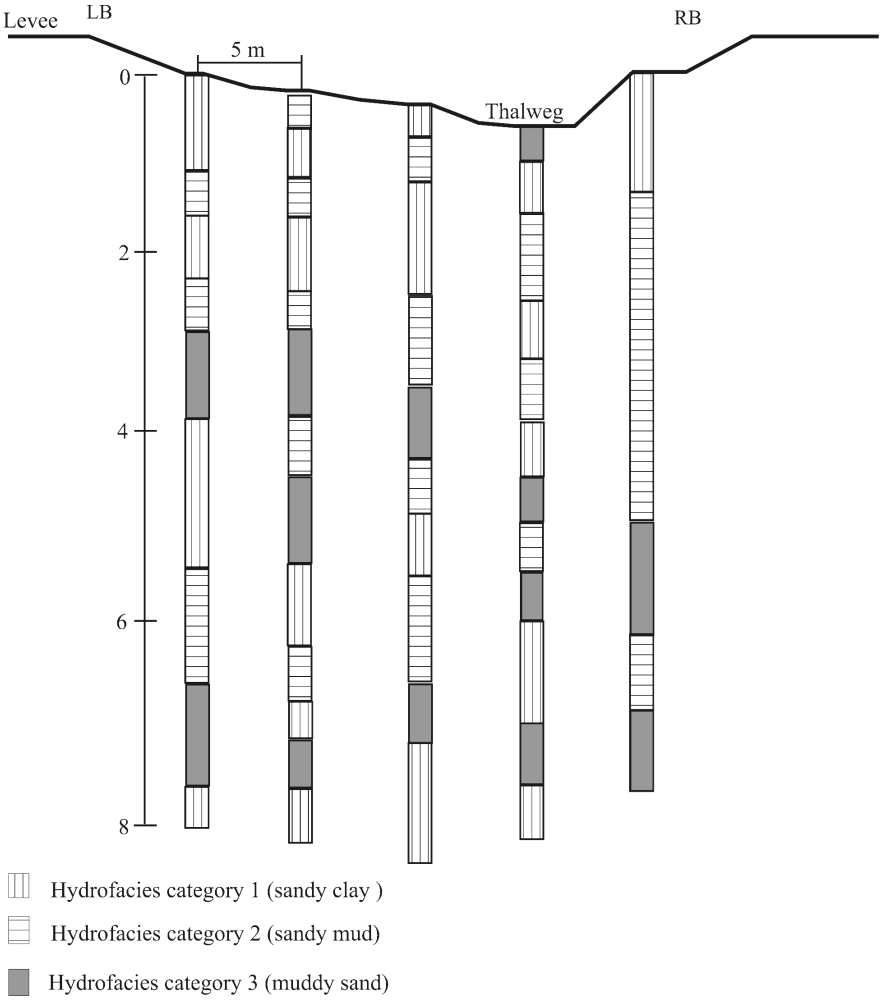

Figure 3.5: Downstream cross-section of lithology beneath the Cosumnes Riverbed. Location of cross section is shown in Figure 3.3. LB and RB designate left bank and right bank, respectively, looking down channel.

We estimated the statistical properties of the heterogeneous alluvial deposits at the Cosumnes that are required for application of TPROGS (hydrofacies mean lengths, global proportions, transition rates) based on the lithological interpretation of bore-hole cuttings and outcrops as described above. Heterogeneity in the alluvial deposits surrounding the Cosumnes River was represented based on three hydrofacies categories. Texture classification and hydraulic properties for each hydrofacies category were developed based on the previously described laboratory measurements. Hydrofacies category 1 (sandy clay) consisted predominately of green and brown clays with some sand and silt. Paleosol that covers part of the riverbed surface at the downstream end of the study site (Professor Tim Horner, Sacramento State, oral communication, 2004) was included into hydrofacies category 1. Hydrofacies category 2 (sandy mud) is a mud that represents floodplain deposits, composed predominately of silts and a small amount of sand and clay. Hydrofacies category 3 (muddy sand) consisted predominately of fine and coarse sand with some silt and clay. There was a small amount of clean sand filling some depressions in part of the channel; however, this sand appeared and disappeared after flow events and was not represented by a hydrofacies type.

We expected to sample clean sand from the subsurface based on other, regional data (Fleckenstein, 2005) and on what is known of depositional processes in fluvial environments (Krumbein and Sloss, 1963; Miall, 1996; Weissmann and Fogg, 1999). The apparent lack of clean sands in our samples could be due to the difficulty of pulling up clean sand with the hand-auguer bucket or mixing of sediment during the drilling. Another likely reason is that our small study area is in a levee (natural overbank deposit) and flood plain environment.

Our lithological data provided sufficient information to calculate vertical transition rates for the development of a vertical Markov-chain model; however, as usual, transition rates estimated for the horizontal directions were unreliable because of an insufficient number of boreholes and insufficiently small borehole spacing relative to lateral variability. Consequently, we used the approach of Carle and Fogg (1997) and developed transition probability matrices based on knowledge of the global facies proportions, estimated mean facies lengths, and facies juxtaposition tendencies.

We estimated the mean lengths for the horizontal directions based on the facies lengths in the riverbank outcrops and those exposed at land surface within the channel and on the floodplain. As described, paleosol was included within hydrofacies category 1 and was the easiest exposed hdyrofacies to discern visually. There were discernable layers of hydrofacies category 1 and 2 in riverbank outcrops upstream and downstream of the study site. These outcrops were consistent with the hydrofacies categories developed from the boreholes, such that they consistent of mixtures of sand, silt and clay. Some of the layers present in the riverbank outcrops pinched off at horizontal distances of 60-80 meters; however, in other areas the riverbank changed shape, such that the terminus of a particular stratigraphic layer could not be identified.

3.3.5. Subsurface-flow model

We used the 3-D non-isothermal multiphase subsurface flow modeling code known as TOUGH2 (Pruess, 1999) to simulate variably saturated flow surrounding the Cosumnes. The purpose of simulating heat flow was to use measured subsurface temperature data to assist in model calibration (Ronan et al., 1998; Constantz et al., 2002). TOUGH2 solves mass and energy balance equations using the method of

integrated finite differences (IFD). These equations are written in general form as (Pruess et al., 1999):

$$\frac{d}{dt}\int_{V_n} M^k dV_n = \int_{\Gamma_n} F^k \bullet n d\Gamma_n + \int_{V_n} q^k dV_n \ , \tag{7}$$

where V_n is an arbitrary volume over which the integration is taken and is specified as model input during the construction of a particular simulation. Γ_n is a closed surface that bounds V_n. The IFD method is not restricted to structured grids so that the shape of a model cell need not be rectangular. The left side of the equation is the accumulation term, where M^k represents the mass or energy per volume and *k* is a subscript that labels the mass or energy component (e.g. water and heat), where *k+1* is always the energy component for mass component *k*. F^k is mass or heat flux and is sources and sinks of a given mass or energy component. *n* is a unit normal vector on the surface element pointing inward. q^k are sources and sinks for mass component *k* integrated over the volume V_n. The mass accumulation term is:

$$M^k = \phi \sum_\beta S_\beta \rho_\beta X_\beta^k \ . \tag{8}$$

The total mass of a component is determined by summing over all fluid phases, β, ϕ is porosity, ρ_β is the density of phase β, S_β is the saturation of phase β, and X_β^k is the mass fraction of component k present in phase β. The accumulation term for heat is:

$$M^{k+1} = (1-\phi)\rho_R C_R T + \phi \sum_\beta S_\beta \rho_\beta u_\beta \ , \tag{9}$$

where ρ_R and C_R are the grain density and specific heat of the sediment, respectively. T is temperature, and u_β is the specific internal energy of phase β. Advective mass flux is a sum over all phases,

$$F^k\big|adv = \sum_\beta X_\beta^k F_\beta \ , \tag{10}$$

and the individual phase fluxes are given by a multiphase version of Darcy's law:

$$F_\beta = \rho_\beta u_\beta = -k\frac{k_{r\beta}\rho_\beta}{\mu_\beta}(\nabla P_\beta - \rho_\beta g)\,, \tag{11}$$

where u_β is the Darcy velocity (volume flux) in phase β, k is the absolute permeability, $k_{r\beta}$ is the relative permeability to phase β, μ_β is the viscosity, and P_β is the sum of the pressure of a reference phase (usually taken to be the gas phase), and the capillary pressure. g is the vector of gravitational acceleration.

The heat flux includes conductive and convective components:

$$F^{k+1} = -\lambda\nabla T + \sum_\beta h_\beta F_\beta \ , \tag{12}$$

where λ is the thermal conductivity, and h_β is the specific enthalpy in phase β. Molecular diffusion of water vapor was not considered. Equations (7-12) are solved together with the equations of state that define the thermodynamic relationships among the primary variables. The main assumption in this approach is that local thermodynamic equilibrium is achieved within a model cell so that the equations of state are applicable (Pruess et al., 1999). This assumption may be restrictive in heterogeneous systems with strong thermal gradients; however, the fine spatial discretization in our model likely alleviates inaccuracies caused by this assumption.

TOUGH2 (Pruess et al., 1999) in its available form does not simulate root-water uptake. The code was therefore modified to implement a root-uptake model as a function of capillary pressure (eq. 6). The root-uptake function was fully coupled to TOUGH2

such that the root-uptake model was implemented into the system of nonlinear equations solved by TOUGH2. Code modifications are included in Appendix E.

3.3.6. Model domain, boundary and initial conditions

The model domain consisted of a 21,500 m^2 area that extended 28 m below the highest elevation of land surface (Figure 3.8). Model cells were 4 m on each side and 0.4 m thick. The number of active cells in the model totaled 69,000. Symmetry was assumed along the thalweg of the stream so that only one side of the system was included. A boundary condition representing the water table was applied to the bottom model layer. A time-variable pressure was assigned to all model cells in the bottom layer according to the regional water table elevation as measured daily, directly beneath the stream.

The measured water surface elevations at the McConnell stage gage (Fig. 3.1) were corrected based on measurements of river depth at the upstream end of the study site and were used to represent the stream depth boundary condition in the model. Boundary conditions were applied to all river and floodplain cells at the surface of the model with an elevation lower than the time-varying river depth (Figure 3.6). The number of cells representing the river was variable in time according to the measured hydrograph of the river. The channel, floodplain and riverbank surface elevations were surveyed along transects using a laser level, and the resulting land-surface elevations were imported into the model to define the elevation of the uppermost active cells. Infiltration by precipitation was neglected in the model because measured water contents near land surface changed very little except in areas of river inundation (Fig. 3.8).

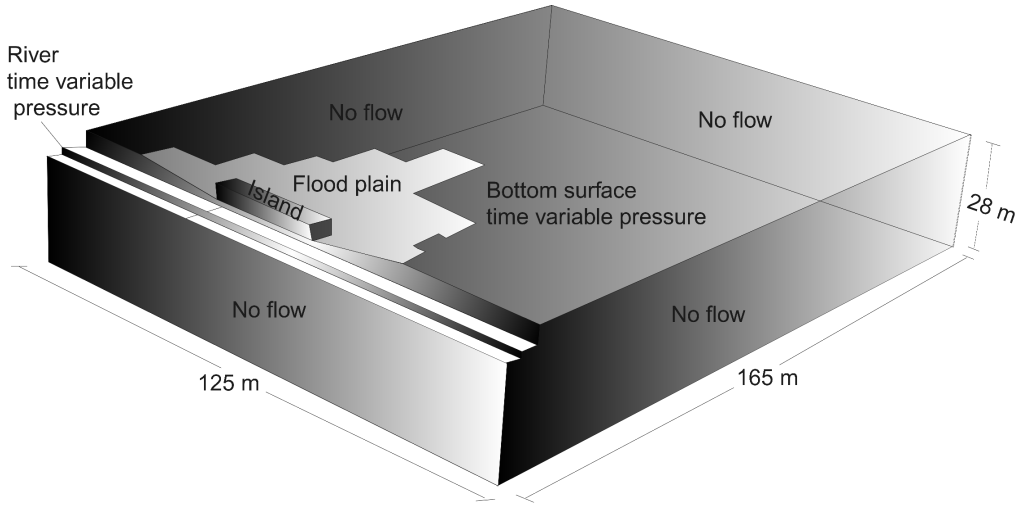

Figure 3.6: Model domain, dimensions and boundary conditions.

Initial conditions were developed by running the model during two sets of forcing conditions. First, the model was run with the boundary conditions representing a static water table without the river boundary conditions. This was done to establish a two-phase equilibrium profile (steady-state capillary fringe) above the water table. Second, the model was run for three consecutive years based on daily stream depth measurements derived from the stage record on the Cosumnes River at McConnell (MCC), (Fig. 3.1). Two years were simulated (January 2000 to the end of December 2002) to establish initial conditions that reflected the seasonal variation in the flow hydrograph. However, a complete water temperature data set was only available for 2003. Consequently, a one-year record of water temperature was repeated for each of the two years. Similarly, due to data limitations a one year record of transpiration demand was repeated during the two years.

Fifty realizations of the alluvial heterogeneity were used in this analysis so that initial conditions were established for each realization. Hydraulic properties used during

the establishment of initial conditions were based on laboratory measurements of core samples from each of the hydrofacies categories (Tables 3.3 and 3.4).

3.3.7. Model calibration

Each of the fifty models with different realizations of heterogeneity was calibrated by linking TOUGH2 to the automated parameter estimation code PEST (Doherty, 2004). Only the saturated hydraulic conductivity for each of the three hydrofacies was adjusted in order to match simulated and measured sediment temperatures and water contents. Other model parameters (e.g. relative hydraulic conductivity parameters, retention parameters, hydrofacies anisotropy) were not adjusted during calibration in order to limit the number of model runs required for PEST to determine a solution. We assumed that the ratio of horizontal to vertical hydraulic conductivity of each hydrofacies was 2.0, which represented only the anisotropy due to layering smaller than the vertical grid size (40 cm), and grain arrangement. Anisotropy due to sediment layering larger than model cells was explicitly modeled by including the hydrofacies stratigraphy.

There were a total of 6990 temperature observations and 280 water content measurements that were used for model calibration (Appendix F). The data used for calibration include measurements distributed in the plan view direction as shown in Fig. 3.3, and at 5-6 incremental depths to 11 m below land surface. The observation data was distributed temporally as daily measurements during the period from December 2002 to January 2004. Temperature measurements were used as a proxy for estimating the advection of heat due to seepage beneath the river. Several studies have demonstrated the use of temperature measurements for estimating streambed seepage and hydraulic conductivity (Ronan et al., 1998; Constantz et al., 2002).

Model calibration served two purposes in this study: to filter non-representative realizations of heterogeneity; and to improve the performance of individual realizations with repsect to observation data. Because of the complex heterogeneity at the Cosumnes, the measured data provide a limited amount of information. This being said, we felt that model calibration was important for estimating streambed seepage for accurately estimating water availability to plants.

Model calibration was evaluated based on the sum of the squared residuals (SSR) between the simulated and measured sediment temperatures and saturations as calculated by the objective function (Doherty, 2002):

$$SSR = \sum_{i=1}^{n} \left[w_i (M_i - S_i)^2 \right], \tag{13}$$

where SSR is the objective function value; i is the observation counter; n is the total number of observations; w_i is the weight applied to observation i; M_i is the measured temperature or saturation for observation i; and S_i is the simulated temperature or saturation for observation i. PEST minimized the objective function using the nonlinear estimation technique known as the Gauss-Marquardt-Levenberg method (Doherty, 2002). In general, the sediment saturation values were lower than the temperature values by a factor of 100 so that the weights (w_i) applied to temperature values were set to 1 and the weights for the saturations were set to 100.

3.4. RESULTS

3.4.1. Analysis of measured data

Simulations used to establish initial conditions for model calibration included the period between January 2000 and December 2002. The period between December 2002 and January 2004 was modeled for calibration, and the results of simulated ET and water budgets for the Cosumnes are presented for the period between January 2004 and October 2005. The year 2004 was a relatively average year of flow and included three flow events that partially inundated the floodplain (Fig. 3.7). The lower floodplain (Fig. 3.3) was partially inundated January 2, 2004, February, 20, 2004 and February, 28 2004. The middle floodplain was inundated on February 28, 2004.

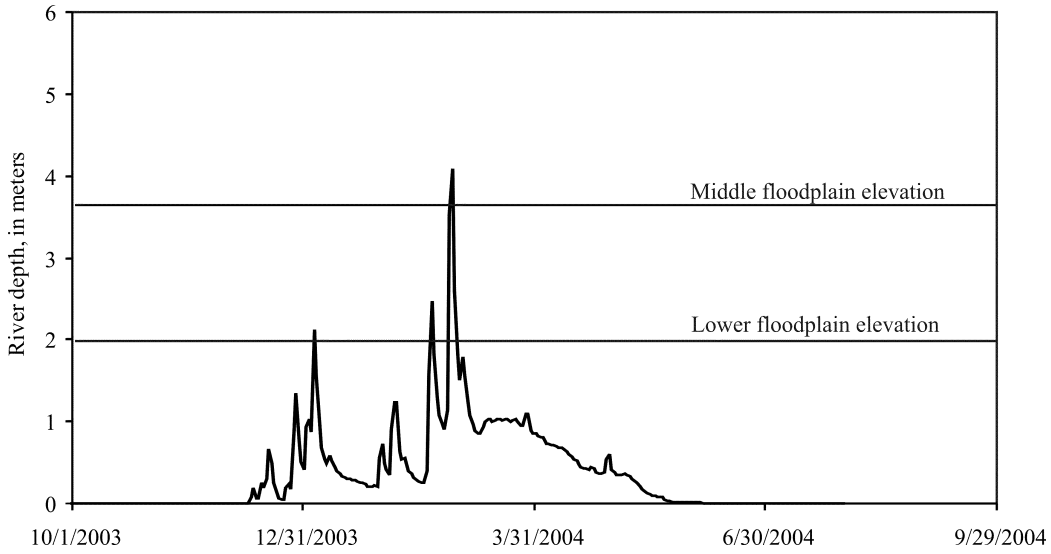

Figure 3.7: Rive depth measured at the McConnell stage gage and corrected to measurements made using a pressure transducer at the upstream end of the study site (MCC; Fig. 3.1).

The three cross-sectional profiles of temperature probes placed beneath the Cosumnes riverbed (Fig. 3.3) provided temperature measurements that could be plotted in 3-D using temperature iso-surfaces (Fig. 3.8). Temperature iso-surfaces show the penetration of cooler water (winter) or warmer water (summer) into the subsurface beneath the riverbed (Fig. 3.8). The variable depths of the temperature iso-surface beneath the riverbed surface show the spatial variability of water seeping from the river into the subsurface (Fig. 3.8). The measured sediment temperatures at 7 m below the riverbed surface varied seasonally 23 C in areas where iso-surfaces are deep and as little as 3 C in areas where iso-surfaces are shallow (Fig. 3.8).

Measurements of sediment water content beneath the floodplain and the levee indicate saturated or near saturated regions in the vadose zone. Beneath the floodplain the sediment water content increases between 3 m and 7 m below the surface in response to lateral subsurface seepage from the river (Fig. 3.9A). Sediment water content increased between December 2003 and July, 2004 above 3 m due to a three flow events that partially inundated the floodplain in January and February (Fig. 3.9A).

Sediment water content within the built levee material (Fig. 3.3) between 1 m and 3.6 m changes very little seasonally and stays relatively wet due to lateral seepage from the river. The nearly constant water content within the levee material, which consisted hydrofacies 1 and 2 above 3 m, may be due to compaction of sediment during construction of the levee which reduced the K of the levee sediment above 3 m (Fig. 3.9B). Beneath 3.6 m the sediment water content varies seasonally and became saturated due to lateral seepage from the river. The regional water table ranged between 17 and 18 m below the surface elevation of the TDR borehole on the levee.

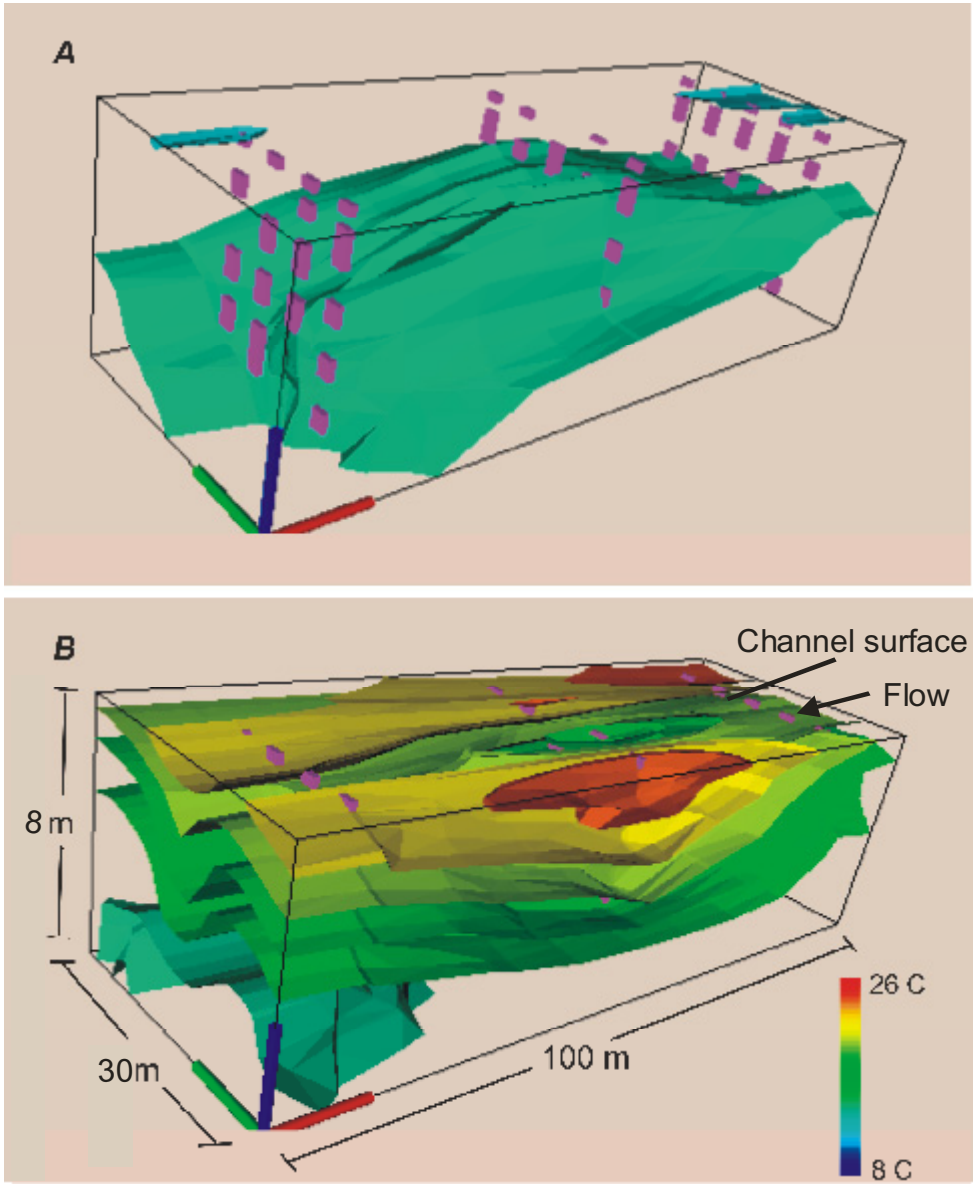

Figure 3.8: 3-D iso-surface plots of measured sediment temperature beneath the Cosumnes Riverbed on (A) 2/1/2003 (flow = 219 cfs) and (B) 6/1/03 (flow = ~100 cfs). Pink boxes represent temperature measurement locations.

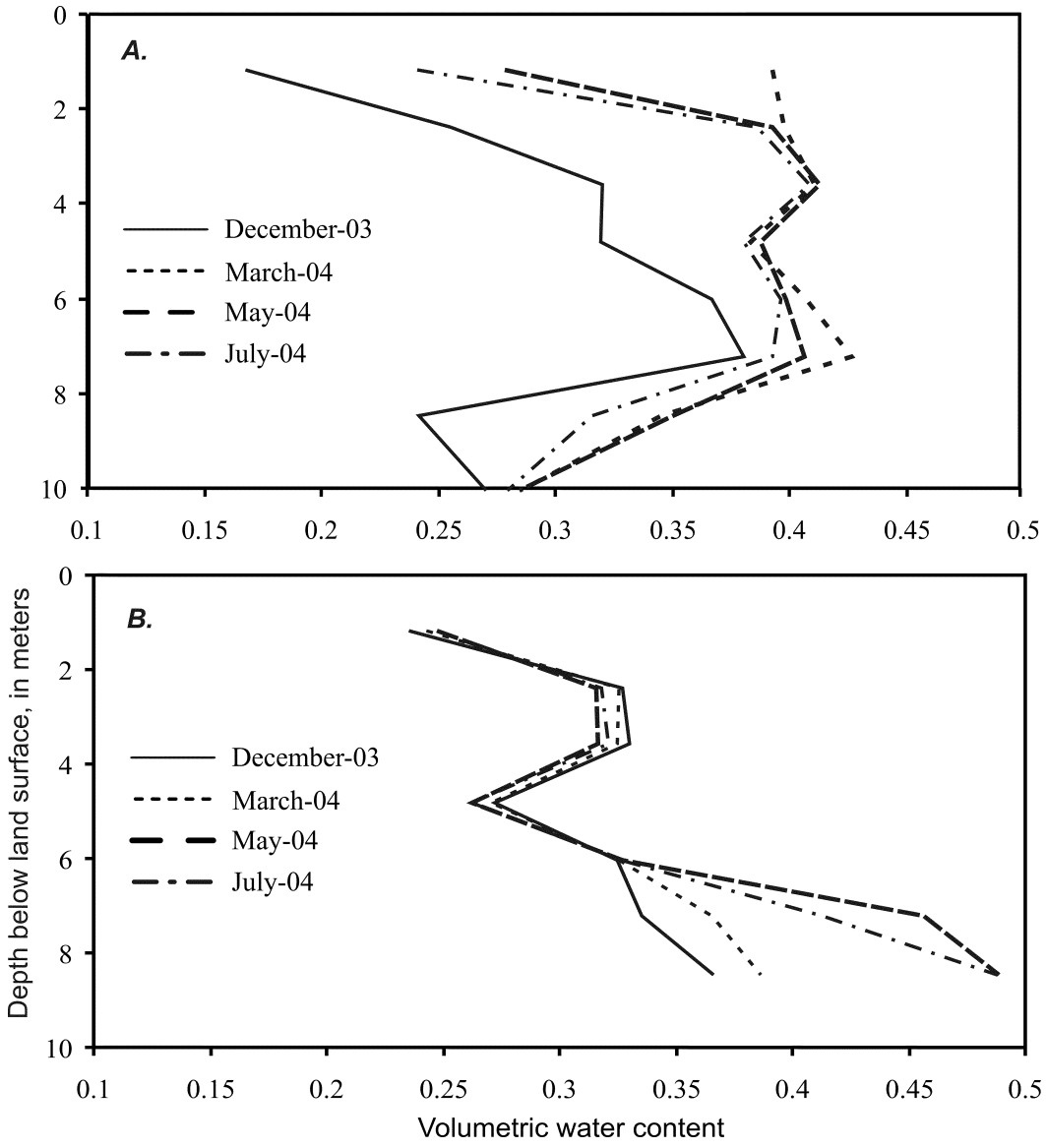

Figure 3.9: Measured TDR sediment water content profiles directly beneath (A) floodplain and (B) built levee.

3.4.2. Hydrofacies delineation and parameterization

We characterized each of the three textural-faces categories based on laboratory measurements of saturated hydraulic conductivity (K), porosity, bulk density, and percent fraction of sand, silt and clay (Table 3.1). Although there is a general correlation among each hydrofaces category and the physical properties of cores from each hydrofacies category, the hydraulic conductivity provides the most consistent correlation (Fig. 3.10).

However, with the exception of bulk density, the averages of these properties within each category correlate well to the texture characterization. For example, the porosity is larger for the finer-grained categories as is the percent clay particles. The hydrofacies categories were characterized as sandy clay (category 1), muddy sand (category 2), and sandy mud (category 3) based on the particle size fractions for each hydrofacies category (Table 3.4).

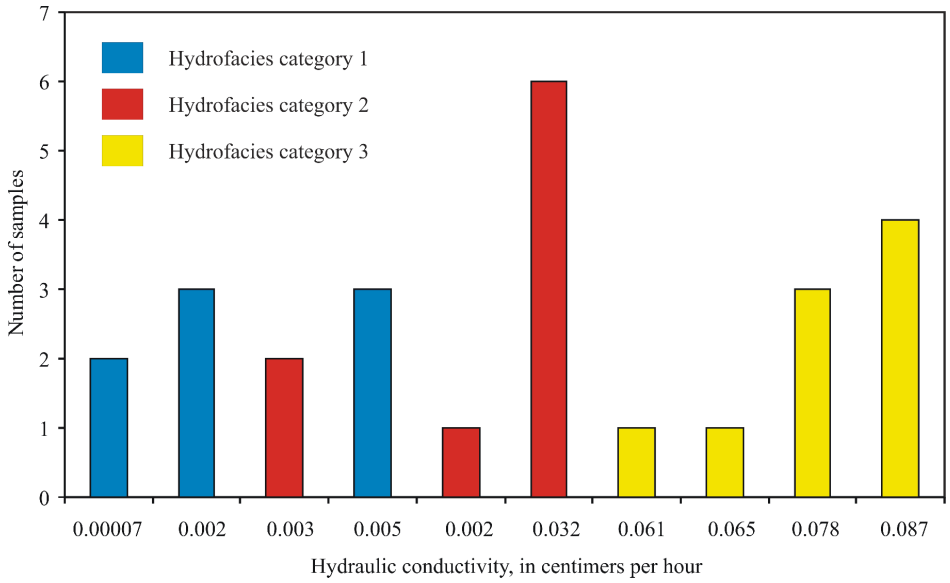

Figure 3.10: Histogram of measured hydraulic conductivity values using the falling-head method.

Relative K and retention parameters for each hydrofacies category were derived based on neural networks that relate easily measurable sediment properties (porosity, bulk density, particle size, and K) to relative K and retention parameters (Fig. 3.11) (Minasny et al., 2004). Although there was a large amount of uncertainty in the estimated parameter values (see 95% confidence intervals shown in Fig. 2.3 for sandy clay and muddy sand hydrofacies). However, there is much more variation in retention parameters among the hydrofacies categories as compared to within a category, as can be seen by comparing the 95% confidence intervals for the muddy sand and sandy clay hydrofacies (Fig. 2.3). Thus, defining the unsaturated flow properties based on hydrofacies categories

may be a satisfactory method of including the effect of heterogeneity in a vadose-zone model.

Table 3.3: Measurements of physical and hydraulic properties on core samples.

Sample #	K (cm/hr)	% mass fraction (<.002mm)	% mass fraction (.002-.063mm)	% mass fraction (.063-.2mm)	Bulk density (g/cm^3)	Porosity (cm^3/ cm^3)	Category[1]
1	$9.2x10^{-5}$	--	--	--	1.64	0.37	1
2	$7.2x10^{-5}$	91.1	1.6	7.25	--	--	1
3	$7.2x10^{-5}$	--	--	--	--	--	1
4	$3.2x10^{-4}$	77.1	4.4	18.5	1.64	0.47	1
5	$1.7x10^{-4}$	80.5	3.3	16.2	1.70	0.44	1
6	$1.8x10^{-3}$	79.3	5.4	15.4	1.74	0.33	1
7	$2.2x10^{-3}$	--	--	--	--	--	2
8	$2.5x10^{-3}$	--	--	--	--	--	2
9	$2.9x10^{-3}$	--	--	--	--	--	2
10	$3.4x10^{-3}$	--	--	--	--	--	1
11	$3.0x10^{-3}$	--	--	--	--	--	1
12	$3.9x10^{-3}$	--	--	--	--	--	2
13	$4.3x10^{-3}$	43.4	38.3	18.3	1.63	0.43	1
14	$4.6x10^{-3}$	15.3	59.0	25.6	1.60	0.39	1
15	$5.0x10^{-3}$	11.1	58.5	30.4	1.71	0.36	2
16	$5.4x10^{-3}$	26.6	51.9	21.5	1.76	0.37	2
17	$5.8x10^{-3}$	--	--	--	--	--	2
18	$6.1x10^{-2}$	--	--	--	--	--	2
19	$6.5x10^{-2}$	--	--	--	--	--	3
20	$7.0x10^{-2}$	3.9	27.1	69.0	1.77	0.33	3
21	$6.6x10^{-2}$	4.8	34.6	60.6	1.69	0.39	3
22	$7.6x10^{-2}$	5.0	33.4	61.6	1.56	0.33	3
23	$7.9x10^{-2}$	--	--	--	--	--	3
24	$8.3x10^{-2}$	--	--	--	--	--	3
25	$8.6x10^{-2}$	1.9	16.2	81.9	1.65	0.39	3
26	$9.1x10^{-2}$	--	--	--	--	--	3

[1]Categories were assigned based on lithological interpretation during drilling of boreholes prior to laboratory measurements.

Table 3.4: Average physical and hydraulic properties of 26 cores taken from the Cosumnes riverbed and banks.

Averages within each category	Muddy sand	Sandy mud	Sandy clay
Porosity (cm^3/ cm^3)	0.36	0.37	0.41
Bulk density (g/cm^3)	1.66	1.77	1.64
K (cm/hr)	$7.7x10^{-2}$	$3.78x10^{-3}$	$1.40x10^{-4}$
% sand	68.7	23.7	14.3
% silt	27.8	52.1	3.6
% clay	4.0	24.3	82.1
Thermal conductivity at residual water content (W/mC°)	0.3	0.16	0.25
Thermal conductivity at saturated water content (W/mC°)	1.30	1.26	1.27
Heat capacity of dry sediment (J/kg C°)	976	985	978
θ_r (cm^3/cm^3)	0.191[1]	0.204[1]	$(6.38x10^{-12})$ [1]
θ_s (cm^3/cm^3)	0.37[1]	0.39[1]	0.59[1]
α 1/cm	0.0083[1]	0.0075[1]	0.0036[1]
n unitless	2.178[1]	1.177[1]	1.113[1]

[1]Values were estimated using NeuroMultistep based on averages of measured physical and hydraulic properties listed in this table (Minasny et al., 2004).

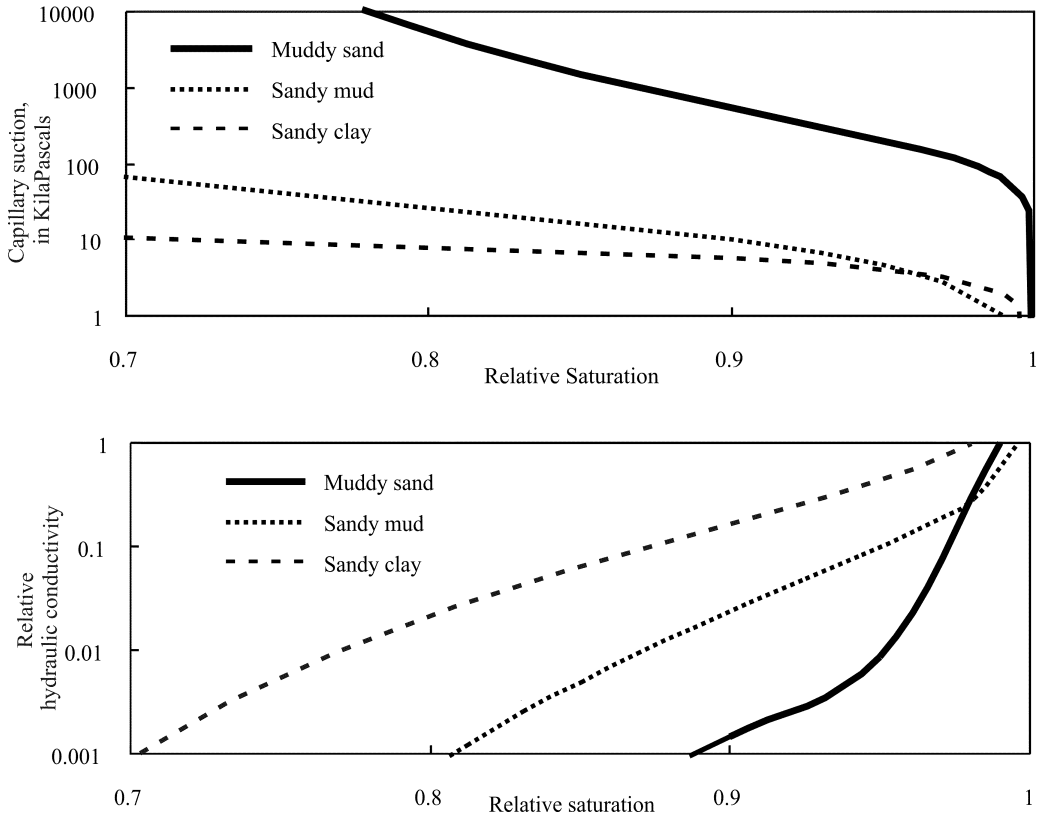

Figure 3.11: A. Retention and B. relative hydraulic conductivity curves. Parameters for Mualem (1976) and van Genuchten (1978, 1980) functions were estimated using NeuroMultistep (Minasny et al., 2004).

3.4.3. Geostatistical simulation

In general the transition probabilities for the vertical direction were smooth for short lags (Fig. 3.12), and thus a continuous Markov-chain model was developed for the vertical direction based on a discrete lag and the transition rates calculated from the transition probabilities (Carle and Fogg, 1997; Carle, 1999).

The Markov-chain models were developed for the horizontal directions based on estimates of facies mean lengths, juxtaposition tendencies, and the volumetric global proportions calculated from the lithologic data. Using this approach, a background category is chosen, such that information does not need to be generated regarding the spatial statistics for the background hydrofacies. The muddy sand was chosen as the

background category because the mean lengths of this facies were the most difficult to ascertain from borehole data. Thus, juxtaposition tendencies and mean lengths were estimated for the muddy sand and sandy clay facies.

The final Markov-chain models for the three principle directions were generated using embedded transition probabilities (Table 3.5). Realizations of the 3-D hydrofacies were then generated using the sequential indicator simulation and the simulated quenching algorithms within the TPROGS suite of geostatistical programs (Carle, 1999). Three realizations of the hdyrfacies distributions are shown in Figure 3.13.

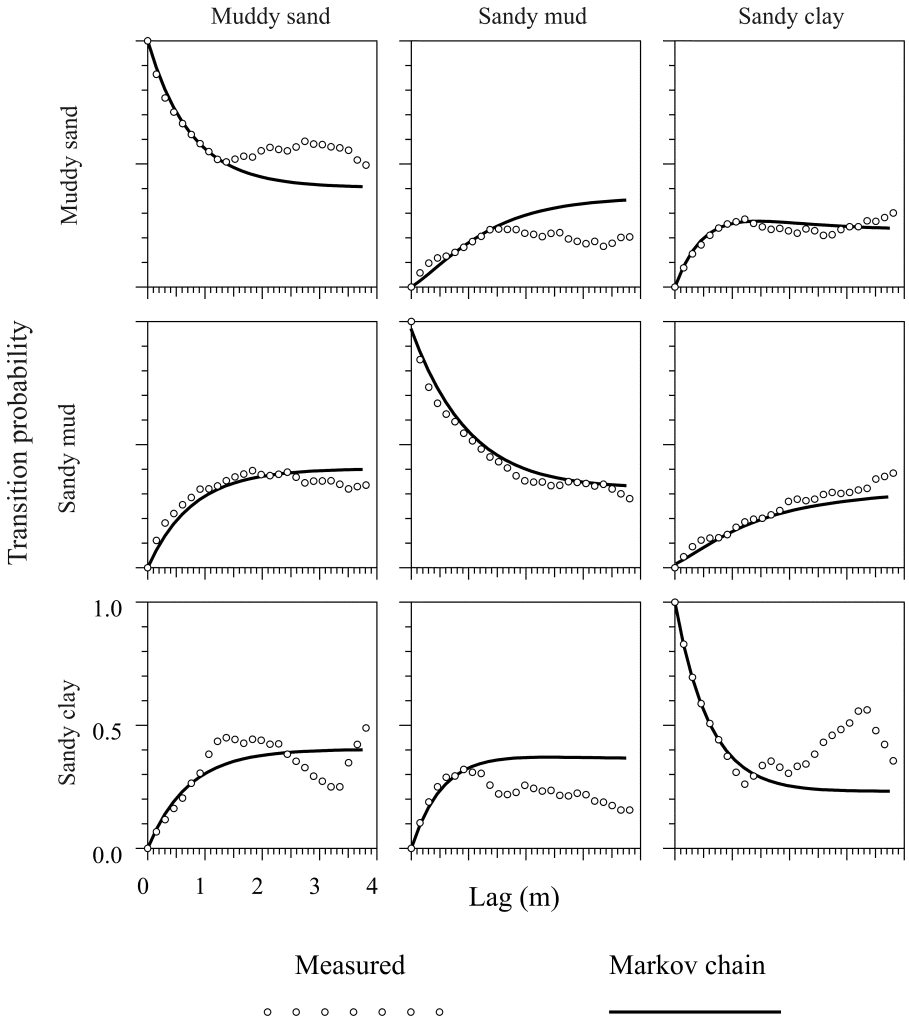

Figure 3.12: Vertical Markov-chain models fitted to measured transition probabilities for a three hydrofacies model.

Table 3.5: Embedded transition probability matrices and mean hydrofacies lengths for geostatistical model (s = muddy sand, m = sandy mud, c = sandy clay).

Vertical (z)-direction

	s	*m*	*c*
s	$\overline{L} = 1.25m$	0.19	0.80
m	0.83	$\overline{L} = 1.59m$	0.32
c	0.44	0.65	$\overline{L} = 0.78m$

Strike (x)-direction

	s	*m*	*c*
s	$\overline{L} = 40.0m$	0.80	0.20
m	0.68	$\overline{L} = 30.7m$	0.32
c	0.34	0.65	$\overline{L} = 40.0m$

Dip (y)-direction

	s	*m*	*c*
s	$\overline{L} = 80.0m$	0.80	0.20
m	0.68	$\overline{L} = 61.38m$	0.32
c	0.34	0.65	$\overline{L} = 80.0m$

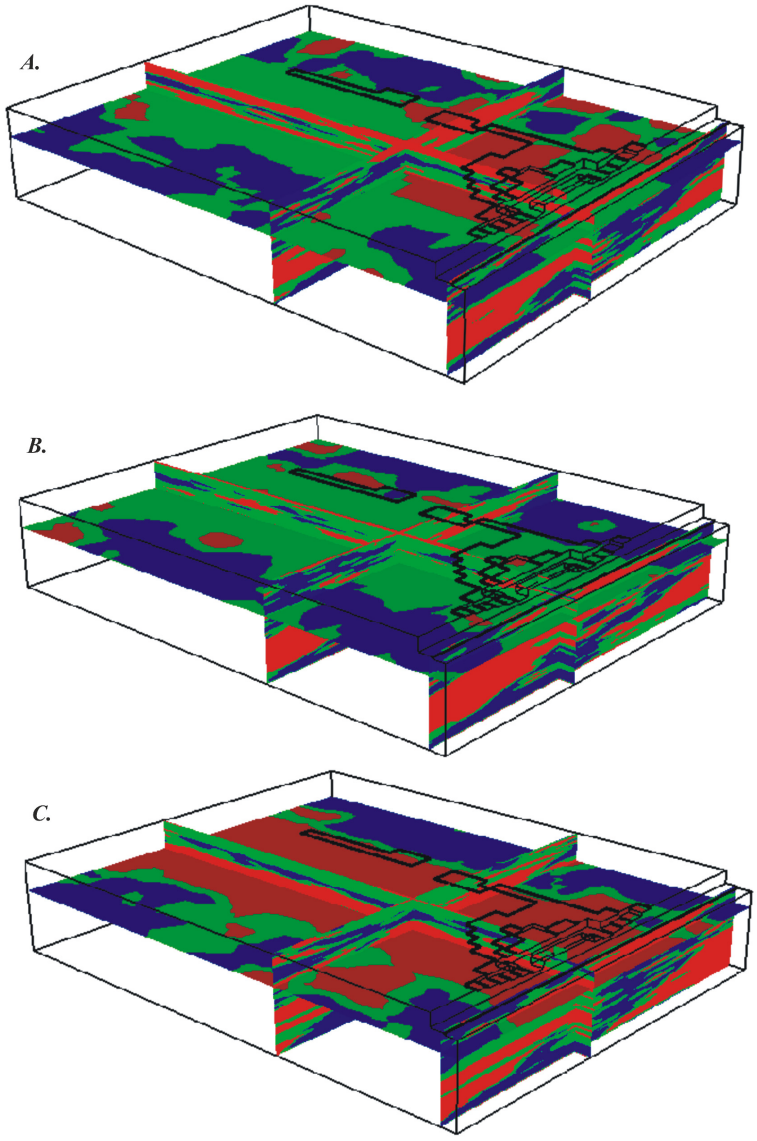

Figure 3.13: Three-facies geostatistical realizations A. rz10; B.rz17, and C. rz30. Red, green and blue colors represent the muddy sand, sandy mud and sandy clay hydrofacies, respectively. The length scales are the same as those shown in Figure 3.6.

3.4.4. Model calibration

In general, most realizations did not provide a reasonable fit to the measured data regardless of the hydraulic conductivity values. Most *SSR* (eq. 13) values for the calibrated realizations remained greater than 80% of the *SSR* values obtained without

parameter estimation, where the K values were based solely on laboratory measurements of hydraulic conductivity.

The small number of realizations that provide a reasonable fit to the measured data is contrary to what is typical for calibrating facies realizations in groundwater flow models (e.g. Fleckenstein et al., 2005). This is likely because the groundwater flow models typically compute residuals based mainly on hydraulic head, whereas the present model computes residuals with both saturation and temperature variables, which represents a more stringent test of model fit. The small number of realizations producing a good fit might also stem from a lack ergodicity among the realizations (i.e., the conditional simulation not preserving the spatial model from realization). This may arise when the correlation lengths are on the same order as the model domain length, resulting in realizations, or portions therein, that either percolate (interconnect) or not. Another study used TPROGS to simulate regional-scale flow and transport and reported that very few realizations provided a good fit to measured groundwater levels and total dissolved solids (G. Pohll, written communication, 2005). In the study by Pohll (written communication, 2005) the model domain was very large as compared to horizontal mean lengths. Thus, the addition of solute transport data (or heat transport data) may limit the number of realizations that fit the data as compared to groundwater level data alone.

Parameter estimation results were compared among realizations by normalizing *SSR* by the median value over all realizations. The median *SSR* was 1.81×10^5 and 4 of the 50 realizations resulted in *SSR* values that were less than 50% of the median value (Fig. 3.14). The four realizations with the lowest *SSR* are rz10, rz17, rz23 and rz30.

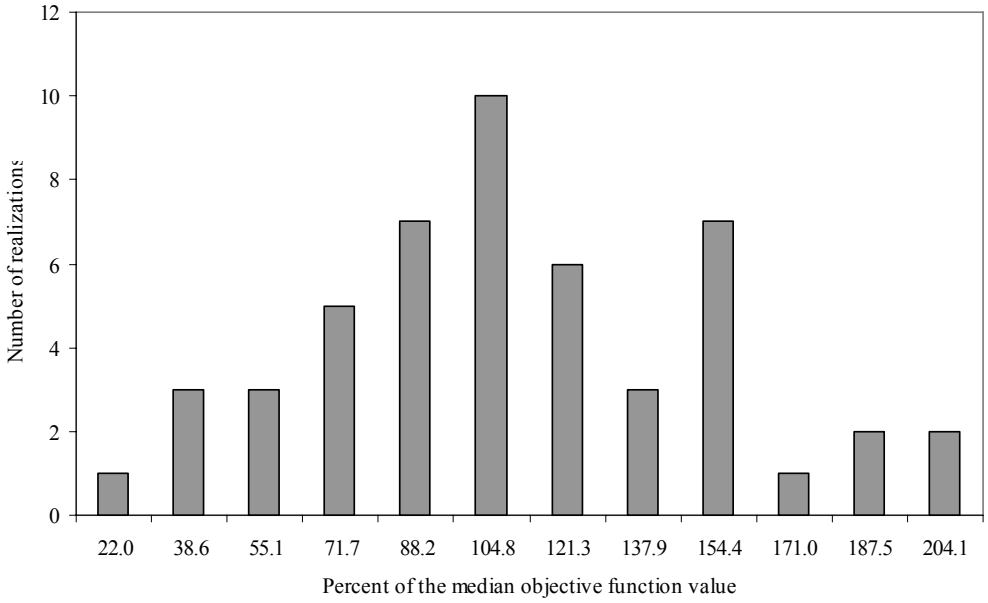

Figure 3.14: Relative sum of the squared residuals from calibration of 50 realizations of heterogeneity. Objective function values are reported as a percent of the median value equal to 23,500 with a total of 7270 observations. The median objective function value was 1.81×10^5.

Realization rz23 resulted in an *SSR* that was only 17% of the median value, whereas the worst was greater than 200% of the median value (Fig. 3.14). As mentioned before, the parameter estimation only improved *SSR* by about 20%, whereas the maximum difference in *SSR* among realizations was 89%. Thus, *SSR* was much more sensitive to the facies structures represented by the different realizations of heterogeneity as compared to changes in the hydraulic conductivity for each hydrofacies.

The measured temperature data indicated that downward advective transport was greater in some areas than in others due to sediment heterogeneity (Fig. 3.8). Temperatures fluctuated seasonally much more in some areas than others. Thus, for the model to fit the measured temperatures well, the realization of heterogeneity had to contain connectivity of the muddy sand in areas of high downward heat transport and a

lack of connectivity in areas without downward heat transport. Accordingly, this occurred to a certain extent in only 4 of the 50 realizations that were analyzed.

Realization rz30 resulted in an objective function value that was 44% of the median value but the resulting hydraulic conductivities were inconsistent with the hdydrofacies designation. The sandy mud took on a higher hydraulic conductivity than the muddy sand, and the normal matrix used to calculate confidence intervals about the estimated parameters was nearly singular (Table 3.5). Thus, rz30 was not used in further simulations. It should be mentioned that only 8 of the 50 realizations resulted in K values that were inconsistent with the hydrofacies designation, and their SSR values were all unacceptable.

A comparison among the estimated K values using PEST on rz23 and those measured in the laboratory indicate very good correspondence for the sandy-mud and sandy-clay hydrofacies; however, the estimated K value for the muddy sand was nearly 100 times greater than the measured value (Table 3.4). This may be because it was difficult to sample the coarse sediment and that the limited number of samples that were measured were not representative of the average K of the category 3 hydrofacies (Fig. 3.5). The comparison among the measured and estimated K values for rz10 and rz17 show a similar result. Adding another hydrofacies category that represents clean sand may have resulted in facies models more representative of the heterogeneity at the Cosumnes.

Confidence intervals can be calculated for the estimated K for each hydrofacies, and are indicative of the sensitivity of *SSR* to changes in K. The confidence intervals can also be used to determine if the estimated K values for each hydrofacies are statistically

different. Confidence intervals for each hydrofacies did not overlap for realizations rz23, and rz17, indicating that the estimated K values were significantly different; however, the confidence interval about the estimated sandy clay for realization rz10 was very wide (Table 3.6). This is likely caused by the model being insensitive to changes in K for sandy clay within the solution space sampled by the parameter estimation code. A 3-D contour plot of the hydraulic conductivity distribution for rz23 displays the distribution of K that resulted in the best fit to observations data (Fig. 3.15).

Table 3.6: Automated parameter estimation results for the four best realizations of heterogeneity. Hydraulic conductivity values and 95 % confidence intervals are reported for each hydrofacies.

Realization				95% confidence limits	
	hydrofacies	Initial value (cm/hr)	Calibrated value (cm/hr)	lower limit (cm/hr)	upper limit (cm/hr)
rz23	muddy sand	$7.7x10^{-2}$	6.25	2.71	14.5
	sandy mud	$3.78x10^{-3}$	$2.65x10^{-2}$	$4.96x10^{-3}$	$1.41x10^{-1}$
	sandy clay	$1.40x10^{-4}$	$4.42x10^{-5}$	$1.64x10^{-5}$	$1.18x10^{-4}$
rz10	muddy sand	$7.7x10^{-2}$	3.05	2.58	3.60
	sandy mud	$3.78x10^{-3}$	1.44	1.35	1.54
	sandy clay	$1.40x10^{-4}$	$5.04x10^{-5}$	$3.56x10^{-14}$	7130.0
rz17	muddy sand	$7.7x10^{-2}$	4.42	$2.84x10^{-1}$	7.29
	sandy mud	$3.78x10^{-3}$	$1.44x10^{-2}$	$4.63x10^{-3}$	$4.50x10^{-2}$
	sandy clay	$1.40x10^{-4}$	$7.21x10^{-5}$	$1.50x10^{-5}$	$3.45x10^{-4}$
rz30	muddy sand	$7.7x10^{-2}$	1.44	--[1]	--[1]
	sandy mud	$3.78x10^{-3}$	144.0	--[1]	--[1]
	sandy clay	$1.40x10^{-4}$	$1.67x10^{-4}$	--[1]	--[1]

[1]Confidence intervals could not be calculated due to a singular normal matrix.

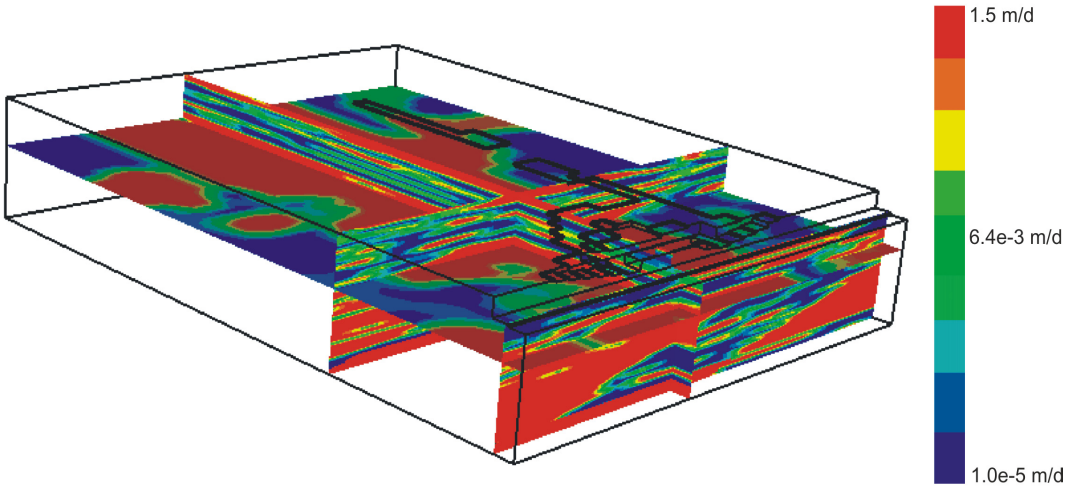

Figure 3.15: Slice planes showing 3-D hydraulic conductivity contours for realization rz23. The length scales are the same as those shown in Figure 3.6.

In order to evaluate the relative fit to observed data, the best fit realization (rz23) was compared to realization rz28, which had in an objective function value (SSR) nearly equal to the median. A comparison among rz23 and rz28 was made based on a plot of the 5, 50 and 95 percentiles of observed versus simulated temperatures (Fig. 3.16). The fit between simulated and measured temperature values for rz23 resulted in a R^2 of 0.82. Percentiles of the measured versus simulated temperature are shown because of the large number of data points obscure the results. The curve of the 50 percentile for rz23 (thick line in Fig. 3.15) was biased above the observed temperatures for cooler temperatures and was biased below observed temperatures for warmer temperatures. Thus, the model had trouble matching measurements that exhibited large seasonal temperature amplitudes in some areas while matching measurements with small seasonal amplitudes in other areas. As described previously, this result is due to the subsurface temperature dependence on connected pathways of high K from the stream to the observation points, which is not represented perfectly by any of the 50 realizations tested. We likely could have achieved

a better fit to the data had we included a forth hydrofacies representing clean sand into the geostatistical conceptual model. The spread in model performance among realizations, as shown by the comparison between the thick line (rz23) and the dashed line (rz28), indicates that the best fit realizations are performing relatively well (Fig. 3.16).

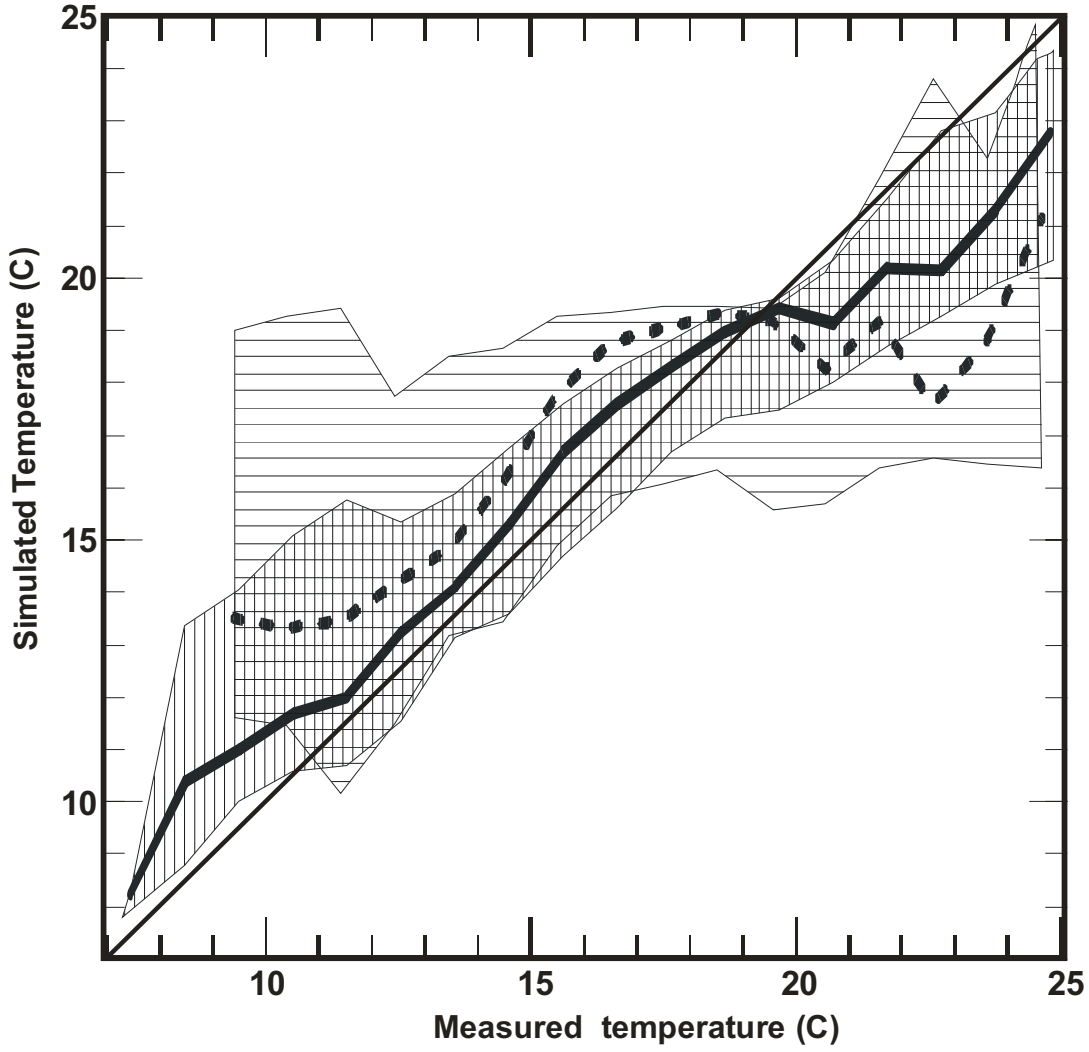

Figure 3.16: Measured versus simulated temperatures for the best fit realization (rz23; solid line) and a realization with an objection function value equal to the median of 50 realizations (rz28; dashed line).The horizontal hatched area spans the 5 and 95 percentiles for rz28 and the vertical hatched area spans the 5 and 95 percentiles for rz23. The thin black line shows a 1:1 correspondence for reference.

The observed and simulated sediment saturations were slightly less correlated than simulated and measured temperatures (R^2 =0.72) (Fig. 3.17); however, comparison between the R^2 values for sediment temperature and saturation may not be valid because there were many more temperature observations than sediment observations, and the R^2 value improves with the number of observations.

The comparison among simulated and measured saturations shows variations in measured saturations in time at certain locations that were not present in the simulated results. At other locations simulated saturations varied more in time than the measured values. The simulated saturations for rz28 was not correlated to the measured values and showed very little seasonal variation in saturation.

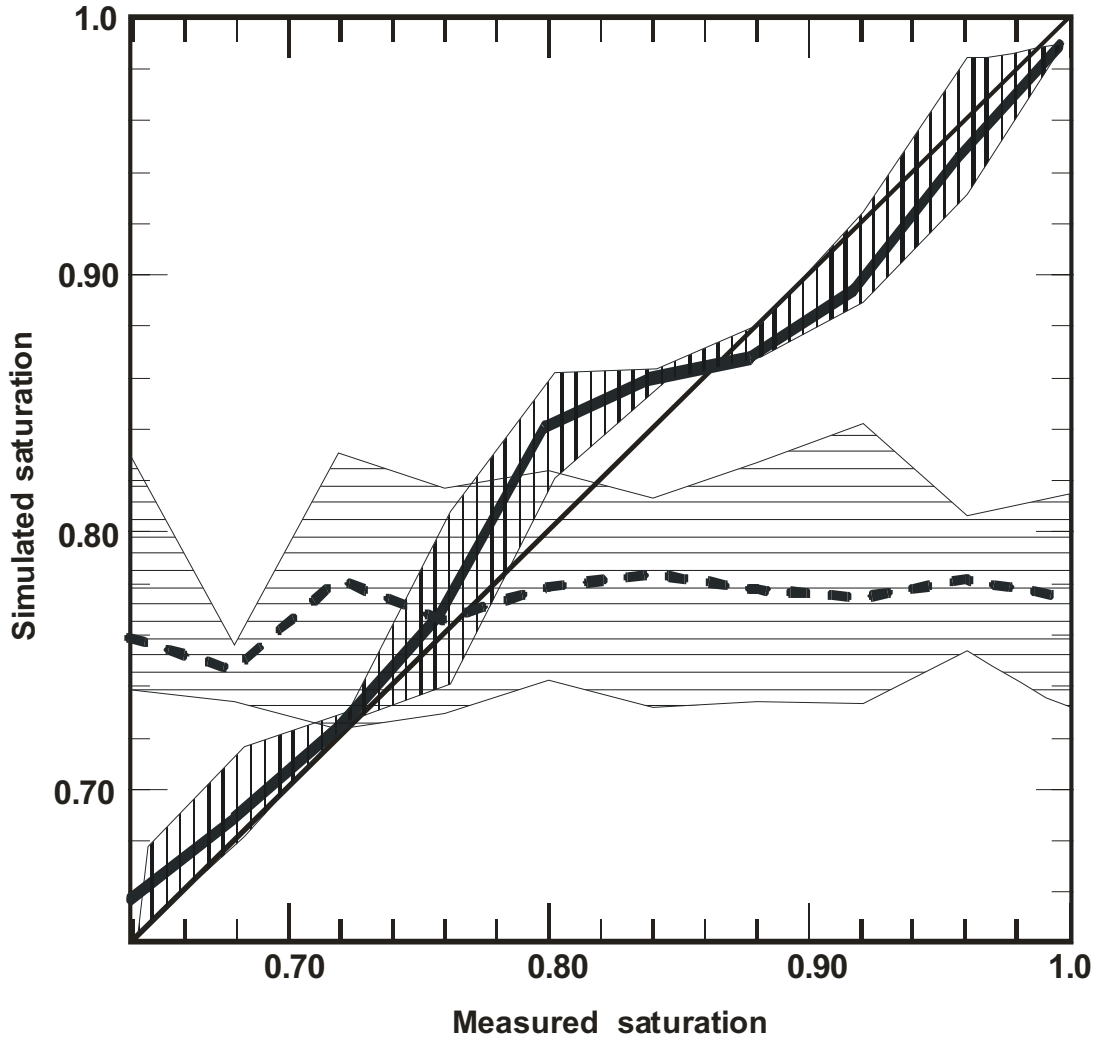

Figure 3.17: Measured versus simulated sediment saturation for the best fit realization (rz23; solid line) and a realization with an objection function value equal to the median of 50 realizations (rz28; dashed line).The horizontal hatched area spans the 5 and 95 percentiles for rz28 and the vertical hatched area spans the 5 and 95 percentiles for rz23. The thin black line shows a 1:1 correspondence for reference.

3.4.5. Perched groundwater and ET simulations

Consistent with field observations, the heterogeneous stratigraphy that was generated based on subjective and measurable information from the Cosumnes resulted in significant lateral seepage that perched within the root zone following the end of flow in the river. Simulated perched groundwater generally is located where high-K sediment is above low-K lenses (Figs. 3.18A and B). Simulated perched groundwater persisted

through the dry season following the winter of 2004, which was an average year of precipitation. Similar to the measured water contents, simulated saturations for July, 2004 indicate significant amounts of saturated sediment within the vadose zone (Fig. 3.18).

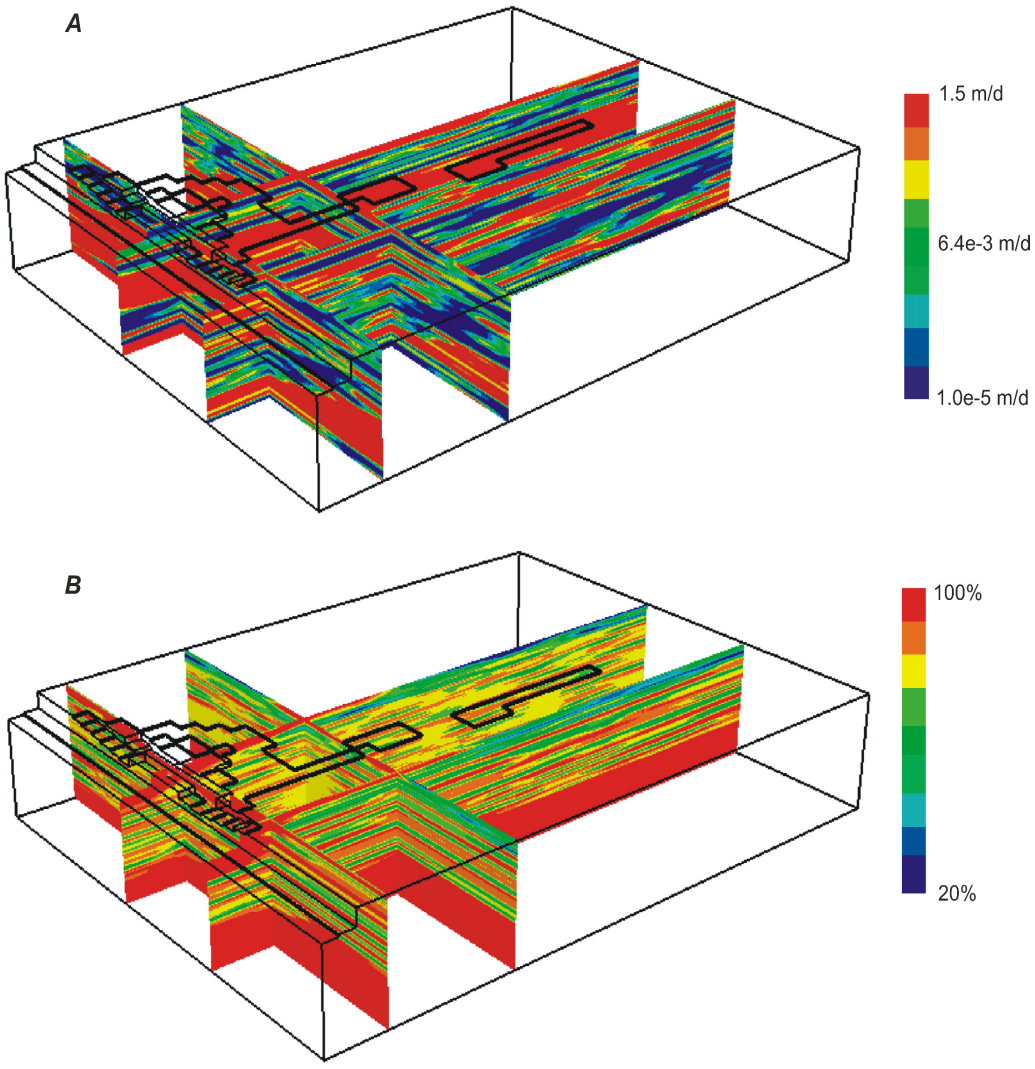

Figure 3.18: (A) Contour plot of K for realization rz23 and (B) Simulated sediment saturation for rz23 showing perched groundwater on 7/1/04. The black lines on the top of domain outline are depressions in land surface elevation. The length scales are the same as those shown in Figure 3.6.

Only the three realizations with the lowest *SSR* were used to simulate ET, namely rz10, rz17 and rz23. Although rz10 and rz17 resulted in *SSR* values that were only 10-15

percent greater than the realization with lowest *SSR* (rz23), they had significant reductions in the amount of modeled area that could support phreatophyte vegetation. This is an indication that amount and distribution of perched groundwater varies somewhat significantly among different realizations of heterogeneity created based on the same Markov-chain models, conditioning and parameter estimation data. However, significant perched groundwater was present in all three realizations.

Results indicate that the simulated ET was less than the PET over most the modeled area; however, simulated ET was near the PET over a substantial proportion of modeled area due to the presence of perched groundwater within the root zone. The simulated ET was close to the PET only where there was substantial perched groundwater within the root zone because the root uptake function for riparian vegetation dropped to zero when capillary pressures were slightly negative (Fig. 3.4). Due to sediment heterogeneity and floodplain inundation, perched groundwater occurred at different locations within the modeled area, such that significant areas were able to supply water for root uptake at PET rate (Figs. 3.19-3.21). In general, the simulated ET that occurred further from the river was taken from deeper in the root zone.

The modeled area that was able to meet the PET varied among realizations and throughout the ET season. Toward the end of the ET season (August 28, 2004) when the storage within the root zone was depleted, rz23 supported the largest area at the demand ET rate equal to 46% of the modeled area outside of the main channel, whereas rz10 and rz17 supported 21% and 23% of the modeled area, respectively. This result could be because rz23 had the greatest muddy sand hydraulic conductivity; however, the degree of lateral connectivity of the muddy sand and continuity of the sandy clay, is likely

important as well. The hydraulic conductivity of the sandy mud hydrofacies was nearly 100 times greater in rz10 as compared to rz23 and rz17, rz10 supported the smallest percentage of modeled area at the PET rate (Figs. 3.19-3.21).

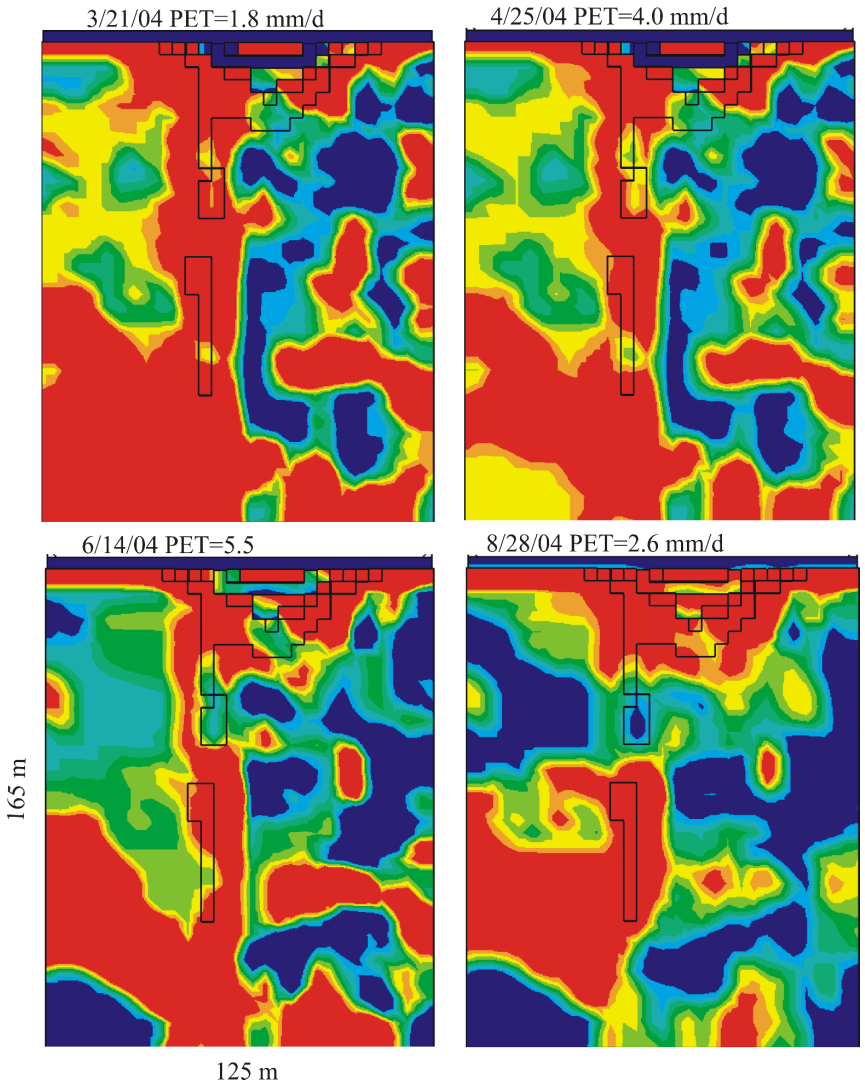

Figure 3.19: Contour plots of ET for hydrofacies model rz23 integrated over rooting depth to 4 m. The red colors represent areas where the simulated ET was within 90% of the demand and other colors represent simulated ET less than 90% of the demand. The blue color indicates that the ET rate is less than half of the potential rate. Black lines on plots indicate model cells with elevations below the top of the riverbank. The river channel runs along the top of the plots. Potential evapotranspiration demand is abbreviated by PET.

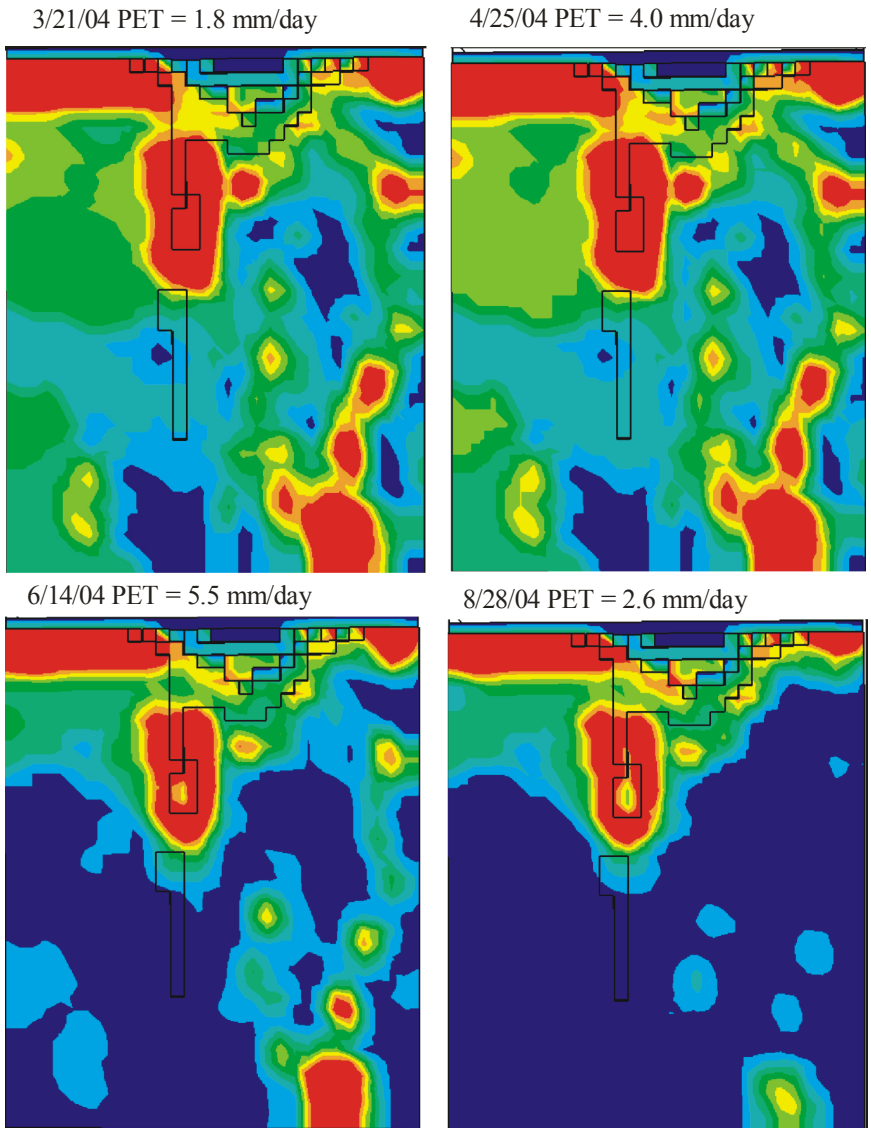

Figure 3.20: Contour plots of ET for hydrofacies model rz10 integrated over rooting depth to 4 m. The red colors represent areas where the simulated ET was within 90% of the demand and other colors represent simulated ET less than 90% of the demand. The blue color indicates that the ET rate is less than half of the potential rate. Black lines on plots indicate model cells with elevations below the top of the riverbank. The river channel runs along the top of the plots. Length scales are the same as those shown in 3.19.

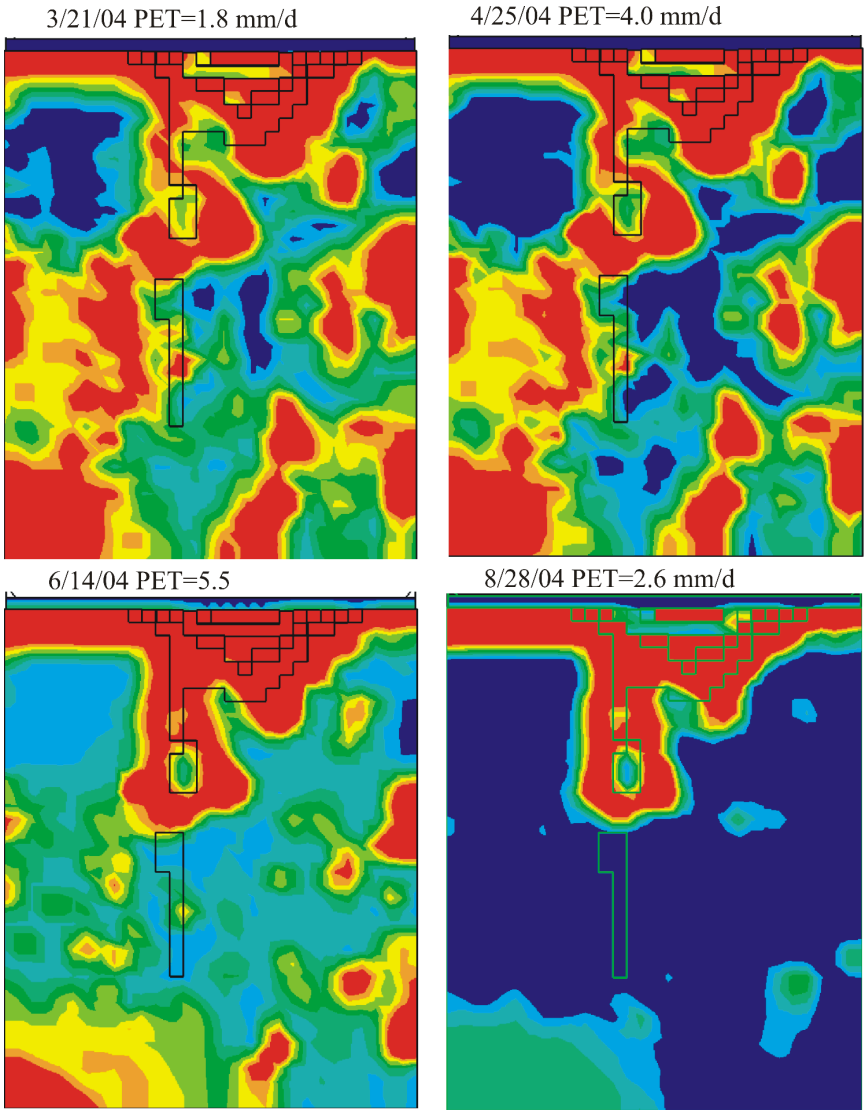

Figure 3.21: Contour plots of ET for hydrofacies model rz17 integrated over rooting depth to 4 m. The red colors represent areas of demand driven ET and other colors represent supply dependent ET. The blue color indicates that the ET rate is less than half of the potential rate. Black lines on plots indicate model cells with elevations below the top of the streambank. Length scales are the same as those shown in 3.19.

The simulated ET rates for rz10 and 17, and to a lesser extent rz23, suggest that the late season water supply limits the amount of the phreatophyte vegetation that can be supported. This is especially true for rz10, which meets the ET demand over 35% of the modeled area into late May; however, as the demand increases into late June the area is reduced to 21%. This is because the storage within the root zone from the previous wet

season has been lost to ET and percolation beneath the root zone, suggesting that if the root zone were to be recharged early June, a larger area along the stream may support phreatophyte vegetation. During water-year 2004, the flood-plain was only partially inundated three times for short periods (1-4 days). Thus, these simulation results suggest that perched groundwater will be available for riparian vegetation even during years of average streamflow and average floodplain inundation. However, water availability to plants decreases significantly in the second half of the ET season, which likely limits the amount of riparian vegetation growing at the study site.

Comparison among the results from the three models with different heterogeneity (Figs. 3.19-3.21) and the actual percent area covered with riparian vegetation at the Cosumnes (Fig. 3.22) suggest that rz23 is over predicting the area that can support riparian vegetation. The percent area covered with riparian vegetation at the Cosumnes that is within the modeled area is about 25% as compared to the simulated result of 46% based on rz23. The simulated area that could support riparian vegetation in rz10 and rz17 (between 21% and 23%) is much closer to the actual area. The actual distribution is somewhat similar in that the model predicts an extension perpendicular to the riparian corridor where the floodplain exists; however, there are areas predicted by the models to support phreatophyte vegetation that do not correspond to the vegetation at the Cosumnes (Fig. 3.22).

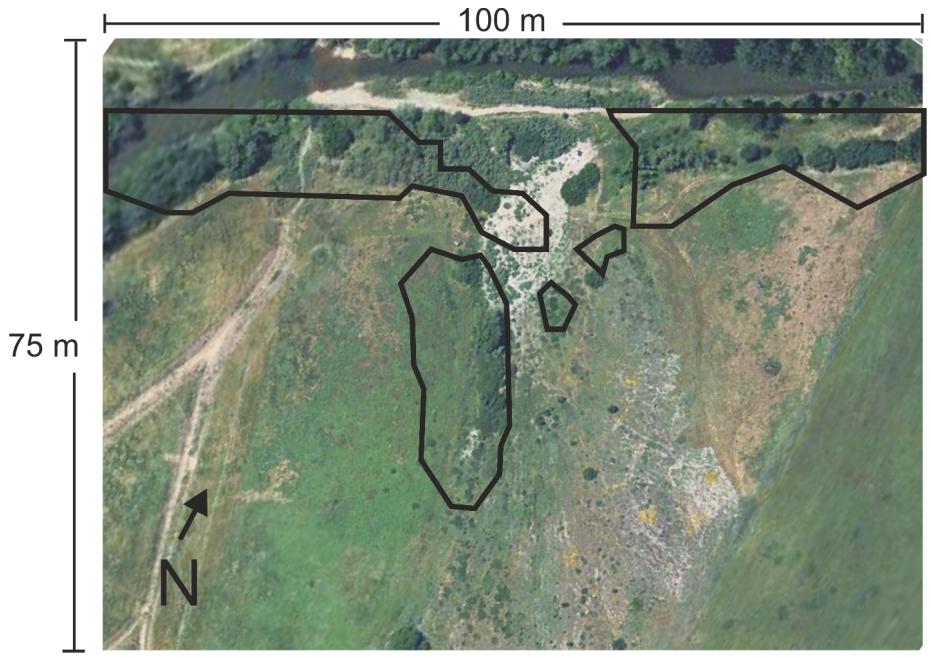

Figure 3.22: Areal photo of study site showing riparian vegetation. Black outlined shapes show the area where the model (rz10) simulated evapotranspiration nearly equal to the PET on 8/28/04.

Discrepancies among the simulated areas that could support riparian vegetation and the actual distribution of riparian vegetation may be due to many factors, such as errors in how sediment heterogeneity and the hydraulic properties were represented in the model, as well as seed dispersal and land use. Much of riparian vegetation that extends away from the river is bounded to the east by an agricultural plot that is plowed (Figure 3.22). However, the fields to the west are not plowed and yet despite the lower land surface elevation, no phreatophyte vegetation grows in this area.

3.4.6. Water budget

The water budget components analyzed in this study include river seepage into the vadose zone, perched groundwater seepage into the river, ET, changes in vadose-zone storage, and regional groundwater recharge. River seepage into the vadose zone was calculated in the model by summing all water leaving cells representing the river and

inundated floodplain boundary conditions. Similarly, perched groundwater seepage into the river was calculated by summing all water entering river and inundated floodplain cells. Regional groundwater recharge was calculated by summing all water that flowed out of the bottom of the layer that was at a minimum 2 m above the regional water table. This was done to minimize the inclusion of water that flowed upward in the capillary fringe during rises in the water table.

Table 3.7 shows the simulated mass balance components for realization rz23, rz10, and a homogeneous model. The K used in the homogeneous model was calculated by taking the geometric average of the three K values used in rz23. Unsaturated parameters for hydrofacies category 2 were used in the homogeneous model. Facies realization rz17 is excluded from the water budget because it was very similar to rz10. The water budget components clearly indicate that the heterogeneity at the Cosumnes enhances storage in the vadose zone, increases ET, and significantly decreases regional groundwater recharge as compared to the homogeneous model.

Facies realization rz23 simulated the greatest amount of river seepage into the vadose zone; however, rz10 simulated the greatest amount of perched groundwater discharge into the river (Table 3.7). Very little water seeped into the river in the homogeneous model (Table 3.7). The simulated ET for rz23 is more than 5 times greater than for the homogeneous model and the simulated ET for rz10 is about 2 times greater than the homogeneous model. The percentage of river seepage that is lost to ET was 65%, 46%, and 32% for models rz23, rz10, and the homogeneous model, respectively (Table 3.7). As described in the previous section, simulated ET distribution for rz10 was the most similar to the actual distribution of vegetation at the Cosumnes. Simulated ET

by riparian vegetation for the homogeneous model occurred within 14 m of the main channel and did not predict the growth of vegetation greater than 50 m from the main channel at the Cosumnes (Fig. 3.22).

Time series plots of the seepage components for rz23 and rz10 indicate large fluctuations in river seepage into the vadose zone corresponding to increases in channel depth, especially during floodplain inundation (January 2, February, 20, and February, 28); seepage increased by a factor of six during floodplain inundation (Fig. 3.23). Perched seepage into the river occurred during the recession limb of the larger flow events as bank storage flowed back into the river. Realization rz23 resulted in very little perched groundwater seepage between flow events, indicating that perched groundwater did not contribute significant baseflow in the river. Realization rz10 did result in about 7 m^3/d of perched groundwater discharge to the river between flow events that lasted through mid June.

The lack of perched groundwater that contributed to baseflow for rz23 and small amount contributed for rz10 is due the riverbed at the study site that primarily contained fine-grained sediment (hydrofacies categories 1 and 2). This is likely because the conditioning data used to develop the hydrofacies models consisted primarily of hydrofacies categories 1 and 2 near the channel surface (Fig. 3.5 and Appendix D). Perched groundwater discharge to the river for rz10 ceased in mid June and is consistent with the river going dry at this time.

Table 3.7: Simulated water budget for Cosumnes River study site totaled from January 4, 2004 to when flow ceased in the river near the end of June 2004.

	Seepage to river, in cubic meters	Seepage from river, in cubic meters	Evapo-transpiration, in cubic meters	% River seepage to vadose zone lost as ET	Recharge, in cubic meters	Change in vadose zone storage, in cubic meters	Mass balance error, in cubic meters
Rz23	1,280	10,100	6,564	65	459	1,786	11
Rz10	1,680	6,490	2,996	46	158	1,651	5
Homogeneous[1]	44	5,190	1,651	32	2,790	714	~0

[1]The K of the homogeneous model was calculated based on the geometric mean of the K values of the three hydrofacies of rz23.

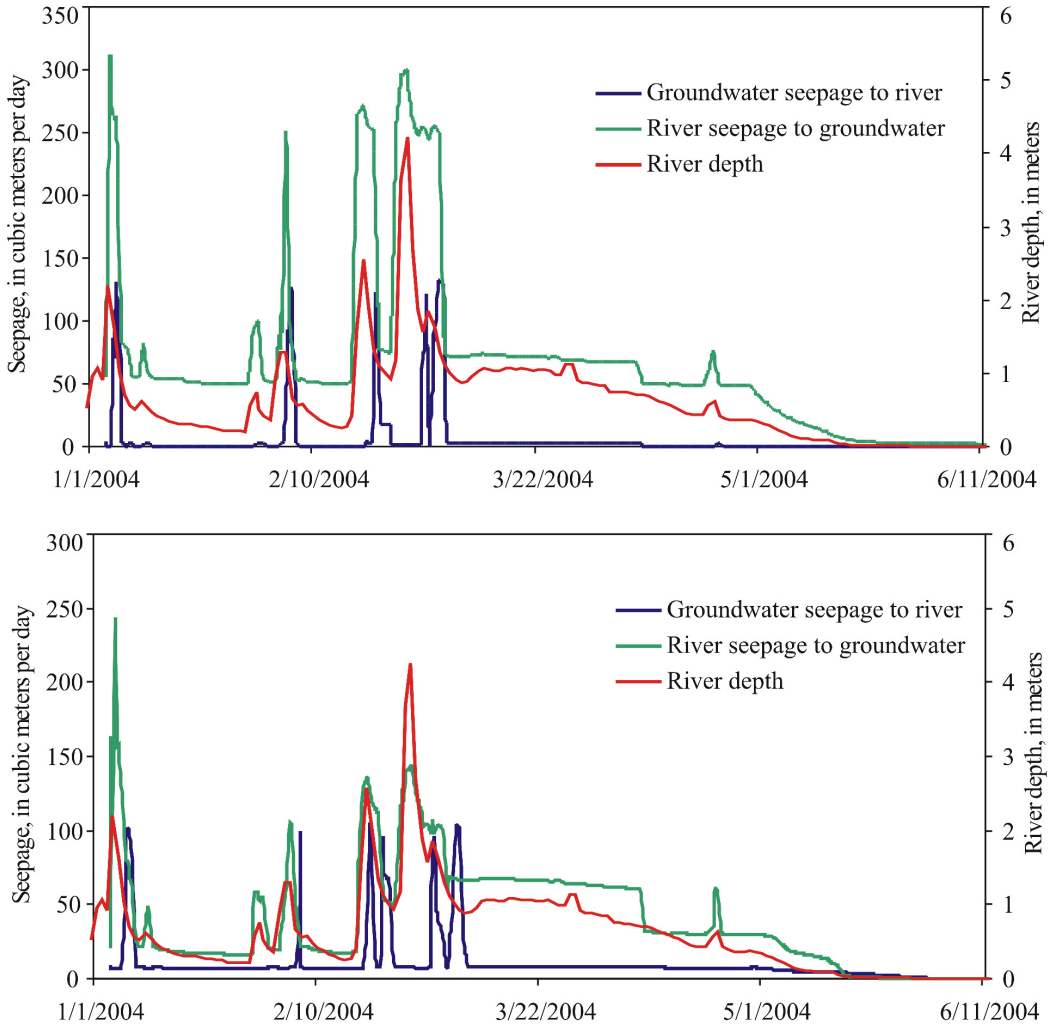

Figure 3.23: Seepage at the Cosumnes River, A. hydrofacies realization rz23, B. hydrofacies realization rz10.

3.5. DISCUSSION

The work presented in this chapter combined previously developed numerical modeling techniques to solve an original problem, perched-groundwater/surface-water interaction. Part of the original contribution of this work is the development of a modeling approach that combines stochastic methods of representing sediment heterogeneity surrounding a river with automated parameter estimation techniques. The modeling presented herein was used to address an important problem with stochastic models, which is how to apply them to predict field conditions. Often times, stochastic models result in a wide variety of solutions (one for each realization) and when averaged together (ensemble average), are unrealistic compared to field data. The geostatistical approach of Carle and Fogg (1997) partly solves this problem by conditioning the geostatistical model with observations of geology and hydrofacies distribution; however, this does not guarantee that simulated results by the flow model will agree with field data. Thus, "conditioning" the geostatistical models using parameter estimation techniques (inverse modeling) can help when applying stochastic models to simulate field conditions.

An improvement to the approach presented herein may be to use pilot-point parameter estimation (Doherty, 2004) with the sequential annealing algorithm in TPROGS to incorporate measures of flow model accuracy (e.g. values of the objective function) directly into the conditioning of the geostatistical model. In this approach, K values are estimated at specific location in the model domain using parameter estimation techniques and these values are then interpreted as a facies type based on the estimated K value. The resulting interpretation of the facies type and location could then be used to

condition the geostatistical model. This approach could significantly reduce the number of simulations required to find optimal facies distributions that honor observations of geology and other measurable quantities such as sediment temperature, water content and pressure.

Applying geostatistical methods to create models of sediment heterogeneity result in large amounts of uncertainty because only a small amount of information describing sediment heterogeneity at a field site can be measured. Consequently, there are an infinite number of equally probable geologic configurations that may result in large variations in model predictions. We conditioned the geostatistical model based on measured information to increase the similarity of the hydrofacies realizations. Despite conditioning, there was a large variance in the model predictions for different facies realizations (e.g., spread in the SSR values). Often in stochastic analyses, a large number of realizations are run and the ensemble of model results are averaged together. Rather than relying on the ensemble average we chose to examine a few of the facies realizations that provided the best fit between measured and simulated sediment temperatures and water contents. One drawback of this approach is that uncertainty in the flow model predictions due to uncertainty in the distribution of hydrofacies was not calculated because so few of the realization fit the measured data.

Another source of uncertainty in the model comes from how the hydrofacies were parameterized. We tried to combine direct measurements of sediment physical, thermal and hydraulic properties with observations of sediment temperature and water content to estimate some of the parameter values. However, several parameters were not measured and were calculated with large amounts of uncertainty, most notably the unsaturated flow

parameters. These parameters could have been included in the model inversions. However, experience indicates that this would have resulted in non-unique solutions, meaningless estimates of both the unsaturated flow parameters and the saturated K values, and would have required many more simulations. A sensitivity analysis on the unsaturated flow parameters would provide much needed insight regarding the effects of these parameters on the model predictions. However, this exercise is left for future work on this topic.

This study was the first to use automated parameter estimation with sediment temperatures as observation data within a 3-D non-isothermal variably-saturated flow model. Although the simulations required significant computing resources (individual simulations required 6-14 hours to run on a Xeon 3.2 GHz, 2.6 GB RAM computer), the inverse modeling results provided a useful method of estimating hydrofacies K-values and evaluating the individual hydrofacies models.

The use of sediment temperature data for estimating sediment K is an underused approach (Anderson, 2005). Sediment temperature beneath a river is dependent on the heat conduction and advection; however, the sediment K affects only the advective component of heat transport. Consequently, when K is small, which causes advection to be small, temperature does not provide useful information to differentiate small values of K from really small values of K. However, temperature worked well in the present study because it helped to define areas of high, medium or low amounts of heat advection corresponding to the three hydrofacies categories. It is likely that temperature is less useful where the channel is covered in hydrofaces category 1 (sandy clay) and advection beneath the channel is very small. The water content data provides additional

information, and the combination of temperature and water content seems to have provided unique estimates of K based on the 95% confidence intervals of the estimated K values for each hydrofacies.

An aspect of this work that deserves more attention is how the discrepancies between the simulated and measured sediment temperatures and water contents affect the overall results of this study. The two realizations analyzed in detail (rz10 and rz23) resulted in SSR values that varied by only 15%, whereas the magnitude of the budgets components varied by as much as 36% for these two models. More work should be done to analyze the variance in water budget predictions for additional realizations that result in relatively good fits to the measured temperature and water content data. Despite differences in water budget predictions, the general conclusions of the model results are the same. These conclusions are that sediment heterogeneity caused water to perch in the vadose zone, increased ET, and decreased regional groundwater recharge as compared to the homogeneous model.

3.6. CONCLUSIONS

Results of this study indicate that perched systems may have a profound effect on the hydrologic budget surrounding rivers where regional groundwater does not contribute the saturated region of the river. This is a significant result because perched systems are mostly ignored in ecological and water resource assessments of rivers. Perched systems can provide a shallow water table to support riparian vegetation. However, unlike the results of Chapter 2, the simulations presented in the chapter did not indicate that perched groundwater discharge to the river in our specific field site is sufficient to maintain flow during the dry season.

Floodplain inundation resulted in a six-fold increase in river seepage into the vadose zone. This suggests that floodplain inundation is a very efficient means of recharging perched groundwater. The channel at our study site was mostly covered with finer sediment, which limited the amount of seepage during low-flow conditions including perched groundwater seepage into the river. From a management perspective, perched groundwater at the study site has the potential to support more riparian vegetation, possibly through artificial recharge, but is likely not ideal for providing baseflow to the river. However, the work in Chapter 2 indicates that there is a potential for perched systems to provide substantial baseflow to the river over other locations of the river where the riverbed contains coarser sediment.

These results indicate that perched systems can significantly affect water availability to different ecological zones surrounding a river and therefore affect stream hydrology and ecosystem functioning. Perched systems also dramatically diminish vertical flow of river seepage to regional groundwater, which by inference also reduces the transport of solutes from surface water to regional groundwater. Because perched systems reduce vertical transport of solutes beneath surface water bodies, there presence in hydrogeologic systems may be beneficial for maintaining good water quality in regional aquifers used for drinking water supplies. For example, managing perched systems in Bangladesh where shallow aquifers are highly contaminated with arsenic could help reduce the vertical transport of arsenic into deeper aquifers that could possibly be used to supplement shallow groundwater used by humans.

Future modeling of the site at the Cosumnes using the model developed in this study may reveal additional insights regarding the hydrologic cycling near rivers. Specifically,

the residence times of water surrounding rivers could be further evaluated possibly by developing tracer tests using information gained from the model. Tracer tests could be especially useful for evaluating the residence time of water in perched aquifers.

3.7. REFERENCES

Anderson, M.P. (2005), Heat as a ground water tracer, vol. 43 no. 6 p.951-958.

Brunke, M. & Gonser ,T. (1997): The ecological significance of exchange processes between streams and groundwater. Freshwater Biology. 37, 1-33.

Busch, D.E., N.L. Ingraham, and S.D. Smith, (1992), Water uptake in woody riparian phreatophytes of the southwestern United States: a stable isotope study. Ecological Applications , 2, 450-459.

Carle, S. F. (1999), TPROGS – Transition Probability Geostatistical Software, Version 2.1, User manual, Hydrologic Sciences Graduate Group, University of California, Davis

Carle, S. F. and G. E. Fogg (1997), Modeling spatial variability with one and multidimensional continuous-lag Markov chains. Mathematical Geology 29, no. 7: 891-918.

Carle, S. F., E. M. La Bolle, G. S. Weissmann, D. Van Brocklin and G. E. Fogg (1998), Conditional simulation of hydrofacies architecture: a transition probability/Markov approach. In: G. S. Fraser, J. M. Davis (eds), Hydrogeologic Models of Sedimentary Aquifers, Concepts in Hydrogeology and Environmental Geology No. 1, SEPM (Society for Sedimentary Geology) Special Publication, 147-170.

Constantz, J., A. E. Stewart, R. G. Niswonger, and L. Sarma (2002), Analysis of temperature profiles for investigating stream losses beneath ephemeral channels, Water Resour. Res., 38 (12), 1316-1326.

Cooley, R.L. and Westphal,, J.A. (1974), An evaluation of the theory of ground-water and river-water interchange, Winnemucca reach of the Humboldt River, Nevada: Desert Research Institute, University of Nevada, Reno, Hydrology and Water Resources Publications No. 19, 74 p.

Cooper, D.J., D.M. Merritt, D.C. Andersen, and R.A. Chimner (1999) Factors controlling the establishment of Fremont cottonwood seedlings on the Upper Green Stream, USA, Regul. Streams : Res. Mgmt. 15: 419–440.

Correll, D.L., Jordan, T.E., Weller, D.E. (1997), Failure of agricultural riparian buffers to protect surface waters from groundwater nitrate contamination. In: Gibert, J., Mathieu, J., Fournier, F. (Eds.), Groundwater/Surface Water Ecotones: Biological and Hydrological Interactions and Management Options, Cambridge University Press, Cambridge, pp. 162–165.

Dahan, O., McDonald, E. V., and Young, M. H. (2003), Development of A Flexible TDR Probe for Deep Vadose Zone Monitoring. Vadose Zone Journal, vol. 2, 2, 270-275.

Department of Water Resources - California (DWR) (1974), Evaluation of ground water resources, Sacramento County, DWR Bulletin ; no. 118-3, The Dept. of Water Resources, Sacramento, 141 pages.

Deutsh, C.V., Geostatistical Reservoir Modeling, Oxford University Press, New York, 2002.

Doherty, John (2004), PEST: Model-Independent Parameter Estimation, Watermark Numerical Computing, Brisbane, Australia.

Dunlap, L.E. Lingren, R.J., and Carr, J.E. (1984), Prjected effects of ground-water withdrawals in the Arkansas River Valley, 1980-99, Hamilton and Kearny Counties, Southwestern Kansas: U.S. Geological Survey Water Resources Investigations Report 84-4082, 168 p.

Fariz, G., and A. Hatough-Bouran (1996), Water and population dynamics: case studies and policy implications, Eds. A. de Sherbnin and V. Domka, Washington, D.C.: American Association of Agricultural Sciences.

Feddes, R.A., E. Bresler, and S.P. Neuman (1974), Field test of a modified numerical model for water uptake by a root system, Water Resour. Res., vol. 10, no 6, 1199-1206.

Feddes, R.A. and P.A.C. Raats (2004), Parameterizing the soil-water-plant root system, in Unsaturated-Zone Modeling: Progress, Challenges and Applications, Papers for

the Frontis Workshop on Unsaturated-Zone Modeling: Progress, Challenges and Applications, Editors: R.A. Feddes; G.H. de Rooij and J.C. van Dam Wageningen, The Netherlands 3-5 October 2004.

Fleckenstein, J.H., Niswonger, R.G., and Fogg, G.E. (2005), Stream-Aquifer Interactions, Geologic Heterogeneity, and Low Flow Management, GROUNDWATER, Special issue from conference: MODFLOW and More 2003: Understanding through Modeling, Golden, CO.

Gardner, W.R. (1991), Modeling water uptake by roots. Irrig. Sci. vol. 12, 109-114.

Gutentag, E.D., F.J. Heimes, N.C. Krothe, R.R. Luckey, and J.B. Weeks (1984), Geohydrology of the High Plains Aquifer in parts of Colorado, Kansas, Nebraska, New Mexico, Oklahoma, South Dakota, Texas, and Wyoming, U. S. Geol. Surv. Prof. Pap., 1400-B, 63p.

Hopmans, J.W., and Bristow, K.L. (2002), Current capabilities and future needs of root water and nutrient uptake modeling. Advances in Agronomy, 77, 103-183.

Hopmans, J.W., and Dane, J.H. (1986), Thermal conductivity of two porous media as a function of water content, temperature, and density, Soil Science, vol. 142, no. 4, 187-195.

Krumbein, W.C. and L.L. Sloss (1963), Stratigraphy and Sedimentation, (2d ed.) San Francisco, W.H. Freeman and Company, 660 p.

Lapham, W.W. (1989), Use of temperature profiles beneath streams to determine rates of vertical ground-water flow and vertical hydraulic conductivity: U.S. Geological Survey Water-Supply Paper 2337, 35 p.

Mason, B., L.G. Berry (1968), Elements of mineralogy, San Francisco, W.H. Freeman and Company, 550 p.

Miall, A. D. (1996), The geology of fluvial deposits: sedimentary facies, basin analysis, and petroleum geology, Springer Verlag, Berlin.

Minasny, B., J. W. Hopmans, T. Harter, S. O. Eching, A. Tuli, and M. A. Denton, (2004) Neural networks prediction of soil hydraulic functions for alluvial soils using multistep outflow data, Soil Sci. Soc. Am. J. 68:417–429

Molz, F.J., (1981) Models of water transport in the soil-plant system: a review, Wat. Resour. Res. Vol. 17, no. 5 1245-1260

Molz, F.J., I. Remson, (1970) Extraction term models of soil moisture used by transpiring plants, Water Resour. Res., vol. 6, no. 5, 1346-1356.

Monteith, J.L. (1965), Evaporation and environment, Symposium of the Society for Experimental Biology, 29, 205-234.

Mualem, Y. (1976), A new model for predicting the hydraulic conductivity of unsaturated porous media: Water Resources Research, v. 12, p. 513-522.

Oaks, D.B. and Wilkinson, W.B. (1972) Modeing of groundwater and surface water systems: I-theoretical relationships between groundwater abstraction and baseflow, Great Britain, Reading Bridge House, Water Resources Board, no. 16, 37 p.

Piper, A. M. & Geological Survey (U.S.) (1939), Geology and ground-water hydrology of the Mokelumne area, California, USGS Water-supply paper 780., US Geological Survey, Washington, 230 p.

Prudic, D.E., 1989, Documentation of a computer program to simulate stream-aquifer relations using a modular, finite-difference, ground-water flow model: U.S. Geological Survey Open-File Report 88-729, 113 p.

Prudic, D.E. and Herman, ,M.E. (1996), Ground-water flow and simulated effects of development in Paradise Valley, a basin tributary to the Humboldt River in Humboldt County, Nevada, U.S. Geological Survey Professional Paper 1409-F, 92 p.

Pruess, K., C. Oldenburg, G. Moridis (1999), TOUGH2 user's guide, version 2.0, Report No. LBNL 43134, Ernest Orlando Lawrence Berkeley National Laboratory, Ca, USA.

Ritzi, R. W., D. F. Dominic, N. R. Brown, K. W. Kausch, P. J. McAlenney and M. J. Basial (1995), Hydrofacies Distribution and Correlation in the Miami Valley Aquifer System. Water Resour. Res. Vol. 31, no. 12: 3271-3281.

Ronan, A.D., D.E. Prudic, C.E. Thodal, and J.E. Constantz (1998), Field study of diurnal temperature effects of infiltration and variably-saturated flow beneath an ephemeral stream, Water Resour. Res., 34(9), 2137-2152.

Sawyer, J.O., Keeler-Wolf, T. (1995), A manual of California vegetation. California Native Plant Society Press. Sacramento, CA, 138 p.

Schaff, S.D., Pezeshki, S.R., Shields Jr, F.D. (2003), The effects of soil conditions on survival and growth of black willow cuttings, Environmental Management. 31(6):748-763.

Schnabel, R.R., Gburek, W.J., Stout, W.L. (1994), Evaluating riparian zone control on nitrogen entry into northeast streams, Ecosystems in the Humid US, Functions, Values and Management, National Association of Conservation Districts Washington DC, pp. 432–445.

Scott, M.L., Friedman, J.M., and Auble, G.T. (1996), Fluvial processes and the establishment of bottomland trees, Geomorphology, 14, 327–339.

Shlemon, R. J. (1998), Quaternary Geology of the Sacramento Area, Field Trip Guidebook, Association of Engineering Geologist, Sacramento Section, Sacramento, CA,

Snyder, K.A., D.G. Williams, and Gempko V.L. (1998), Water source determination for cottonwood, willow and mesquite in riparian forest stands. Pages 185-188, In Wood, E.F., A.G. Chebouni, D.C. Goodrich, D.J. Seo, and J.R. Zimmerman, technical coordinators. Proceedings from the Special Symposium on Hydrology. American Meteorological Society, Boston, Massachusetts.

Tabacchi, E., L. Lambs, H. Guilloy, A. Planty-Tabacchi, E. Muller, H. Decamps (2000), Impacts of riparian vegetation on hydrological processes, Hydrol. Process., 14, 2959-2976.

Van Genuchten, M. Th. (1980) A closed form equation for predicting the hydraulic conductivity of unsaturated soils. Soil Sci Am J, 44, p. 892-898.

Van Genuchten, M.T. and Hoffman, G.J. (1984), Analysis of crop salt tolerance data. In: Shainberg, I. and Shalhevet, J. eds. Soil salinity under irrigation: processes and management. Springer, Berlin, 258-271. Ecological Studies no. 51.

Van Genuchten, M.T. (1987), A numerical model for water and solute movement in and below the root zone. USDA-ARS, US Salinity Laboratory, Streamside. Research Report no. 121.

Vionnet, Leticia BG. And Thomas Maddock III, (1992), Modeling ground-water flow and surface/ground-water interactions for the San Pedro Basin—Part 1—Mexican border to Fairbank, Arizona. Department of Hydrology and Water Resources. HWR No. 92-010.

Vrugt, J.A., J.W. Hopmans, J. Simunek (2001a), Calibration of a two-dimensional root-water-uptake model. Soil Sci. Soc. Am. J., vol. 64, pp1027-1037.

Weissmann, G. S. and G. E. Fogg (1999), Multi-scale alluvial fan heterogeneity modeled with transition probability geostatistics in a sequence stratigraphic framework. Journal of Hydrology 226, no. 1-2: 48-65

Wesseling, J.G., 1991. Meerjarige simulatie van grondwaterstroming voor verschillende bodemprofielen, grondwatertrappen en gewassen met het model SWATRE. DLO-Staring Centrum, Wageningen. Rapport / DLO-Staring Centrum no. 152.

Whisler, F.D., A. Klute, and R.J. Millington, (1968) Analysis of steady state evapotranspiration from a soil column, Soil. Sci. Soc. Am. Proc., 32, 167-174, 1968.

Whitehead, D. and Dye, P.J. (1998), Regulation of stomatal conductance and transpiration in forest canopies. Tree Physiology, 18 (8/9), 633-644.

Williams, M., Rastetter, E.B., Fernandes, D.N., et al. (1996), Modeling the soil plantatmosphere continuum in a Quercus-Acer stand at Harvard Forest: the regulation of stomatal conductance by light, nitrogen and soil/plant hydraulic properties. Plant, Cell and Environment, 19 (8), 911-927.

Wood, W.W. (2003), A Fresh Water Odyssey: some observations on the global resource, Groundwater, vol. 41, pp 300-305.

Zuo, Q. and R. Zhang (2002), Estimating root-water-uptake using an inverse method, Soil Science, vol. 176, no. 9, 561-571.

CHAPTER 4: PERCHED SYSTEMS: IMPLICATIONS FOR ECOHYDROLOGY AND FLOODPLAIN MANAGEMENT

4.1. INTRODUCTION

The interdependence of hydrology and the distribution, structure, and function of ecosystems at the catchment scale has been termed ecohydrology (Zalewski, 2000). Ecohydrology encompasses how water and ecosystems can be managed to enhance processes that are beneficial to water quality and the health of aquatic and terrestrial organisms. Perched systems could be important to ecohydrology because they are components of the hydrologic budget in some systems.

While the interactions within any ecosystem may be complex and difficult to describe, the role of perched systems to aquatic and riparian habitats are quantifiable and important. In Chapters two and three, the role of perched systems in stream and riparian ecoystems was addressed. However, perched systems may play another important role in ecosystem function by connecting the surface and subsurface and making possible the movement of water and chemicals through the hyporeic zone. In addition to providing water during periods of low availability, perched systems also facilitate physical and microbial transformation of stream water (e.g. nutrient cycling), thereby changing water composition. Together, these roles make perched systems an important asset to a managed system. In this chapter, the context for managing perched systems is provided.

Chapter 2 used conceptual numerical modeling to estimate the amount of baseflow that perched systems could provide to streams. The work in Chapter 3 put the hypothetical results of Chapter 2 in perspective with a real system; however, this small study site on the Cosumnes River likely represented only a subset of perched system

conditions and their relations to the hydrology of that system. In the present chapter, we consider the possibility that the various hypothetical simulations presented in Chapter 2 may represent different regions of a stream or river. Using the results of Chapter 2, we consider whether perched systems could sustain systems where regional groundwater no longer or only partially contributes to the saturated region of a stream. We also introduce how perched systems may benefit ecosystems that function in streams that are ephemeral.

The influences of perched systems on riparian vegetation are also discussed. Perched systems occur beneath rivers underlain by a vadose zone, and accordingly may be associated with systems that are stressed by limited water availability. For this reason, in addition to addressing how perched systems may benefit riparian vegetation and the corresponding benefit to the entire ecosystem, we briefly consider how riparian vegetation may decrease streamflow and negatively affect aquatic organisms. This point is important in how it relates to the management of perched systems, possibly for enhancing riparian ecosystems.

Chapter 1 introduced the various ecological zones surrounding a stream, which included the hyporheic zone. The analysis in Chapters 2 and 3 did not explicitly evaluate the influence of perched systems on the hyporheic zone. However, by demonstrating that perched systems can enhance lateral hydraulic gradients and seepage into a stream, we showed that perched system can provide the necessary hydraulic conditions to support a hyporheic zone. Accordingly, we consider perched systems as surrogates for regional groundwater by supporting hyporheic zones.

This chapter concludes with areas for future work and directs how water-resource management might be adapted to include the possible benefits of perched systems to ecosystems and water resources development.

4.2. AQUATIC AND TERRESTRIAL WATER REQUIREMENTS

4.2.1. Stream baseflow

Perched systems can maintain flow in a stream when hydrogeologic conditions are favorable. For example, in the hypothetical simulations of Chapter 2 a perching layer that extended beneath a 1-km length of stream caused between 10 and 50 l/s of perched system seepage into the stream. These flow rates could provide enough water to support migrating salmon and other organisms living in some streams depending on channel geometries and streamflow velocities. However, even for ideal perching conditions, the flow provided by a single perched system will seep back into the subsurface where perching layers do not exist. For streamflow to be continuous over the entire length of a stream, water must be provided by other sources such as from other perched systems, regional aquifers, or tributary streams. Accordingly, to examine the overall benefit of perched systems to stream ecosystems, the hydrogeologic setting of the entire length of a stream should be considered.

Geologic conditions that are ideal for the existence of perched systems near streams include high-K channel deposits overlying a low-K perching unit. Previous studies that have examined driller's logs and that have mapped the geology of alluvial depositional environments indicate that laterally extensive low-K deposits in juxtaposition with coarse channel deposits are a common occurrence (Johnson et al., 1968; Weissman and Fogg; 1999; Fleckenstein et al., 2005). Streams often flow over heterogeneous alluvial sediment

and perched systems may be a common occurrence where regional groundwater does not contribute to the saturated region of a stream.

In this chapter we consider two possible hydrogeologic conditions for systems that are supported by perched systems. One possible condition occurs where streams receive no baseflow from regional groundwater and consequently, flow that connects through the entire channel occurs only during periods of high runoff. The other possible condition is described by systems that have historically been perennial but groundwater pumping, diversions and climate change have caused reductions in baseflow contributed by regional-groundwater seepage. These two conditions may be considered end members that bound a range of possible hydrogeologic systems that could be benefited by perched systems.

For systems where the entire length of a stream is underlain by a vadose zone, flow provided by perched systems could, at most, generate streamflow where perched conditions exist. Flowing water would occur only for ideal geologic conditions that result in quantities of perched groundwater seepage similar to the highest values estimated in Chapter 2 (10-50 l/s). These regions of flow could support aquatic ecosystems that expand and move to other locations along a stream during periods of runoff. Managing perched systems in these types of systems by banking water during periods of runoff could significantly enhance ecosystem integrity.

If such a system was benefited by the presence of perched systems that were less ideal for providing baseflow, seepage may not be high enough for water to flow in the channel. However, perched systems may still provide aquatic habitat. For example, as runoff recedes in an ephemeral stream, water is left in depressions of the channel to form

pools. Without the benefit of a perched system, these pools quickly dry out due to evaporation and seepage into the subsurface. Perched groundwater seepage into a stream can persist for longer than 6 months following a streamflow event for a variety of hydrogeologic conditions (Chapter 2). Perched systems could maintain pools in ephemeral streams throughout a dry season even for moderately low seepage rates. Pools in ephemeral streams that are supplied by regional groundwater have been identified previously in the literature for providing important dry-season refuges for aquatic organisms, including fish (Erskine et al., 2005).

Often times, aquatic ecosystems in ephemeral streams are physiologically adapted to a higher degree of water stress. However, ecosystems in perennial streams could be very sensitive to stress caused by decreased water availability. Thus, small changes in water availability may result in drastic shifts in ecosystem community structure. Perched systems could potentially prevent drastic changes or damages to stream ecosystems by providing water during critical periods of water stress.

Systems that may receive the greatest benefit from perched systems are those that are still partially in contact with regional groundwater in some areas and that support ecosystems accustomed to perennial stream flow. Perched systems may benefit these systems by providing supplemental streamflow and by decreasing seepage losses where regional groundwater levels are well below the elevation of the streambed. Supplemental streamflow provided by perched groundwater, possibly enhanced by management strategies, could make an important difference for sustaining aquatic habitat in water-stressed perennial systems.

4.2.2. Riparian vegetation

Ecohydrology has often described the interrelationships between hydrology and vegetation (Rodriguez-Iturbe, 2000; Rains et al., 2004). Riparian vegetation is beneficial to river ecosystems because they provide habitat for river fauna, enhance nutrient cycling, reduce sediment load, and regulate stream temperatures by providing shade (Brunke and Gonser, 1997).

Groundwater-level decline can result in shifts in community population structure due to variations in plant tolerance to water table depth and sediment saturations (Stromberg et al., 1996). Species of riparian vegetation that are obligate phreatophytes are especially sensitive to regional groundwater level decline. An example is when woody vegetation with broad canopies, such as willow and cottonwood, are replaced by low lying shrubs such as tamarix that are physiologically adapted to a higher degree of water stress (Stromberg et al., 1996). These shifts occur when water availability is diminished below some threshold, such as when water tables fall below the riparian root zone. Organisms adapted to canopy vegetation often cannot live in low-lying shrubs and changes in vegetation type may be accompanied by shifts in the entire riparian ecosystem community structure.

Perched systems could potentially lessen the effects of regional groundwater level decline on phreatophyte vegetation (Chapter 3). Model results indicated that low-K deposits in the vadose zone can saturate the root zone of riparian vegetation near a river and alleviate water stress in the absence of a regional water table. These results are supported by the presence of willows of various ages growing along the Cosumnes greater than 50 m from the river where regional groundwater levels are greater than 15 m below land surface. However, there are unanswered questions regarding whether

increasing the growth of riparian vegetation in water-stressed environments will be beneficial to aquatic organisms.

Despite the large body of work that describes the interrelationships between riparian vegetation, groundwater and surface water, the effects of riparian vegetation on overdeveloped water supplies is an issue of current study. In highly stressed systems, riparian vegetation has the potential to negatively impact stream organisms through competition for available water. However, there is no research that supports this assertion. The results in Chapter 2 indicate that riparian vegetation may reduce potential benefits of perched systems by diminishing the amount seepage into a stream by 30%. Additionally, the results from Chapter 3 indicated that for a 1-year period the amount of water lost to evapotranspiration (ET) could be as high as 46 to 65 % of the stream seepage into the vadose zone at the Cosumnes. Accordingly, management of perched systems to increase riparian vegetation should consider the sustainability of increasing demands for water.

Riparian vegetation may also increase water availability through groundwater recharge during flooding by slowing peak flows and increasing the time during floodplain inundation. The results of Chapter 3 indicate the floodplain inundation is likely very important for recharging perched systems. Depending on the rate of ET losses during low flow periods when water availability is most critical, the effect of riparian vegetation may or may not enhance overall water availability. The simulation modeling techniques presented in Chapter 3 could be useful for quantifying the net effects of ET for determining whether or not perched systems should be managed to enhance the growth or riparian vegetation in a particular system.

4.3. CONNECTIVITY BETWEEN RIVER AND SUBSURFACE ECOSYSTEMS

Chapters 2 and 3 did not address explicitly how perched systems might benefit the hyporheic zone. However, the modeling results of Chapters 2 and 3 indicate that perched systems can create strong lateral and upward hydraulic gradients, as evidenced by the simulated quantities of perched groundwater seepage into a stream. More detailed analysis of hyporheic zone processes are required to provide a detailed description of how perched systems might benefit these systems. However, the present work offers a foundation upon which future work can be developed.

Concepts discussed in the previous section relate solely to potential benefits of perched system hydrology by increasing water availability to aquatic and terrestrial habitats. The traditional definition of an ecosystem includes biotic and abiotic interrelationships. Biotic and abiotic transformation of components of water may also influence water quality.

In addition to understanding the effects perched systems have on their related stream and riparian habitats, it is important also to understand how the perched systems affect water composition and quality. Another important aspect of ecohydrology concerns how ecosystems affect hydrology. For example, ecosystems can change the quality of water when microbes oxidize and reduce organic and inorganic compounds that are dissolved in water. Perched systems have the potential to be important for nutrient cycling and temperature moderation of stream water by providing connectivity among stream and subterranean habitats.

The hyporheic zone is recognized as providing a high degree of connectivity between streams and the subsurface and is characterized by gradients in pressure,

temperature and chemicals (Brunke and Gonser, 1997). Movement of water through the hyporheic zone are responsible for transferring heat and chemical energy between stream and subterranean organisms. Important metabolic reactions occur in the hyporheic zone that improves surface-water quality and ecosystem integrity.

Connectivity between surface and subterranean habitats occurs only when seepage occurs both from the subsurface into the stream and from the stream into the subsurface. Bidirectional seepage is caused by the influence of a regional groundwater system that exerts pressures beneath a stream that exceed pressures exerted by the stream water. Fluxes of water and chemicals between a stream and the hyporheic zone may be enhanced by hydraulic gradients caused by the streambed topography, slope, and stream velocity and stream depth. However, without the influence of groundwater, only minimal amounts of water will seep back into a stream regardless of streamflow and geomorphic conditions. Consequently, a hyporheic zone cannot exist without the lateral hydraulic gradients that are created by groundwater flowing directly beneath a stream.

Because groundwater is required for a hyporheic zone to exist, regional-groundwater level decline may diminish connectivity between stream and subterranean zones. Where there are extensive perching layers beneath a stream, pressures created by perched systems may be strong enough to maintain a hyporheic zone. Thus, perched systems may function as a surrogate for regional groundwater to support hyporheic zones and maintain connectivity among stream and subterranean ecosystems.

The idea that perched systems can support hyporheic zones leads to the possibility of studying hyporheic flow in streams not supported by regional groundwater. The study of hyporheic zones has only considered alpine streams and small to medium streams in

humid environments (Brunke and Gonser, 1997). Perched systems and other hydrogeologic conditions such as spring flow likely create regions in ephemeral streams where hyporheic zones exist. An area for future research is on hyporheic-zone processes in ephemeral streams such as in semi-arid environments and in systems where regional groundwater levels have declined.

4.4. MANAGING PERCHED SYSTEMS

Conceptually, perched systems represent storage reservoirs beneath streams. Similar to regional groundwater, these systems can be very beneficial because they store water beneath the ground where water is insolated from the influence of high temperatures at the surface. However, as with regional aquifers, perched systems are susceptible to contamination that could compromise their benefits to streams or other surface-water systems. Perched systems are also susceptible to groundwater pumping where regional groundwater levels have declined. Wells that are screened within a perched system may inadvertently drain a perched system beneath a stream and increase seepage losses from a stream. Determining the potential of perched systems for benefiting a stream system provides a basis for managing and protecting this resource.

Water-resource management has, in some cases, adapted to try and consider the natural environment to sustain ecosystems while supplying enough water for human consumption. However, the role of ecohydrology in water-resource management is largely dependent on politics and conflicting perceptions regarding the value of ecosystems. Perched systems are likely not valuable for providing water for human consumption directly. Thus, many of the political difficulties that are encountered while

trying to preserve regional groundwater for ecosystem integrity will not apply to the preservation of perched systems.

Water-resource management of surface water systems may be enhanced by using perched systems to store water during periods of high water availability for use during dry periods, similar to groundwater banking or surface reservoirs. The reason this seemingly obvious concept is important is that presently, vadose zones that contain perched systems are not considered useful for storing water. Thus, the first step toward managing perched systems is to change our conventional thinking regarding vadose zone hydrology. Then it is easy consider that many of the techniques and hurdles associated with water banking to recharge regional groundwater systems may be applied to recharge perched systems. Possibly the most important aspect of managing perched systems will be to develop methods for locating perched systems and identifying ideal hydrogeologic conditions for their enhancement.

Management activities that may enhance the benefits of perched systems will likely have variable degrees of success depending on the system. The clearest opportunity is to recharge perched systems by enhancing floodplain inundation. For example, installing sluice gates where constructed levees are located could enhance floodplain inundation. The gates could be opened during flooding and then closed again before water drains back into the channel. Of course, these activities have to be balanced by considering other possible consequences. Other options for recharging perched systems include streamflow augmentation, shallow well injection, and infiltration basins.

Perched systems are likely to be relatively sensitive to changes in climate. Unlike regional aquifers, perched systems are much more limited in storage. The residence time

for water in perched systems storage is typically much shorter than for regional aquifers storage. Perched systems probably rely on year-to-year recharge and are likely much more sensitive to changes in climate. Relying heavily on perched systems for providing water to streams may become problematic during periods of drought.

As regional groundwater levels continue to decline worldwide, the potential of perched systems for mitigating the resulting loss of stream ecosystems will become more apparent. The present work provides a limited description of the physics of perched systems and their potential for being important components of hydrologic systems. Nonetheless, this work provides a basis for further study of perched system and the development of management programs for the maintenance and restoration of stream ecosystem integrity.

4.5. REFERENCES

Brunke, M. and Gonser ,T. (1997): The ecological significance of exchange processes between streams and groundwater. Freshwater Biology. 37, 1-33.

Erskine, W. D., Saynor, M. J., Erskine, L., Evans, K. G., and Moliere, D. R. (2005), A preliminary typology of Australian tropical rivers and implications for fish community ecology. Marine and Freshwater Research 56, 253–267.

Fleckenstein, J.H., Niswonger, R.G., and Fogg, G.E. (2005), Stream-Aquifer Interactions, Geologic Heterogeneity, and Low Flow Management, GROUNDWATER, Special issue from conference: MODFLOW and More 2003: Understanding through Modeling, Golden, CO.

Johnson, A.I., Moston, R.P., and Morris, D.A. (1968), Physical and hydrologic properties of water-bearing deposits in sibsiding areas in Central California, U.S.Geol. Survey Prof. Paper 497-A, 71 p.

Rains, M.C., Mount, J.F., and Larsen, E.W. (2004), Simulated changes in shallow groundwater and vegetation distributions under different reservoir operations scenarios. Ecological Applications 14(1):192-207.

Rains, M.C., Fogg, G.E., Harter, T., Dahlgren, R.A., and Williamson, R.J., (In Press) The role of perched aquifers in hydrological connectivity and biogeochemical processes in vernal pool landscapes, Central Valley, California. Hydrological Processes vol. 20, no. 1, p. xx.

Rodriguez-Iturbe, I. (2000), Ecohydrology: a hydrologic perspective of climate–soil vegetation dynamics. Wat. Resour. Res. 36, 3–9.

Stromberg, J.C., Tiller, R., Richter, B. (1996), Effects of ground water decline on riparian vegetation of semi-arid regions: The San Pedro River, AZ. Ecological Applications 6, 113-131.

Weissmann, G. S. and G. E. Fogg (1999), Multi-scale alluvial fan heterogeneity modeled with transition probability geostatistics in a sequence stratigraphic framework, Journal of Hydrology 226(1-2), p. 48-65.

Zalewski, M. (2000), Ecohydrology—the scientific background to use ecosystem properties as management tools toward sustainability of water resources. Ecol. Engng 16, 1–8.

APPENDIX A: PLOTS OF PERCHED WATER TABLES SIMULATED IN CHAPTER 2

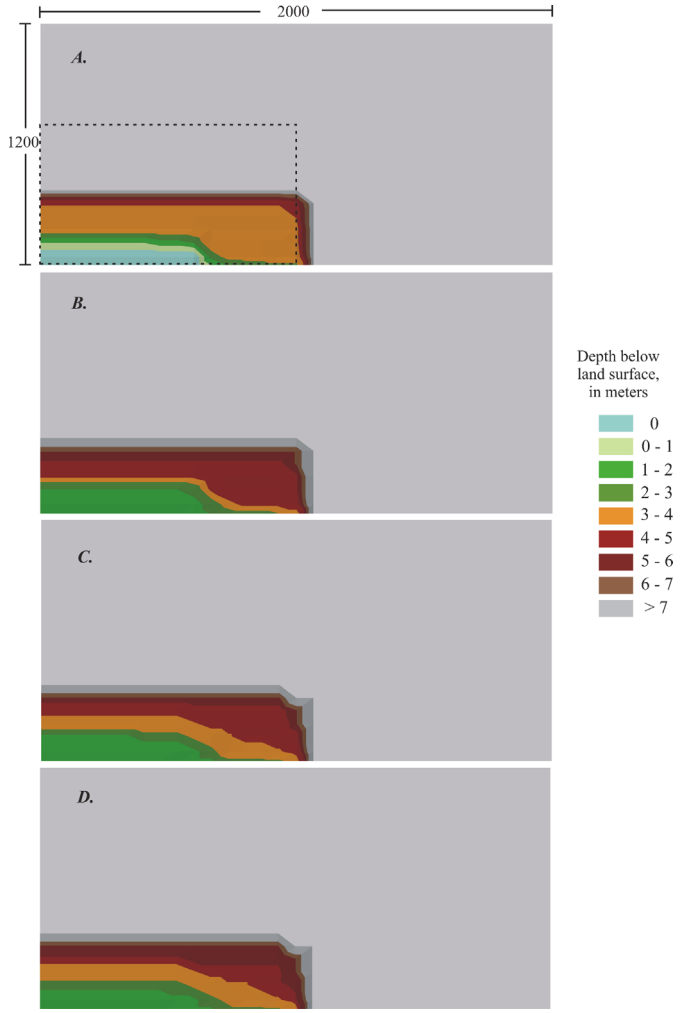

Perched water table depths for model scenario 1 with a coarse sediment K = 0.83 m/d and a perching unit K = 5.0×10^{-6}, after A. 0 days; B. 58 days; C. 173 days; D. 243 days. Black dashed line shows the footprint of the perching layer and the gray area shows the model domain.

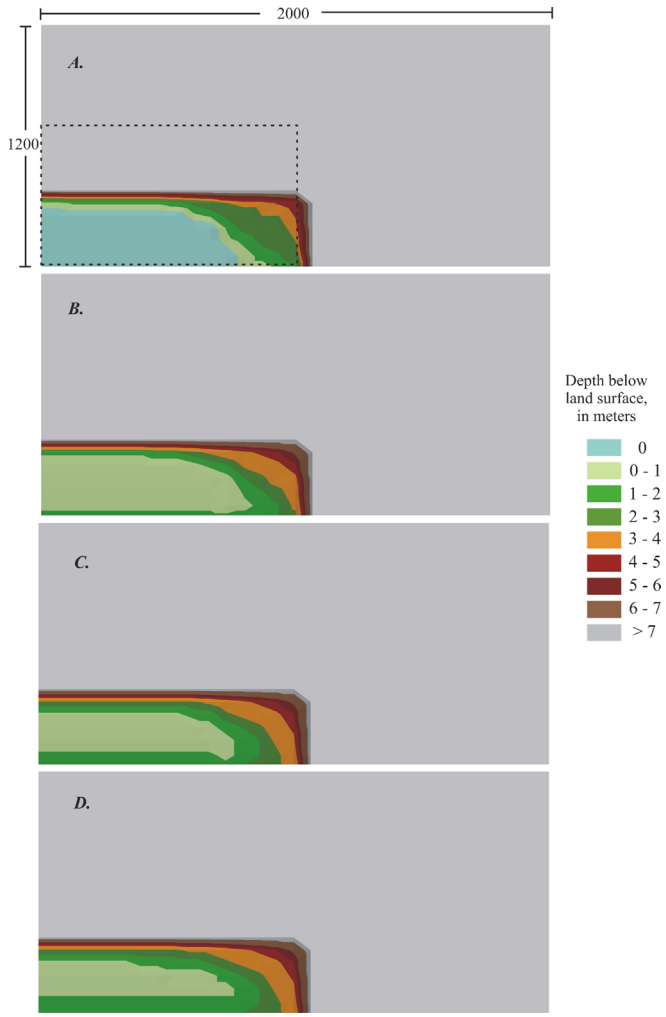

Perched water table depths for model scenario 2 with a coarse sediment K = 5.81 m/d and a perching unit K = 5.0×10^{-6}, after A. 0 days; B. 58 days; C. 173 days; D. 243 days. Black dashed line shows the footprint of the perching layer and the gray area shows the model domain.

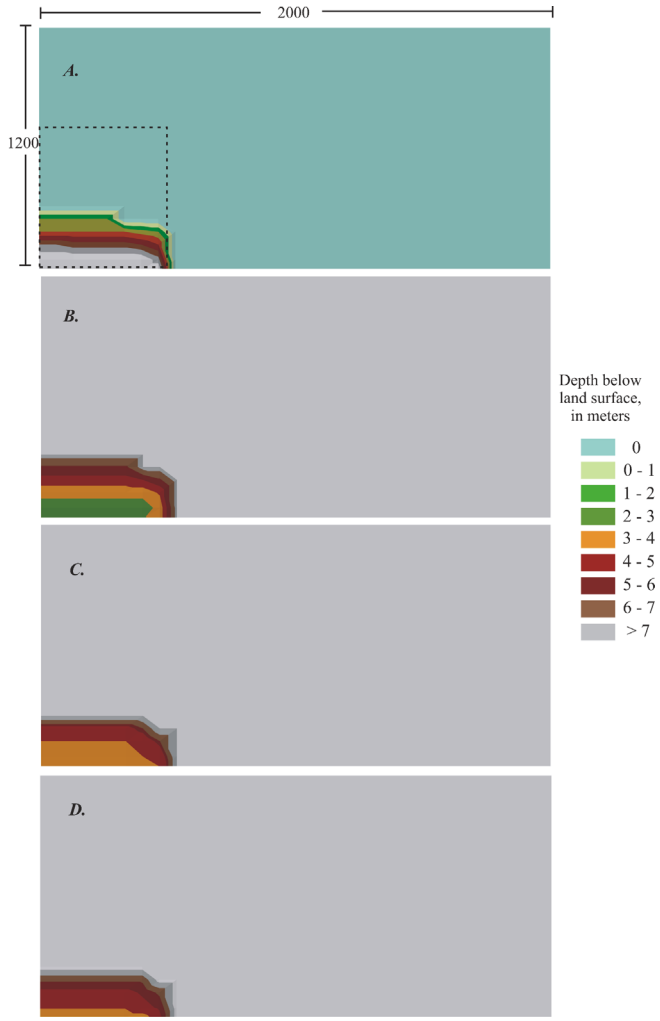

Perched water table depths for model scenario 7 with a 200 m long perching layer, a coarse sediment K = 0.83 m/d, and a perching unit K = 5.0×10^{-4}, after A. 0 days; B. 58 days; C. 173 days; D. 243 days. Black dashed line shows the footprint of the perching layer and the gray area shows the model domain.

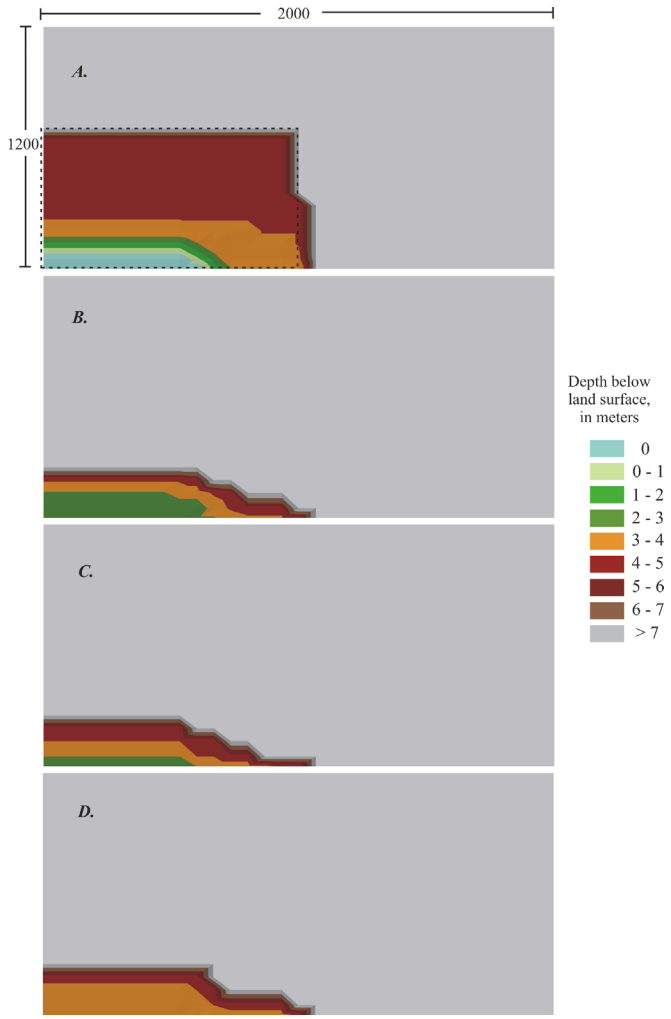

Perched water table depths for model scenario 8 with a perching layer 2.5 meters below land surface, a coarse sediment K = 0.83 m/d, and a perching unit K = 5.0×10^{-4}, after A. 0 days; B. 58 days; C. 173 days; D. 243 days. Black dashed line shows the footprint of the perching layer and the gray area shows the model domain.

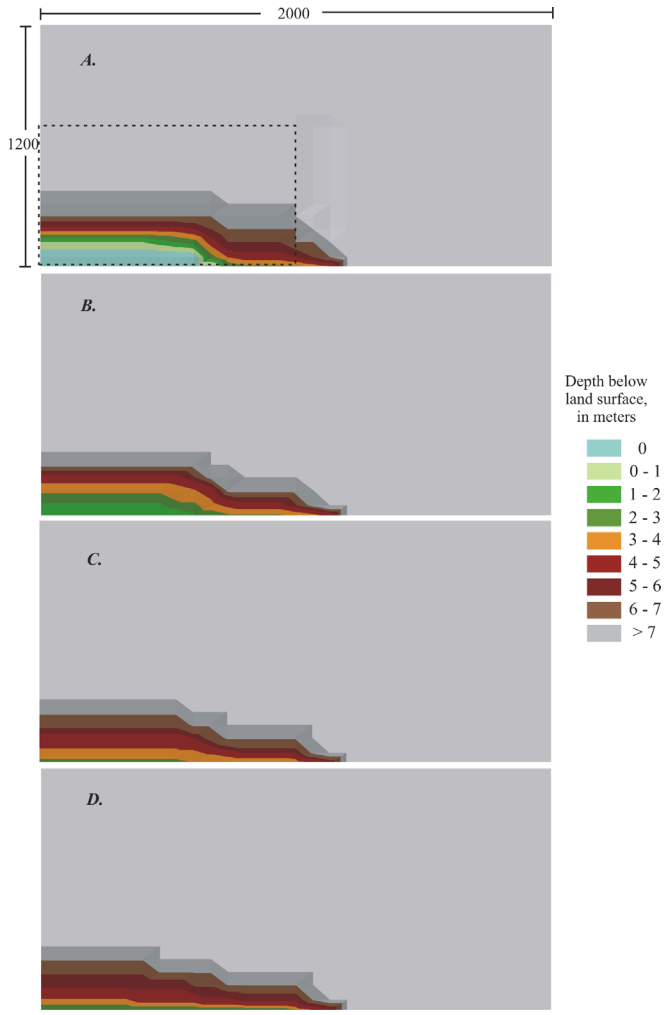

Perched water table depths for model scenario 9 with a perching layer 5.5 meters below land surface, a coarse sediment K = 0.83 m/d, and a perching unit K = 5.0×10^{-4}, after A. 0 days; B. 58 days; C. 173 days; D. 243 days. Black dashed line shows the footprint of the perching layer and the gray area shows the model domain.

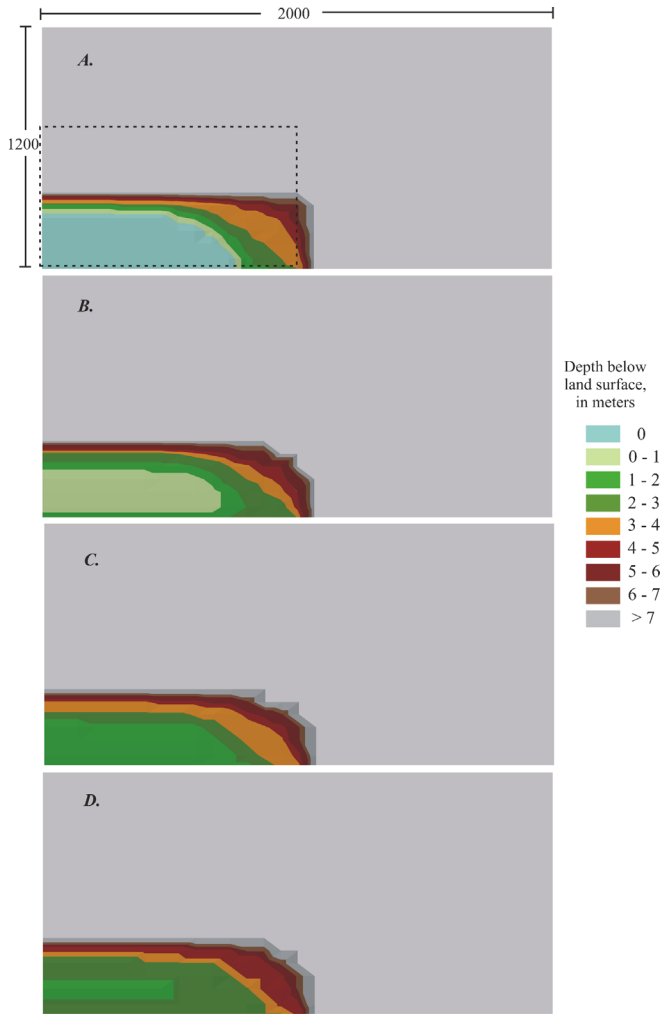

Perched water table depths for model scenario 10, which is the same as scenario 1 with ET, a coarse sediment K = 0.83 m/d, and a perching unit K = 5.0×10^{-4}, after A. 0 days; B. 58 days; C. 173 days; D. 243 days. Black dashed line shows the footprint of the perching layer and the gray area shows the model domain.

APPENDIX B: LABORATORY MEASUREMENTS OF SATURATED HYDRAULIC CONDUCTIVITY USING THE FALLING HEAD METHOD

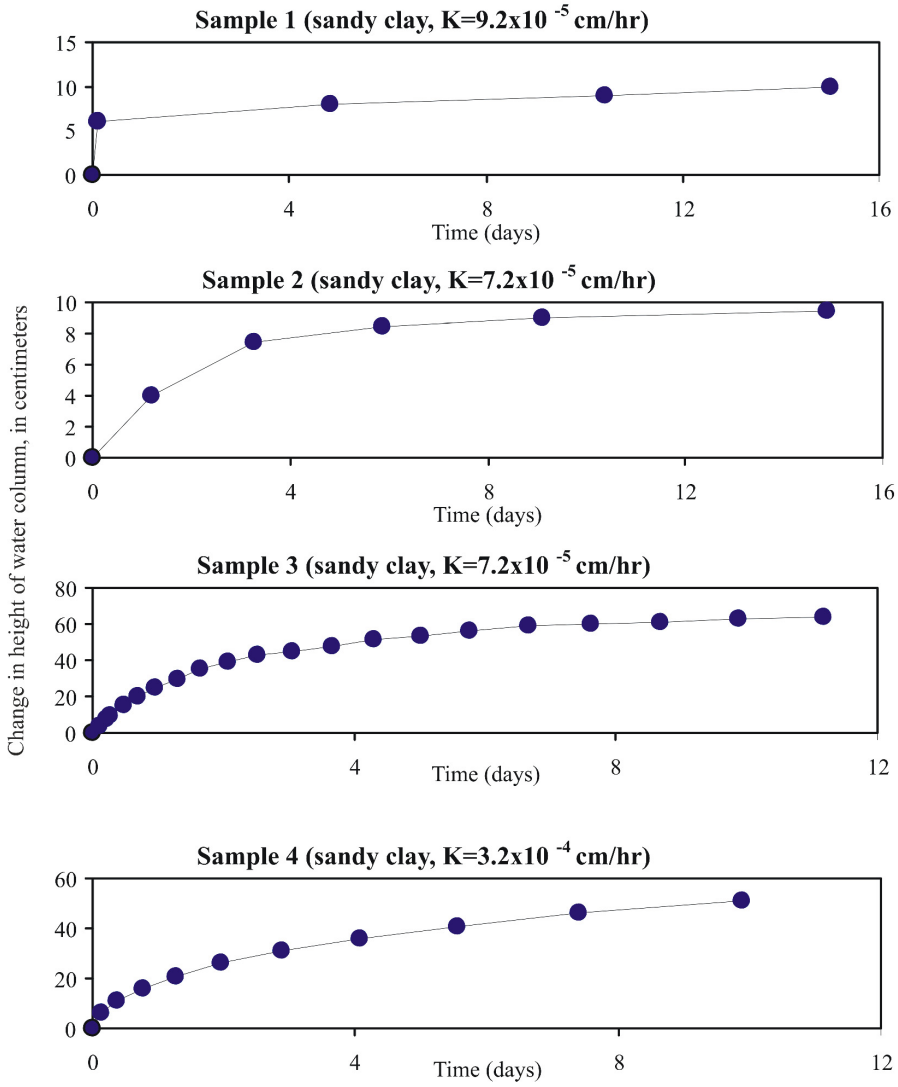

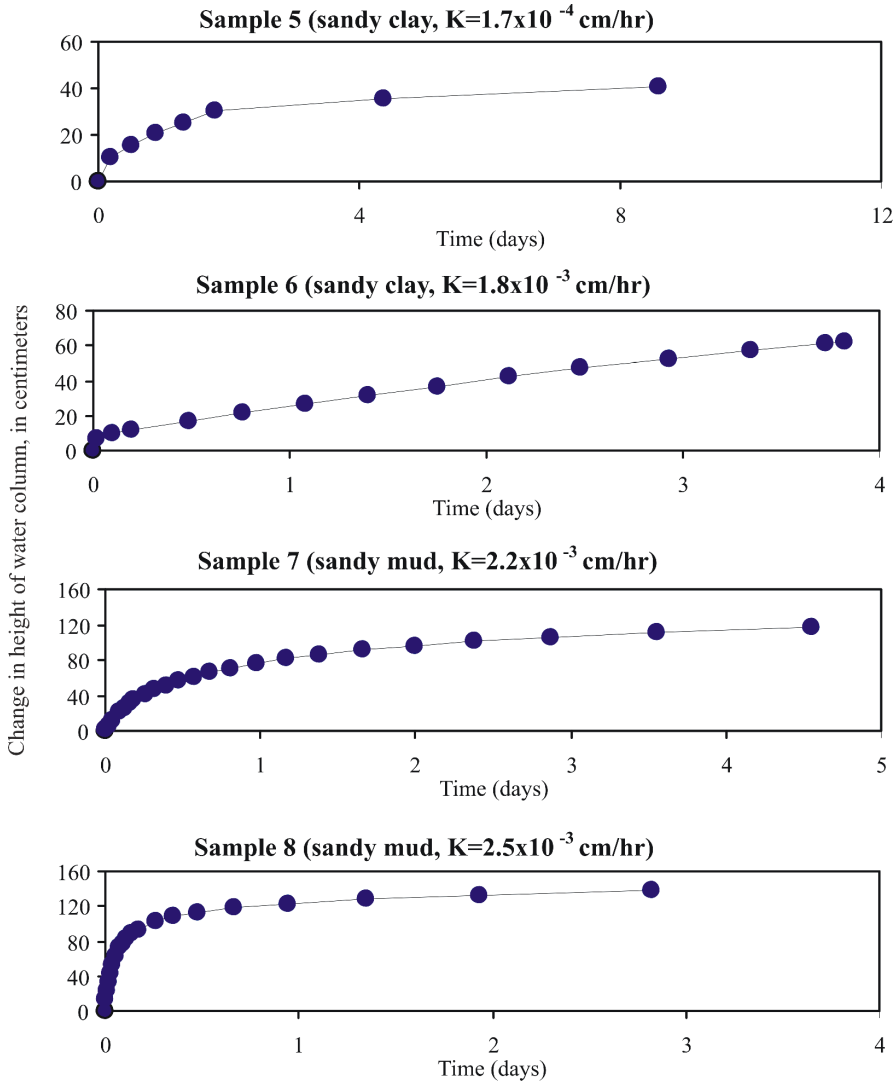
Sample 5 (sandy clay, K=1.7x10 -4 cm/hr)
60
40
20
0
0
4
8
12
Time (days)
Sample 6 (sandy clay, K=1.8x10 -3 cm/hr)
Change in height of water column, in centimeters
80
60
40
20
0
0
1
2
3
4
Time (days)
Sample 7 (sandy mud, K=2.2x10 -3 cm/hr)
160
120
80
40
0
0
1
2
3
4
5
Time (days)
Sample 8 (sandy mud, K=2.5x10 -3 cm/hr)
160
120
80
40
0
0
1
2
3
4
Time (days)

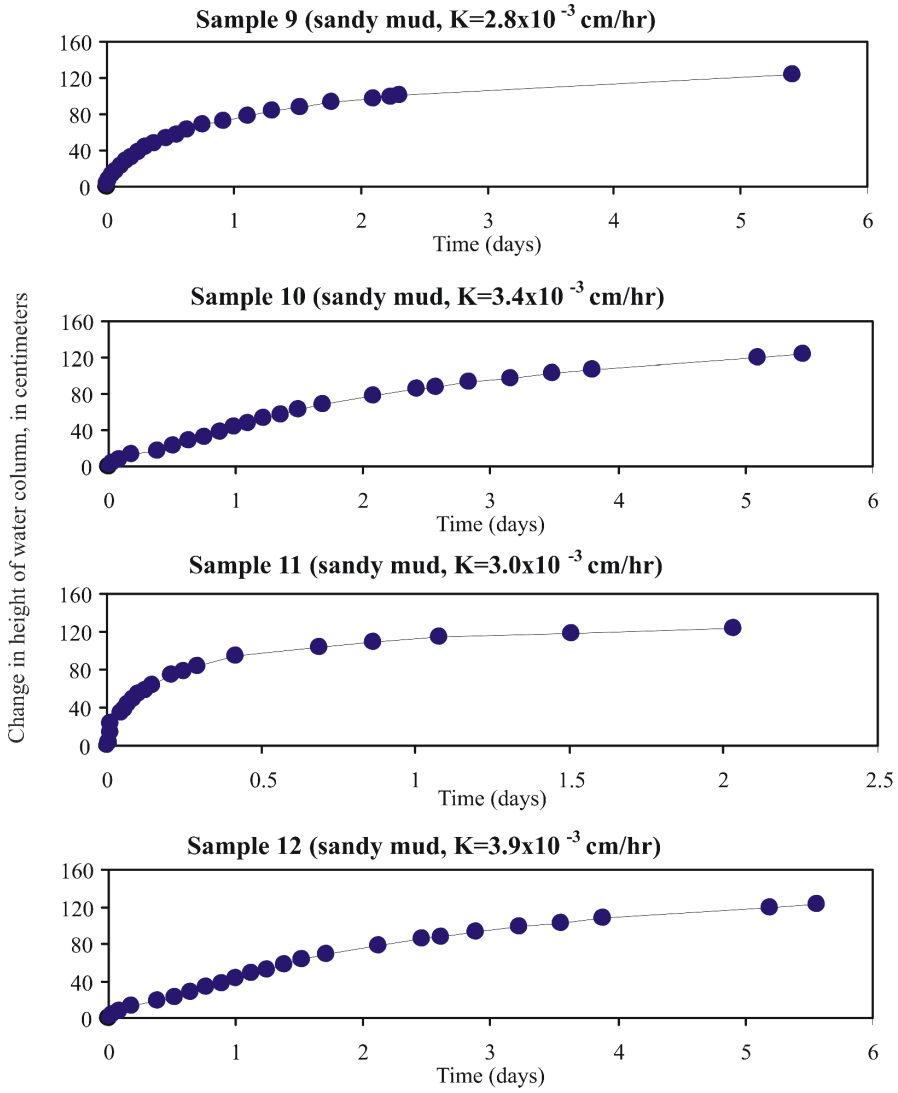
Sample 9 (sandy mud, K=2.8x10 -3 cm/hr)
Sample 10 (sandy mud, K=3.4x10 -3 cm/hr)
Sample 11 (sandy mud, K=3.0x10 -3 cm/hr)
Sample 12 (sandy mud, K=3.9x10 -3 cm/hr)
Change in height of water column, in centimeters
Time (days)
0
40
80
120
160
0.5
1
1.5
2
2.5
3
4
5
6

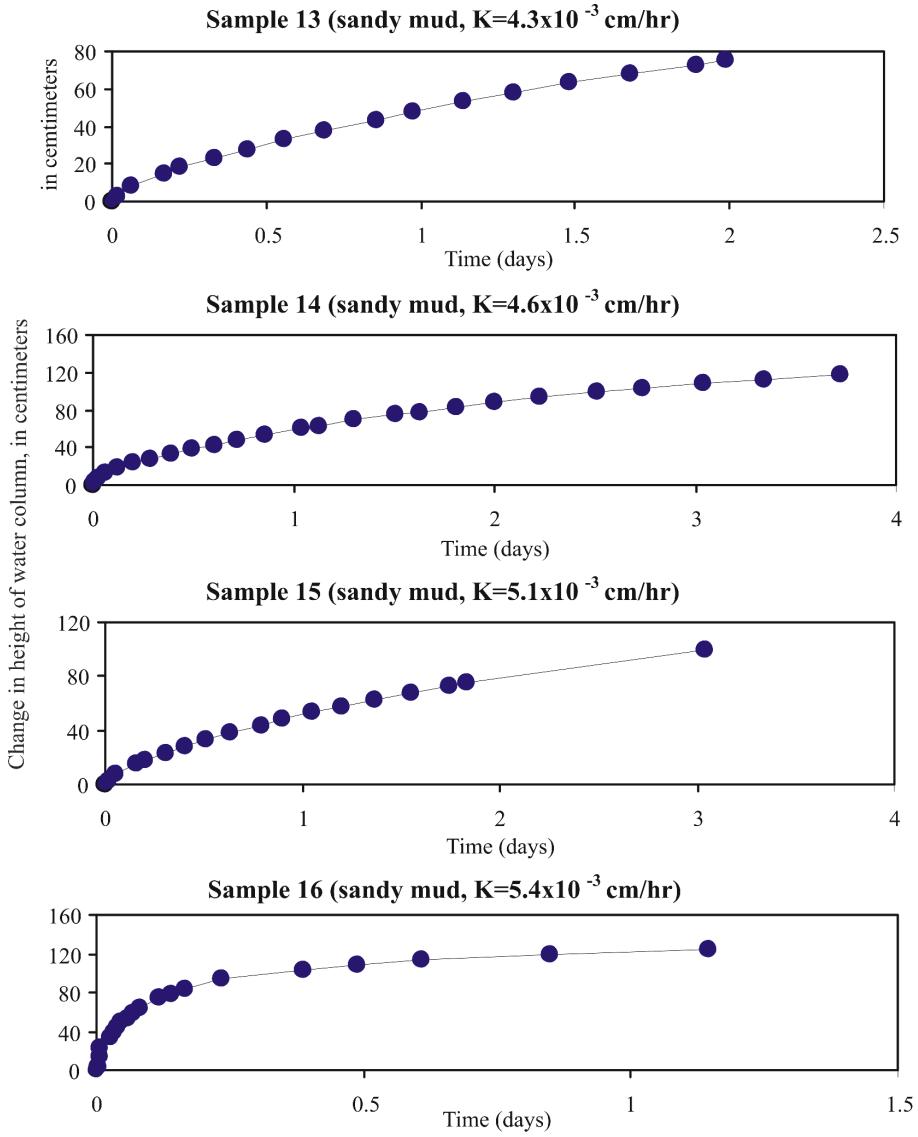
Sample 13 (sandy mud, K=4.3x10 -3 cm/hr)
in cemtimeters
80
60
40
20
0
0
0.5
1
1.5
2
2.5
Time (days)
Sample 14 (sandy mud, K=4.6x10 -3 cm/hr)
Change in height of water column, in centimeters
160
120
80
40
0
0
1
2
3
4
Time (days)
Sample 15 (sandy mud, K=5.1x10 -3 cm/hr)
120
80
40
0
0
1
2
3
4
Time (days)
Sample 16 (sandy mud, K=5.4x10 -3 cm/hr)
160
120
80
40
0
0
0.5
1
1.5
Time (days)

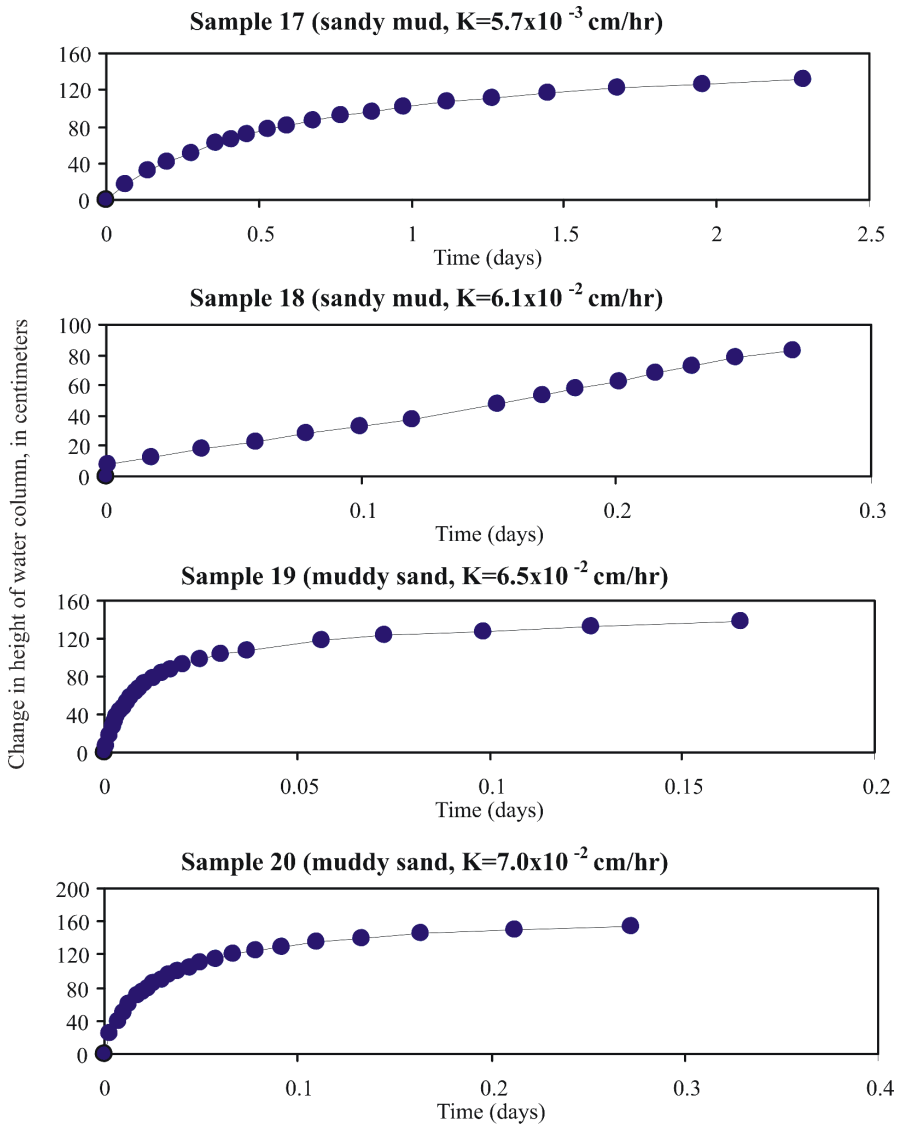
Sample 17 (sandy mud, K=5.7x10 -3 cm/hr)
160
120
80
40
0
0
0.5
1
1.5
2
2.5
Time (days)
Sample 18 (sandy mud, K=6.1x10 -2 cm/hr)
Change in height of water column, in centimeters
100
80
60
40
20
0
0
0.1
0.2
0.3
Time (days)
Sample 19 (muddy sand, K=6.5x10 -2 cm/hr)
160
120
80
40
0
0
0.05
0.1
0.15
0.2
Time (days)
Sample 20 (muddy sand, K=7.0x10 -2 cm/hr)
200
160
120
80
40
0
0
0.1
0.2
0.3
0.4
Time (days)

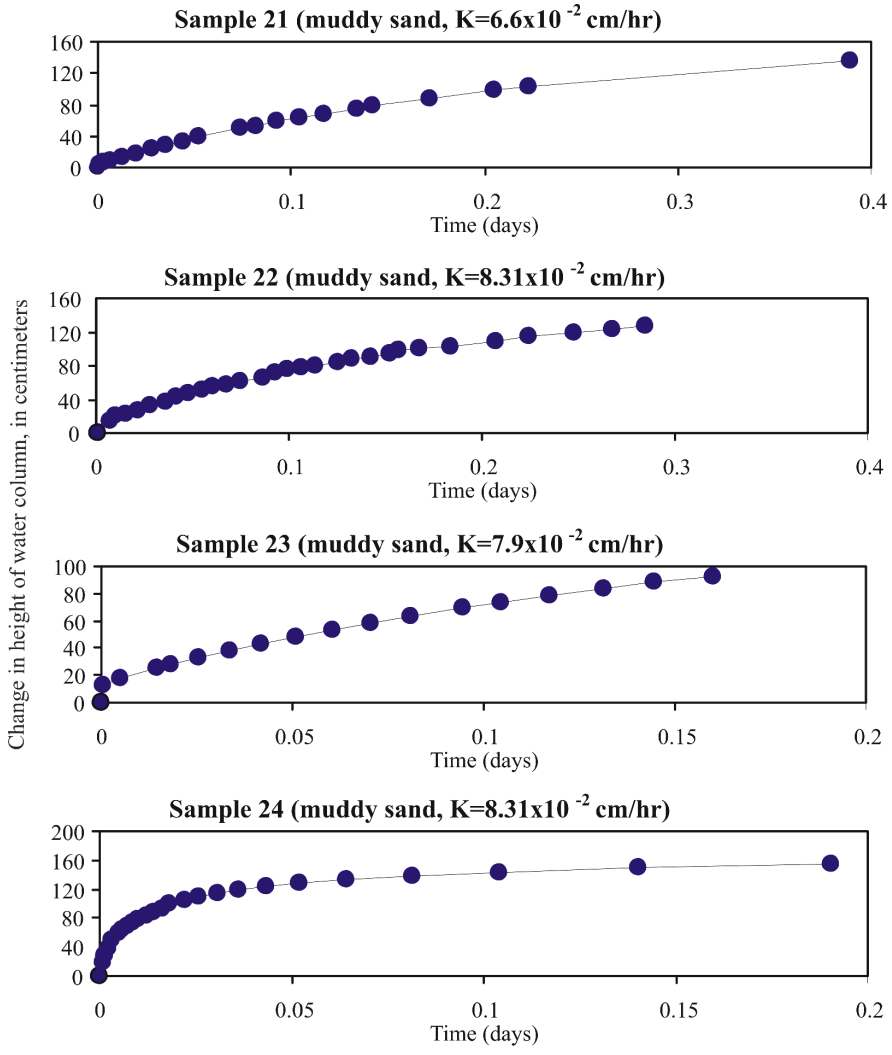
Sample 21 (muddy sand, K=6.6x10 -2 cm/hr)
160
120
80
40
0
0
0.1
0.2
0.3
0.4
Time (days)
Sample 22 (muddy sand, K=8.31x10 -2 cm/hr)
Change in height of water column, in centimeters
160
120
80
40
0
0
0.1
0.2
0.3
0.4
Time (days)
Sample 23 (muddy sand, K=7.9x10 -2 cm/hr)
100
80
60
40
20
0
0
0.05
0.1
0.15
0.2
Time (days)
Sample 24 (muddy sand, K=8.31x10 -2 cm/hr)
200
160
120
80
40
0
0
0.05
0.1
0.15
0.2
Time (days)

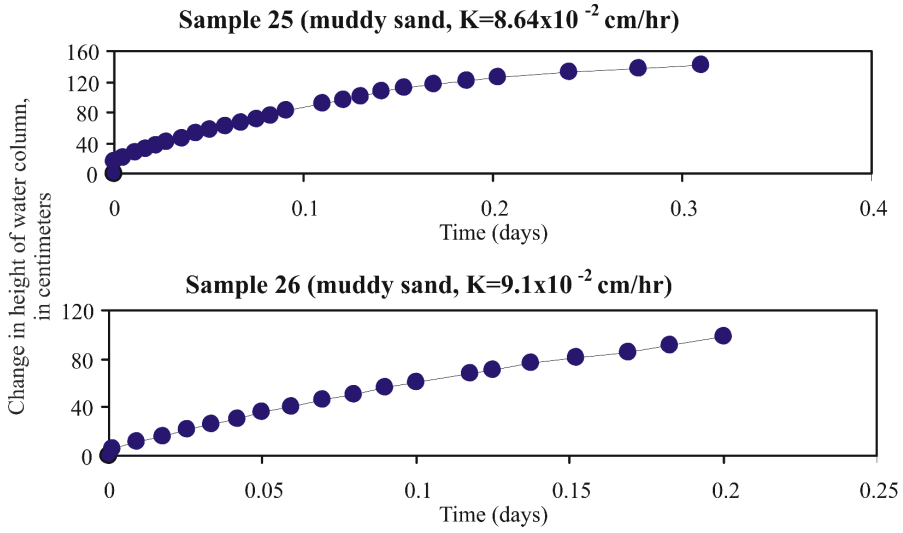
Sample 25 (muddy sand, K=8.64x10 -2 cm/hr)
160
120
80
40
0
0
0.1
0.2
0.3
0.4
Time (days)
Change in height of water column, in centimeters
Sample 26 (muddy sand, K=9.1x10 -2 cm/hr)
120
80
40
0
0
0.05
0.1
0.15
0.2
0.25
Time (days)

APPENDIX C: LABORATORY MEASUREMENTS OF THERMAL CONDUCTIVITY USING A HOT WATER BATH AND INVERSE SIMULATIONS OF CONDUCTIVE HEAT TRANSPORT

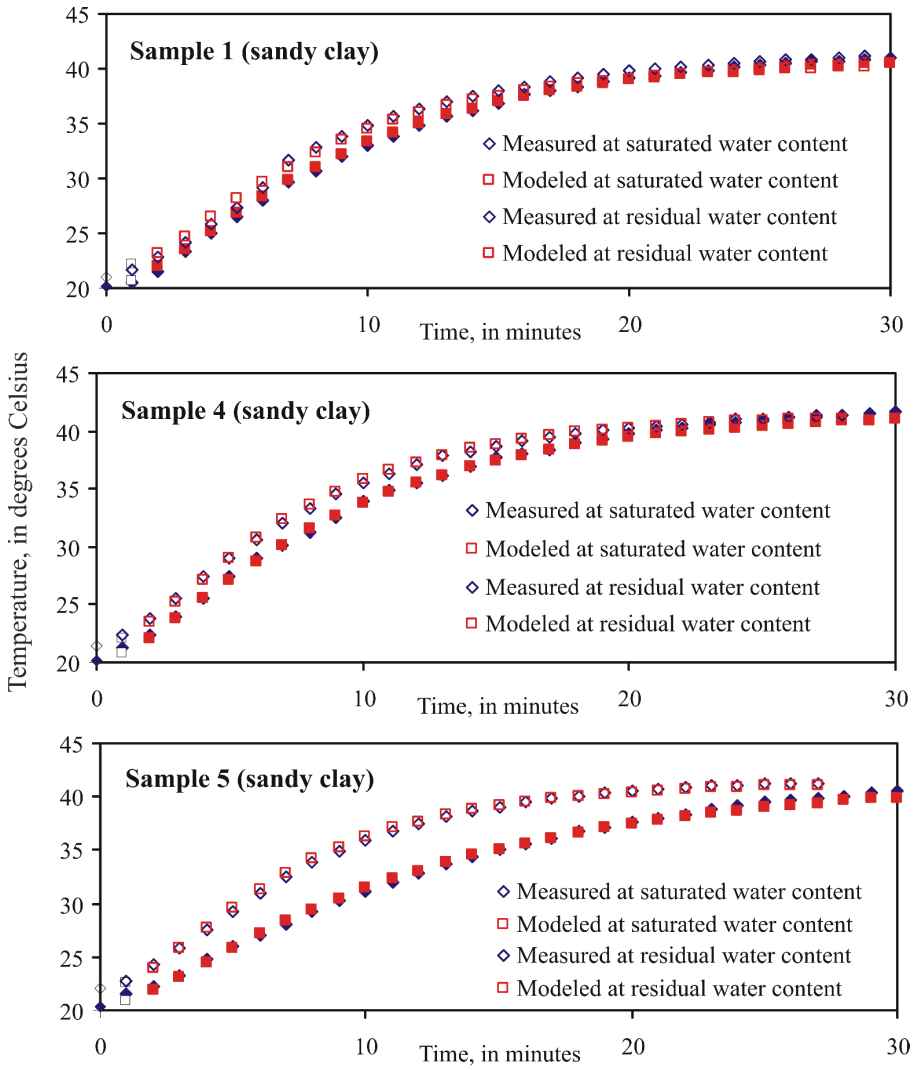

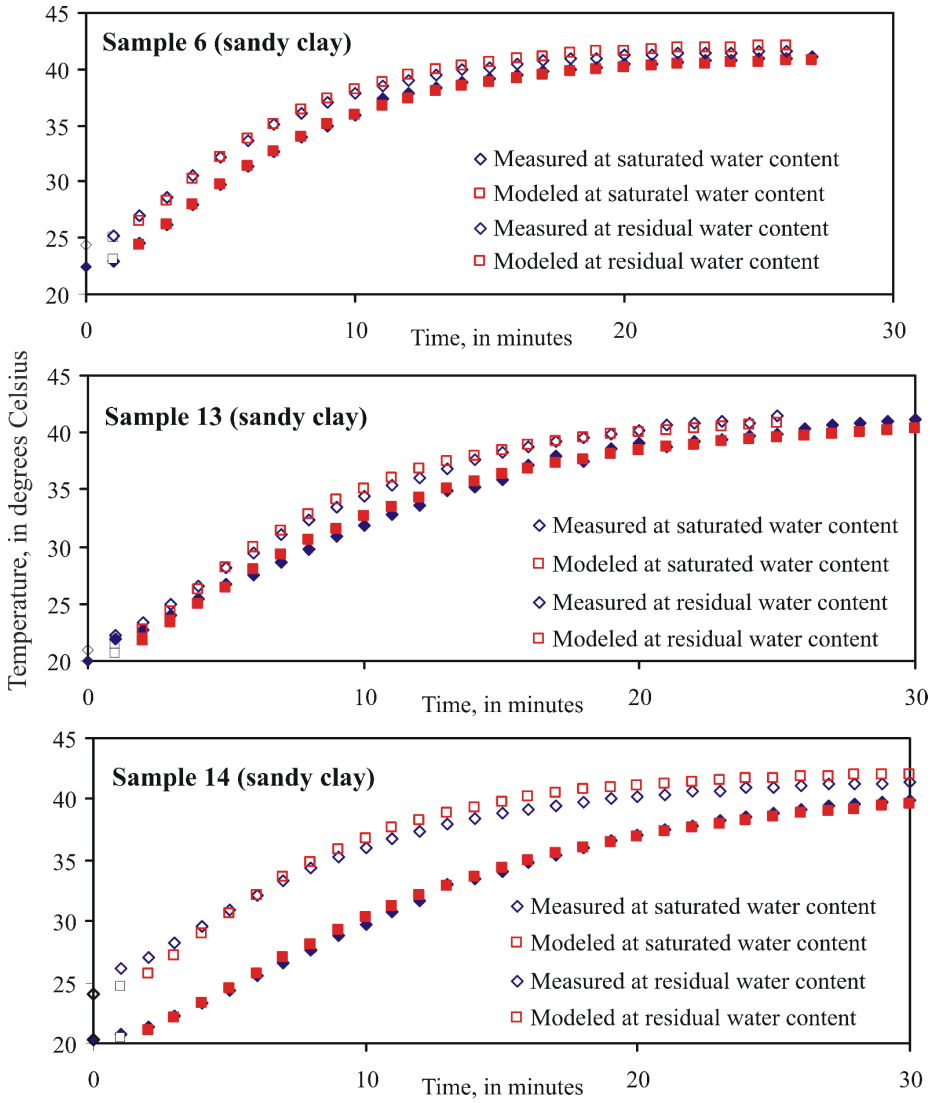
Sample 6 (sandy clay)
Measured at saturated water content
Modeled at saturatel water content
Measured at residual water content
Modeled at residual water content
Sample 13 (sandy clay)
Measured at saturated water content
Modeled at saturated water content
Measured at residual water content
Modeled at residual water content
Sample 14 (sandy clay)
Measured at saturated water content
Modeled at saturated water content
Measured at residual water content
Modeled at residual water content
Temperature, in degrees Celsius
Time, in minutes
Time, in minutes
Time, in minutes
0
10
20
30
20
25
30
35
40
45

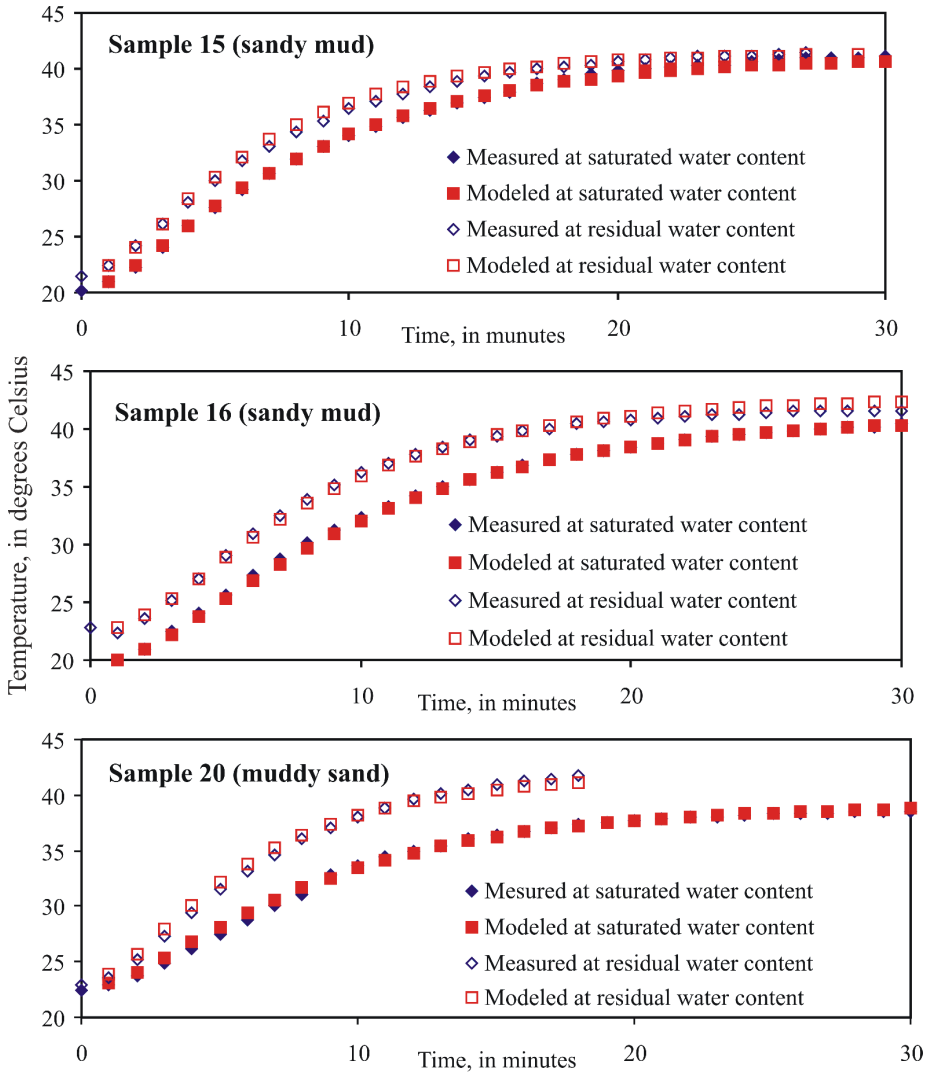
Sample 15 (sandy mud)
Measured at saturated water content
Modeled at saturated water content
Measured at residual water content
Modeled at residual water content
Time, in munutes
Temperature, in degrees Celsius
Sample 16 (sandy mud)
Measured at saturated water content
Modeled at saturated water content
Measured at residual water content
Modeled at residual water content
Time, in minutes
Sample 20 (muddy sand)
Mesured at saturated water content
Modeled at saturated water content
Measured at residual water content
Modeled at residual water content
Time, in minutes

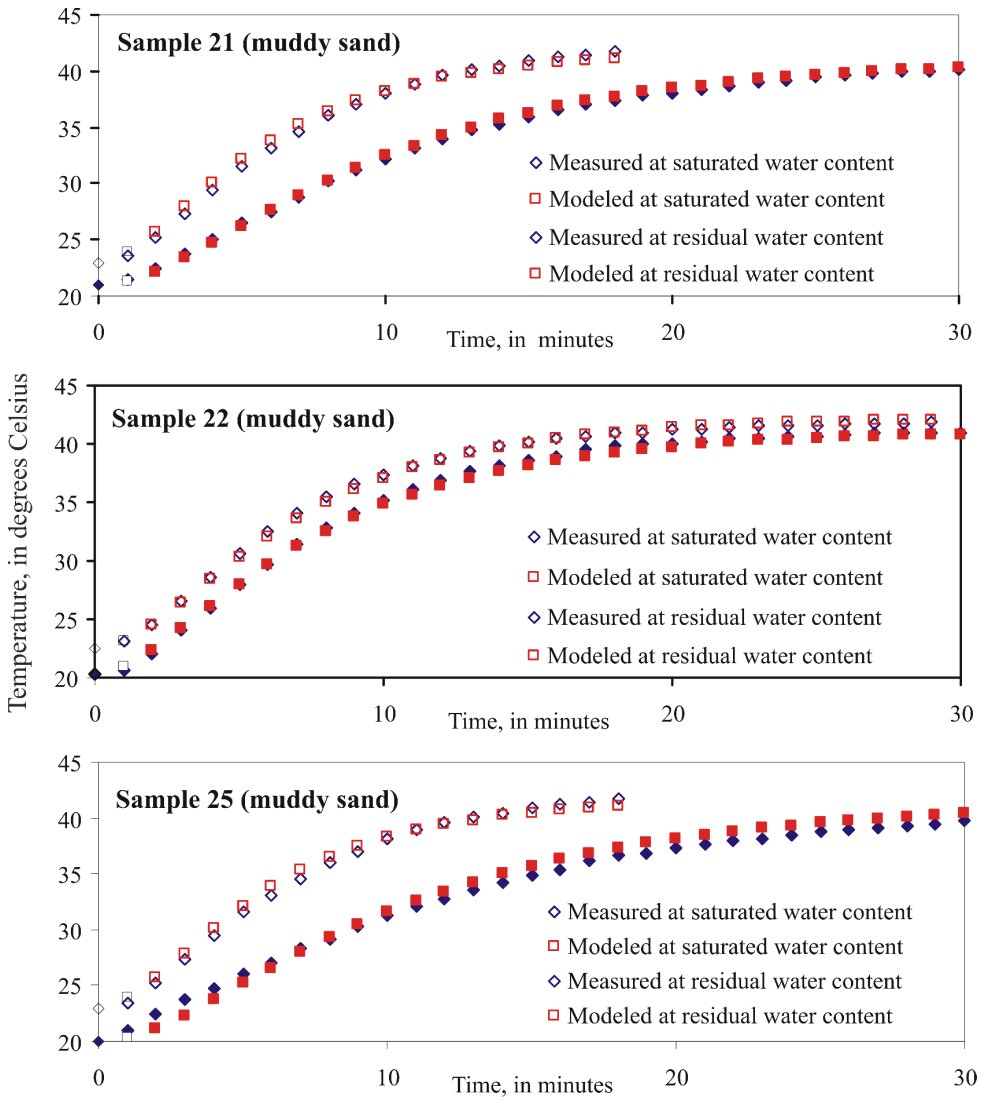
Sample 21 (muddy sand)
Measured at saturated water content
Modeled at saturated water content
Measured at residual water content
Modeled at residual water content
Time, in minutes
Sample 22 (muddy sand)
Measured at saturated water content
Modeled at saturated water content
Measured at residual water content
Modeled at residual water content
Time, in minutes
Temperature, in degrees Celsius
Sample 25 (muddy sand)
Measured at saturated water content
Modeled at saturated water content
Measured at residual water content
Modeled at residual water content
Time, in minutes
45
40
35
30
25
20
0
10
20
30

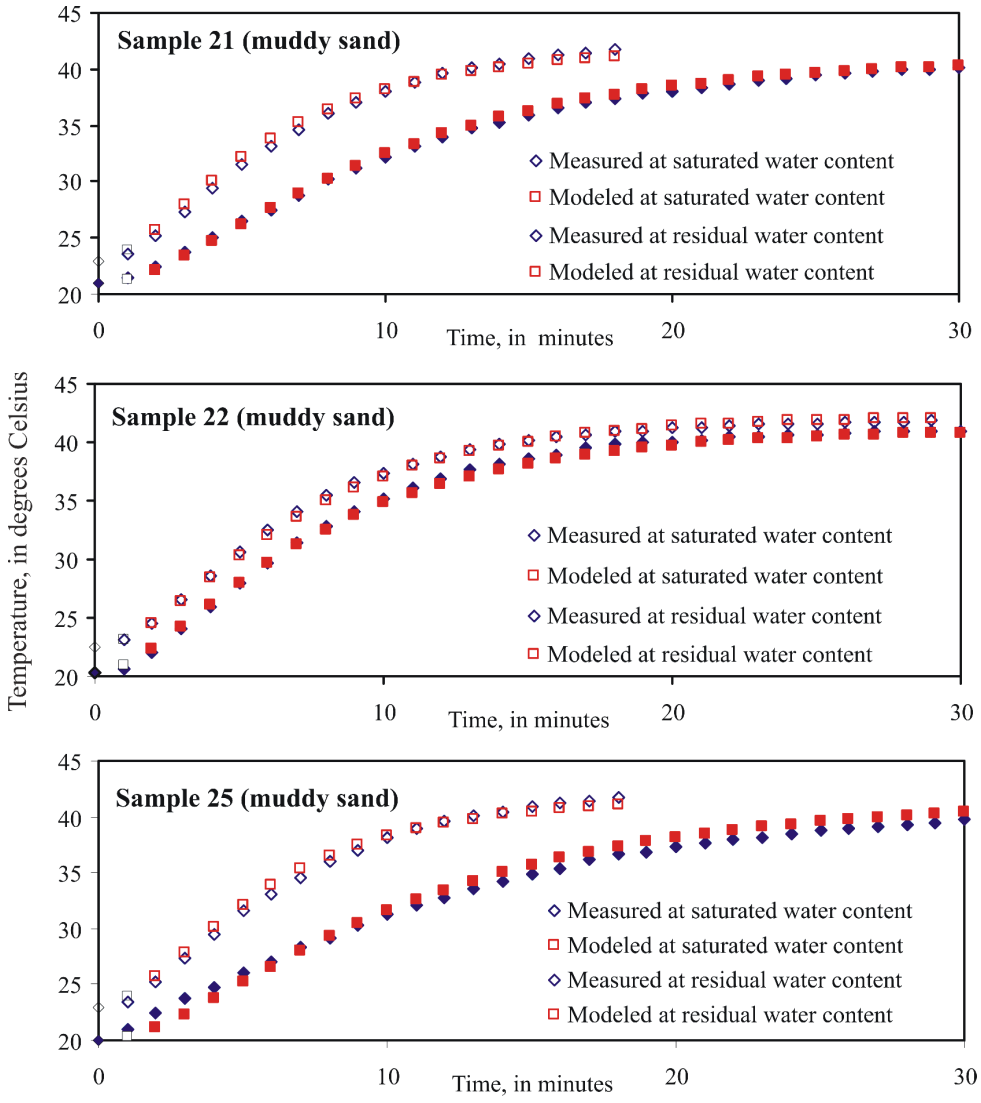
Sample 21 (muddy sand)
Measured at saturated water content
Modeled at saturated water content
Measured at residual water content
Modeled at residual water content
Time, in minutes
Sample 22 (muddy sand)
Measured at saturated water content
Modeled at saturated water content
Measured at residual water content
Modeled at residual water content
Time, in minutes
Temperature, in degrees Celsius
Sample 25 (muddy sand)
Measured at saturated water content
Modeled at saturated water content
Measured at residual water content
Modeled at residual water content
Time, in minutes
45
40
35
30
25
20
0
10
20
30

APPENDIX D: TEXTURE ANALYSIS OF CORE SAMPLES AND DRILL CUTTINGS USED TO DEVELOP GEOSTATISTICAL MODEL

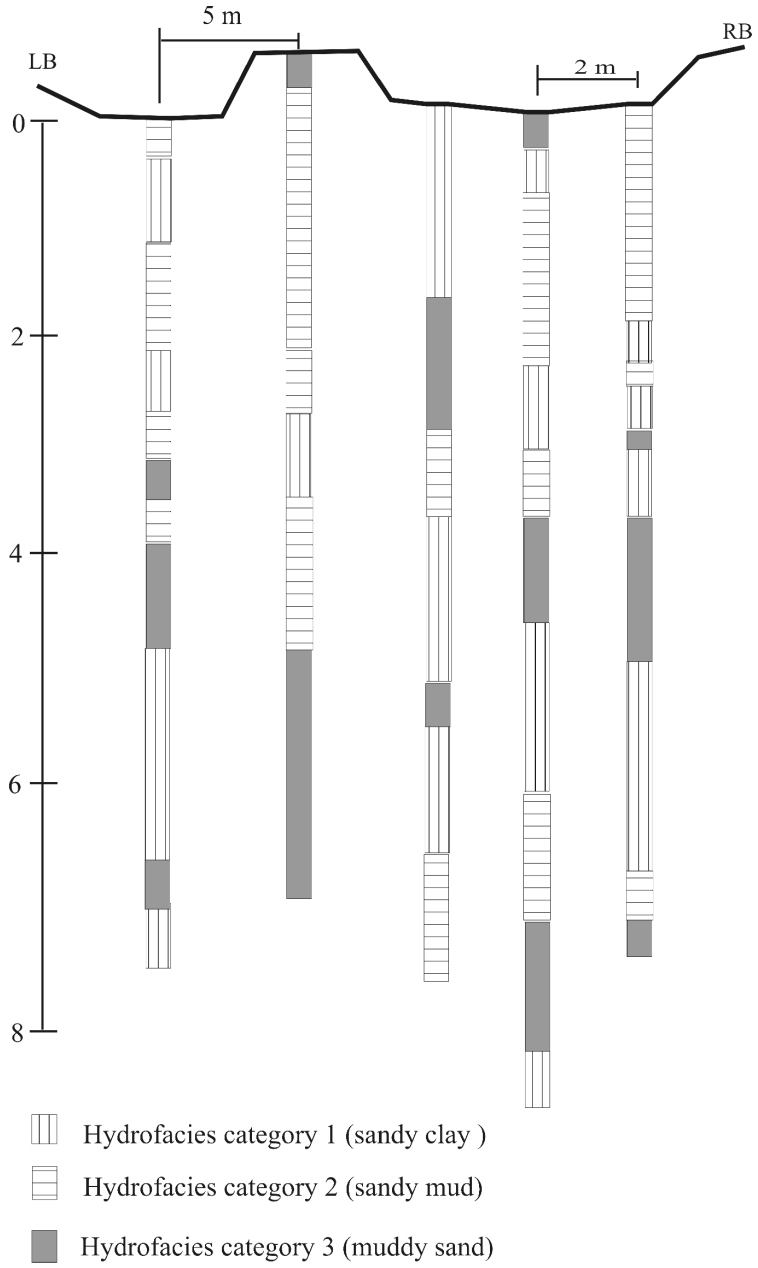

Texture analysis of core samples and drill cuttings for the cross section located at the center of the study site. Locations are shown in Figure 3.3.

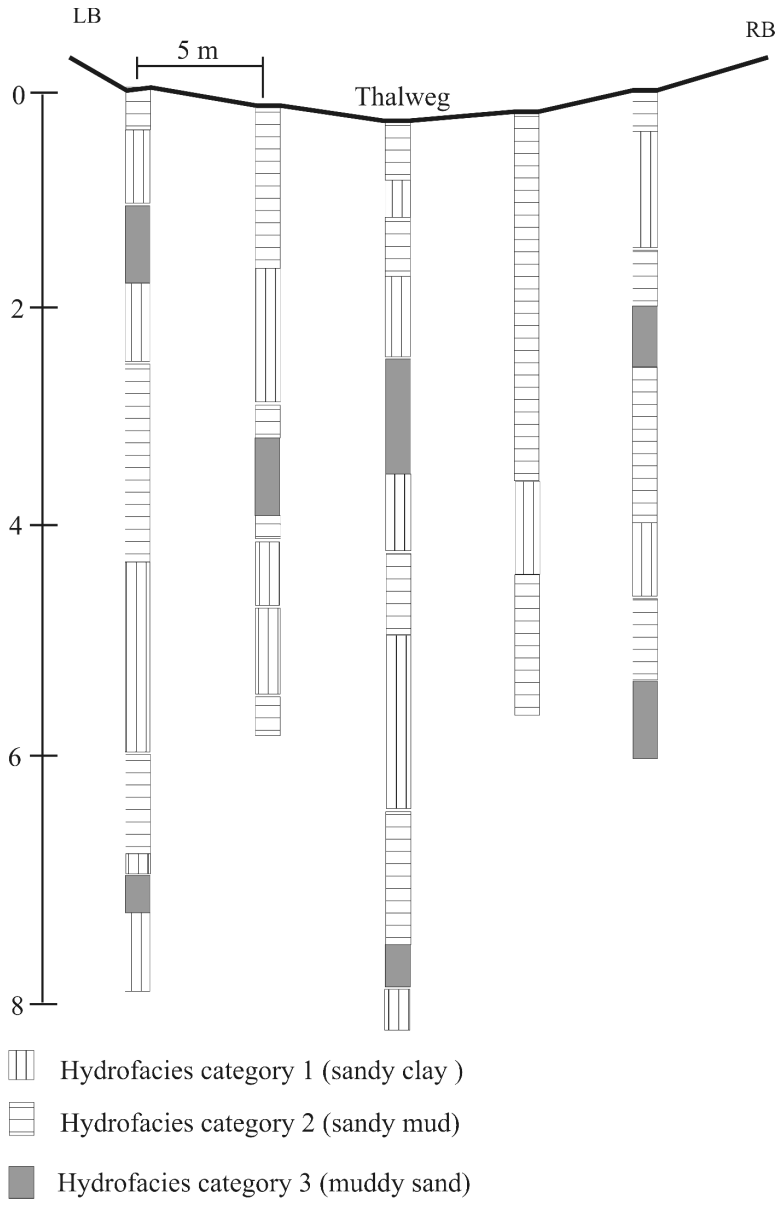

Texture analysis of core samples and drill cuttings for the cross section located at the upstream end of the study site. Locations are shown in Figure 3.3.

APPENDIX E: TOUGH2 SOURCE CODE MODIFIED TO SIMULATE ROOT UPTAKE

```
CCCCC The following lines of code designated by the initials RGN were added
ccccc to the source file t2f.f begining on line 2047.
C The code that handles pressure dependent well deliverability
c was modified to consider ET uptake as a function of capillarity
C...Line 2047 of the source code file 2tf.f of TOUGH2
      IHALVE=0
C
   52 ITER=0
      NOW=0
C-----PRINTOUT OCCURS FOR NOW=1
C
      NOWTIM=0
      IF(ITI.NE.0) CALL TSTEP
      DELTEX=DELT
      KON=1
C
    3 CONTINUE
C
C    added these lines to interpolate PET from a text file
C    4/20/05 RGN
      TOLF2=1.0e-4
      numdata=52
      do i=1,numdata
        fold=abs(SUMTIM-tt2(i))
        if (fold .le. TOLF2) then
c
          pet22=pet2(i)
        elseif (SUMTIM .gt. tt2(i) .AND. SUMTIM .lt.
     c       tt2(i+1))then
c
          pet22=((pet2(i+1)-pet2(i))/(tt2(i+1)-
     c      tt2(i)))*SUMTIM+pet2(i+1)-((pet2(i+1)-
     c      pet2(i))/(tt2(i+1)-tt2(i)))*tt2(i+1)
c
        end if
      end do
C     This is original code from TOUGH2
C-----COME HERE FOR NEXT ITERATION.
C
      IF(ITER.NE.0) GOTO19
      DO20 N=1,NEL
      NLOC=(N-1)*NK1
      DO20 K=1,NK1
      DX(NLOC+K)=0.
   20 CONTINUE
C
   19 CONTINUE
C     end of original TOUGH2 code

C zero out ET array. RGN
```

```
      do N=1,1201
      etact(N)=0.0
      end do
C
C This is original code from TOUGH2
c  included to find location of code changes.
      ITER=ITER+1
      ITERC=ITERC+1
C
      FORD=FOR*DELTEX
C
C-----COMPUTE ACCUMULATION-, SOURCE-, AND FLOW-TERMS.
      CALL MULTI
      IF(IGOOD.EQ.3) GOTO 50
C
C-----CHECK FOR CONVERGENCE.
      IF(RERM.LE.RE1) GOTO51

C...Line 3894 of the source code file 2tf.f of TOUGH2
c
C
C=====COMPUTE FLOW RATES FOR EACH PHASE AND TOTAL RATE FOR WELL ON
C     DELIVERABILITY.==================================================
C     This code was changed to consider only the liquid phase.
c
c     DPRES=0.
c     IF(M.EQ.2) DPRES=DELX(JLOCP+1)
c     DELP=X(JLOCP+1)+DX(JLOCP+1)+DPRES+PAR(J2LNP+6)-PWB(N)
C-----COMPUTE MASS FLOW RATE.
c     FF((N-1)*NPH+NP)=FF((N-1)*NPH+NP)*pin*DELP
c     changed this whole subroutine to use ET function rgn
c     check to see if ET demand has been met (1200 cells per layer).
      hpfive = -1000.
      ppp=3.0
      ttxt = ELEG(N)
      itxt = iDumbText2INT( ttxt)
      iftest=mod(itxt-49201,1200)+1
      totet = 0.0
c  sum up ET for cells above. Any demand left?
       ik=iftest
       if(itxt<49201)then
        ik=0
       end if
       if(ik.ge.1)then
        DPRES=0.
        IF(M.EQ.2) DPRES=DELX(JLOCP+1)
        delp=X(JLOCP+1)+DX(JLOCP+1)+DPRES+PAR(J2LNP+6)
        if(delp.ge.0.0)delp=1.0D-30
        if(M==3.and.np==2)etleft=pet22-etact(ik)
         FF((N-1)*NPH+NP)=(1.0/(1.0+(delp/hpfive)**ppp))*etleft
         if(FF((N-1)*NPH+NP)<0.08*etleft)FF((N-1)*NPH+NP)=0.0
        if(M==3.and.np==2)etact(ik)=etact(ik)+FF((N-1)*NPH+NP)
        if(etleft.lt.0.0)etleft=0.0
        if(M==3.and.np==2)ik=ik+1
       else
        FF((N-1)*NPH+NP) = 0.0
```

```
            end if
          G(N)=G(N)-FF((N-1)*NPH+NP)
          FFS=FFS+FF((N-1)*NPH+NP)
      C
      C=====ENDOFDELIVERABILITYSECTION-modified to simulate
ET.====================================
      C
```

APPENDIX F: MEASURED SEDIMENT TEMPERATURE AND WATER CONTENT

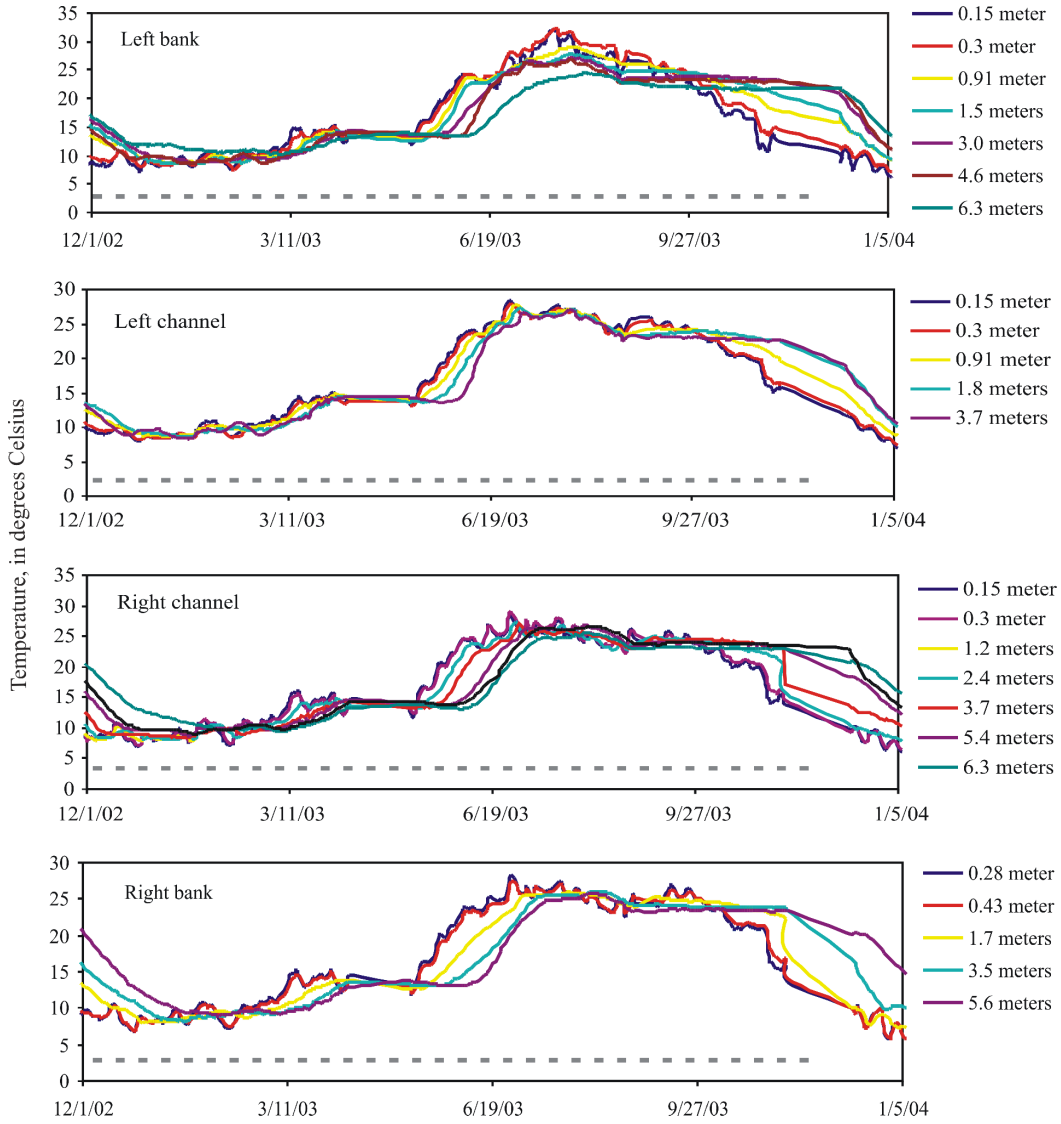

Measured sediment temperatures at the cross-section located at the upstream end of the study site. Locations are shown in Figure 3.3. Dashed gray line indicates the period measurements were used for calibration.

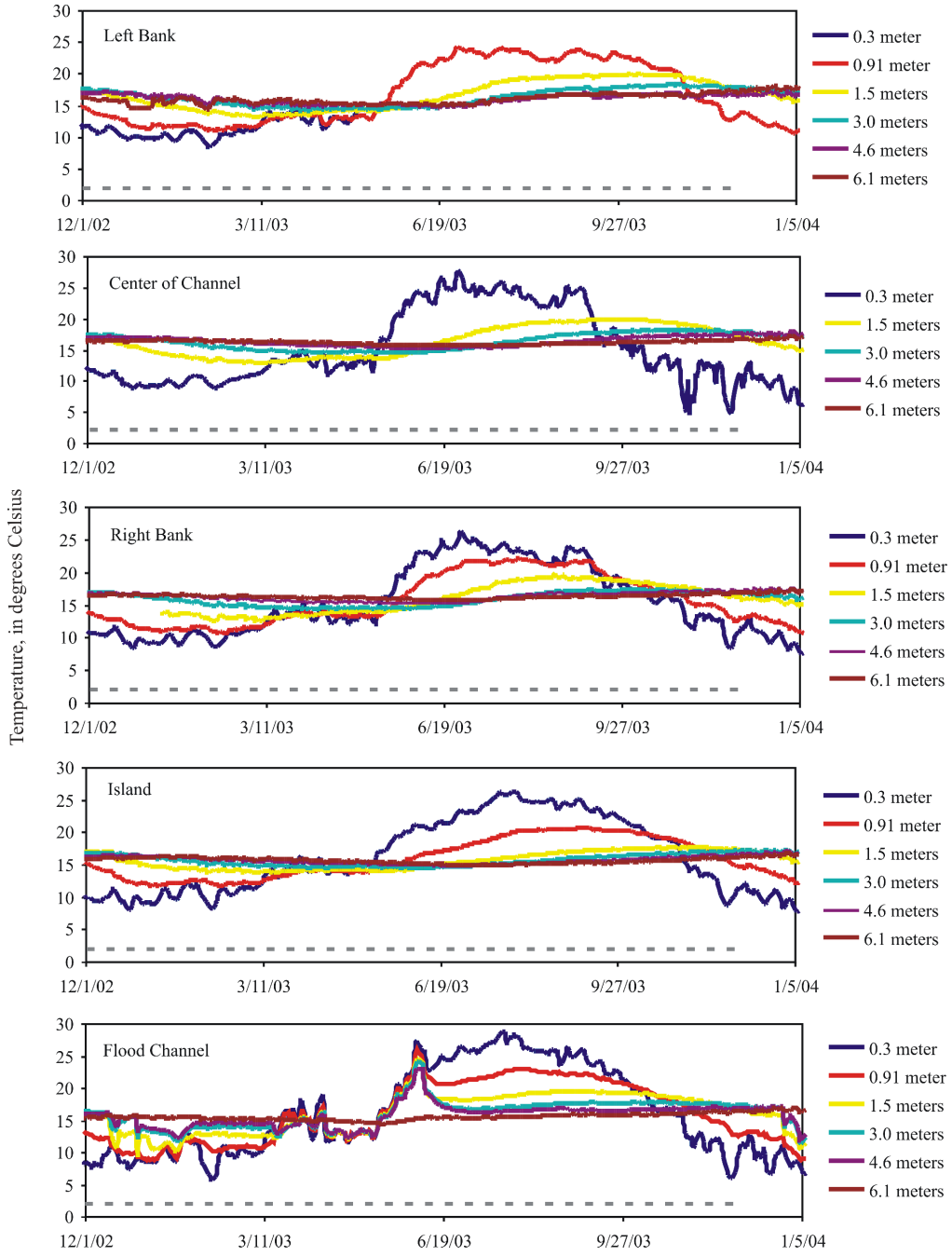

Measured sediment temperatures at the cross-section located at the center of the study site. Locations are shown in Figure 3.3. Dashed gray line indicates the period measurements were used for calibration.

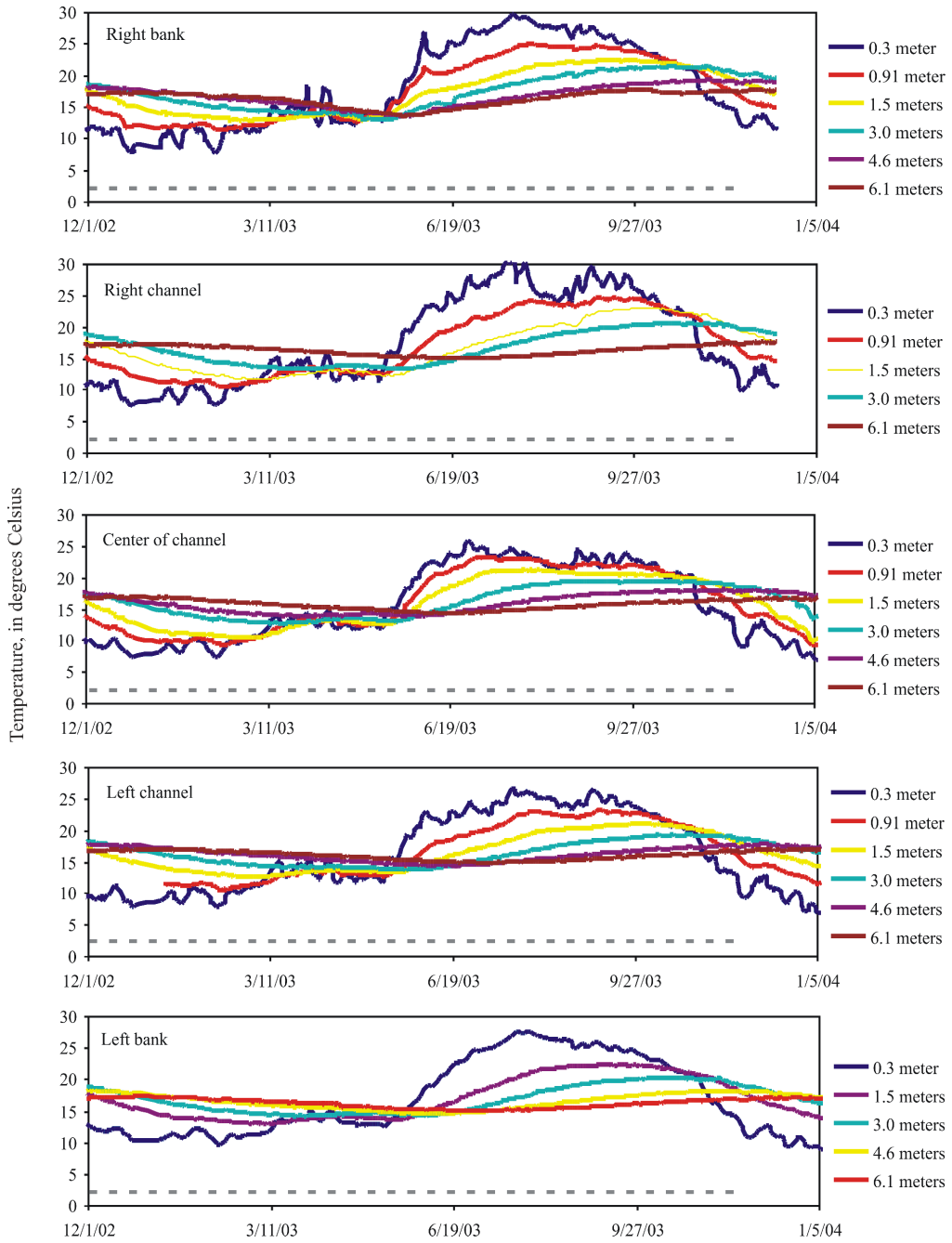

Measured sediment temperatures at the cross-section located at the downstream end study site. Locations are shown in Figure 3.3. Dashed gray line indicates the period measurements were used for calibration.

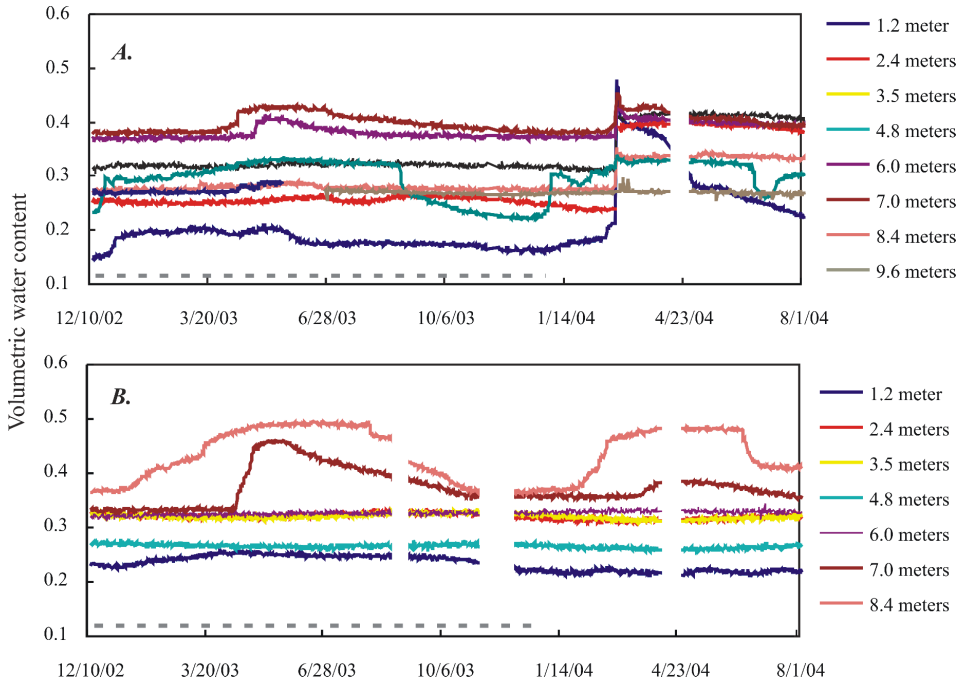

Measured sediment water content: A. Beneath the floodplain and B. beneath the constructed levee. Locations are shown in Figure 3.3. Dashed gray line indicates the period measurements were used for calibration.